الجمهورية الجزائرية الديمقراطية الشعبية

PEOPLE'S DEMOCRATIC REPUBLIC OF ALGERIA

وزارة التعليم العالي والبحث العلمي

Ministry of Higher Education and Scientific Research

جامعة أبي بكر بلقايد – تلمسان –

University of Abou Bekr Belkaid – Tlemcen –
Faculty of Technology

THESIS

Presented to obtain of the degree of **Doctorate**, **3rd Cycle**

In: Mechanical engineering

Specialty: Energetics

By: CHIKH Mohammed El Amine

Subject

Contribution to the improvement of the energy efficiency of solar sorption refrigeration systems: application to absorption systems

Contribution à l'amélioration de l'efficacité énergétique des systèmes frigorifiques solaires à sorption : application aux systèmes à absorption

Publicly defended on 18 / 06 / 2026, in front of the jury composed of:

M. GHERNAOUT Mohammed El Amine	Pr.	Univ. Tlemcen	President
M. BENRAMDANE Mohammed	Pr.	Univ. Tlemcen	Thesis director
M. ALIANE Aabdennour	Dr.	Univ. Tlemcen	Thesis co-director
M. SAIM Rachid	Pr.	Univ. Tlemcen	Examiner
M. BOUSBAA Hamza	Pr.	ENP. Oran	Examiner

Academic year: 2025-2026

Acknowledgments

First and foremost, I express my deepest gratitude to God Almighty, the source of strength, wisdom, and perseverance, who has guided and supported me throughout the completion of this work.

I would like to extend my sincere appreciation to my thesis supervisors, **Professor Mohammed BENRAMDANE** and **Dr. Aabdennour ALIANE**, for their invaluable guidance, patience, and continuous support. Their scientific expertise, insightful advice, and encouragement were essential to the successful accomplishment of this research.

I am also profoundly grateful to the members of the examination committee **Professor Mohammed El Amine GHERNAOUT**, **Professor Rachid SAIM** and **Professor Hamza BOUSBAA** for the honor they have given me by evaluating this work. Their time, effort, and constructive comments have greatly contributed to improving the quality of this thesis.

My heartfelt thanks go to my dear mother and my sisters for their unconditional love, unwavering support, and constant encouragement. I am equally grateful to my family and friends for their understanding, motivation, and comforting presence during the most challenging moments of this journey.

This research was conducted at the Applied Energy and Thermal Laboratory (ETAP), Department of Mechanics, Faculty of Technology, at the University of Tlemcen. I sincerely acknowledge this institution for providing the necessary technical and scientific resources, as well as a stimulating research environment conducive to academic excellence.

Finally, to everyone who contributed, directly or indirectly, to the completion of this work, I extend my sincere and heartfelt gratitude.

Dedication

In loving memory of my Father, who will always remain in my heart.

To my dear Mother, with all my gratitude and love.

To my beloved sisters: Meriem, Djamila, Fatima Zohra, and Khadidja.

To my uncles and cousins, for their constant support.

To all my family, whose love has guided me.

To my darling Merwa, for her inspiration and encouragement.

To my friends, especially Farouk, Walid, Sofiane, Mohammed Abdelbassit, Nouredinne, Abdou and Adnen, for their companionship and support.

To all those who have devoted their time to science, and to those who use knowledge to serve humanity and promote its well-being.

Mohammed El Amine . . .

ملخص

يوفر التبريد بالامتصاص الذي يعمل بالطاقة الشمسية باستخدام مزيج الأمونيا والماء (NH_3–H_2O) حلاً مستداماً للتبريد في المناطق ذات الإمكانات الشمسية العالية. تتناول هذه الأطروحة تطوير نموذج ديناميكي حراري في حالة الاستقرار لنظام تبريد بالامتصاص الشمسي أحادي التأثير يعمل بمزيج NH_3–H_2O، استناداً إلى معادلات توازن الكتلة والطاقة والتوازن، وتم حلها باستخدام برنامج «Engineering Equation Solver» (EES).

وقد فحصت دراسة بارامترية تأثيرات درجة حرارة المولد، ودرجة حرارة المبخر، وضغوط الماص/المكثف، وتركيز الأمونيا على معامل الأداء (COP). وتُظهر النتائج أن معامل الأداء يزداد مع ارتفاع درجة حرارة المولد حتى نقطة مثلى، وبعدها تحدّ عدم قابلية العودة عن التغييرات من تحقيق مكاسب إضافية، في حين أن ارتفاع تركيز الأمونيا يحسّن معامل الأداء عن طريق تقليل نسبة الدوران. وعلى العكس من ذلك، تؤدي زيادة درجة حرارة المبخر إلى انخفاض معامل الأداء بسبب التغيرات في توازن المحلول.

وبلغ الحد الأقصى لمعامل الأداء (COP) الذي تم الحصول عليه 1.28، عند Ph = 7 بار، و Pb = 1 بار، و٪x = 25، ودرجة حرارة المولد في نطاق 110–115 درجة مئوية. وتم التحقق من صحة النموذج بمقارنته بالبيانات المنشورة، حيث أظهرت النتائج توافقًا جيدًا. وتحدد هذه النتائج مناطق التشغيل المثلى وتقدم إرشادات تصميمية لتحسين أداء التبريد بالامتصاص الشمسي في المناطق ذات الإشعاع العالي مثل الجزائر.

الكلمات المفتاحية :الطاقة الشمسية، التبريد، الامتصاص، التركيز، معامل الأداء، الأمونيا–الماء.(NH_3–H_2O)

Abstract

Solar-driven absorption refrigeration using the ammonia–water (NH_3–H_2O) pair offers a sustainable cooling solution for regions with high solar potential. This thesis develops a steady state thermodynamic model of a single-effect NH_3–H_2O solar absorption refrigeration system, based on mass, energy, and equilibrium balances, and solved using Engineering Equation Solver (EES).

A parametric study examined the effects of generator temperature, evaporator temperature, absorber/condenser pressures, and ammonia concentration on the coefficient of performance (COP). Results show COP increases with generator temperature up to an optimum, beyond which irreversibility limits further gains, while higher ammonia concentration improves COP by reducing the circulation ratio. Conversely, increasing evaporator temperature reduces COP due to shifts in solution equilibrium.

The maximum COP obtained was 1.28, at Ph = 7 bar, Pb = 1 bar, x = 25%, and a generator temperature of 110–115°C. The model was validated against published data, showing good agreement. These findings identify optimal operating regions and offer design guidelines for improving solar absorption cooling performance in high-irradiation regions such as Algeria.

Key words: Solar energy, Refrigeration, Absorption, concentration, COP, NH_3-H_2O.

Résumé

La réfrigération par absorption solaire utilisant le couple ammoniac-eau (NH_3–H_2O) offre une solution de refroidissement durable pour les régions à fort potentiel solaire. Cette thèse développe un modèle thermodynamique en régime permanent d'un système de réfrigération par absorption solaire NH_3–H_2O à simple effet, basé sur les bilans de masse, d'énergie et d'équilibre, et résolu à l'aide du logiciel Engineering Equation Solver (EES).

Une étude paramétrique a examiné les effets de la température du générateur, de la température de l'évaporateur, des pressions de l'absorbeur et du condenseur, ainsi que de la concentration en ammoniac sur le coefficient de performance (COP). Les résultats montrent que le COP augmente avec la température du générateur jusqu'à un point optimal, au-delà duquel l'irréversibilité limite tout gain supplémentaire, tandis qu'une concentration plus élevée en ammoniac améliore le COP en réduisant le rapport de circulation. À l'inverse, l'augmentation de la température de l'évaporateur réduit le COP en raison de modifications de l'équilibre de la solution.

Le COP maximal obtenu était de 1,28, pour Ph = 7 bar, Pb = 1 bar, x = 25 % et une température du générateur comprise entre 110 et 115 °C. Le modèle a été validé par rapport à des données publiées, montrant une bonne concordance. Ces résultats identifient les plages de fonctionnement optimales et fournissent des lignes directrices de conception pour améliorer les performances du refroidissement par absorption solaire dans les régions à fort ensoleillement telles que l'Algérie.

Mots-clés : Énergie solaire, Réfrigération, Absorption, Concentration, COP, NH_3–H_2O.

Summary

General introduction

Chapter 1 Solar resource assessment 5

I.1. Introduction **5**

I.2. Sun **6**
I.2.1 Fundamental Properties of the Sun 6
I.2.2. Earth motion 7
I.2.3. Apparent solar path 8
I.2.4. Celestial Sphere 9
I.3. Astronomical data 10
I.3.1 Equatorial coordinates 10
I.3.1.1 Solar declination 10
I.3.1.2 Hour angle of the sun 11
I.3.1.3 Solar time 12
I.3.2. Horizontal coordinates of the sun 12
I.3.2.1 Sun azimuth (χ) 12
I.3.2.2 Solar altitude angle 13
I.3.3 Geographical coordinates 13
I.3.3.1 Latitude of location (φ) 13
I.3.3.2 Longitude (L) 14
I.3.3.3 Altitude (z) 14

I.4 Solar radiation **14**
I.4.1. Direct radiation 15
I.4.2. Diffuse radiation 15
I.4.3. Global radiation 16

I.5 Solar Resource in Algeria **16**

I.6. General of solar thermal collectors **17**
I.6.1. Stationary solar collectors 18
I.6.1.1 Flat plate collectors (FPC) 18
I.6.1.2 Evacuated tube collectors (ETC) 18
I.6.1.3 Solar air collectors (SAC) 19
I.6.1.4 Unglazed collector 20
I.6.2. Concentrating solar collectors (CSC) 20
I.6.2.1. Parabolic trough collectors (PTC) 20
I.6.2.2. Parabolic dish reflectors (PDR) 21
I.6.2.3. Fresnel collectors (FC) 21
I.6.2.4. Heliostat field collectors (HFC) 22
I.6.3. Future Research Trends 22

I.7. Conclusion **23**

Chapter 2 Cooling and refrigeration technologies 25

II.1. Introduction 25

II.2. Solar energy 25

II.3. Solar refrigeration 25

II.4. Electrically driven 27
II.4.1. Photovoltaic (PV) 27
II.4.2. Vapour compression 28
II.4.3. Thermo electric 30

II.5. Thermally driven 31
II.5.1. Thermo-mechanical cooling 31
II.5.1.1. Rankine cycle 31
II.5.1.2. Ejector cycle 32
II.5.2. Sorption process cooling 33
II.5.2.1. Open sorption systems 33
II.5.2.1.1. Liquid desiccant 34
II.5.2.1.2. Sorption solid 35
II.5.2.1.3 Desiccant cooling 35
II.5.2.2. Closed sorption systems 36
II.5.2.2.1 Adsorption system 36
II.5.2.2.2 Absorption system 38

II.6. Types of absorption cycles 43
II.6.1. Single effect absorption cycle 43
II.6.2. Double-effect absorption cycle 43
II.6.3. Half-effect solar absorption cycle 44
II.6.4. Triple-effect solar absorption cycle 45

II.7. Difference between absorption and adsorption 46
II.7.1. Absorption 46
II.7.2. Adsorption 46

II.8. Thermal energy storage 47

II.9 Market distribution of solar cooling technologies 47
II.9.1. Market overview of small-scale chillers 48

II.10. Literature review 50

II.11. Conclusion 59

Chapter 3 Thermodynamic study of absorption refrigeration 61

III.1. Introduction 61

III.2. Description of the absorption cycle 62
III.2.1. Generator 62

III.2.2. Condenser 62
III.2.3. Expansion Valve 63
III.2.4. Evaporator 64
III.2.5. Absorber 64
III.2.6. Solution pump 65
III.2.7. Solution heat exchanger 65
III.2.8. Overall cycle operation 66

III.3. Thermodynamic study 66

III.4. Working constraints 72
III.4.1. Hypotheses 72
III.4.2. Operating Parameters 73
III.4.3. Binary working couple 73

III.5. Conclusion 74

Chapter 4 Results and discussions 76

IV.1. Introduction 76

IV.2. Model setup 78

IV.3. Results and discussion 78

IV.4 Interpretations 79
IV.4.1. First study (Ph=7bar) 79
IV.4.2. Second study (Ph=8bar) 85
IV.4.1. Third study (Ph=10bar) 91

IV.5. Model validation 98

IV.6 Conclusion 98

General conclusion 101

References

List of figures

Figure I. 1 Sun 7
Figure I. 2 Orbital Motion of the Earth Relative to the Sun 7
Figure I. 3 Determining the position of the sun 9
Figure I. 4 Circles on the Celestial Sphere 10
Figure I. 5 Annual variation of declination 11
Figure I. 6 Variation in the hour angle as a true solar time 12
Figure I. 7 Horizontal reference point 13
Figure I. 8 Solar radiation 14
Figure I. 9 Spectral analysis of solar radiation 15
Figure I. 10 Pyrheliometer 15
Figure I. 11 Pyrometer 16
Figure I. 12 Pyranometer 16
Figure I. 13 Global regions with high potential for Solar Power. 17
Figure I. 14 Algeria global horizontal irradiation 17
Figure I. 15 Schematic view of flat plate collectors (FPC) 18
Figure I. 16 Schematic of evacuated tube collector 19
Figure I. 17 Schematic of solar air collector (plate version) 19
Figure I. 18 Unglazed solar collector 20
Figure I. 19 Schematic diagrams of parabolic trough collector (PTC) 21
Figure I. 20 Schematic diagrams of parabolic dish reflectors (PDR) 21
Figure I. 21 Schematic diagram of Fresnel collector (FC) 22
Figure I. 22 Schematic diagram of heliostat field collectors (HFC) 22

Figure II. 1 Schematic representation of a solar thermal cooling system 26
Figure II. 2 Classification of solar cooling systems 27
Figure II. 3 Solar photovoltaic (PV) cooling system 28
Figure II. 4 Illustration and schematic representation of a solar-powered vapour compression refrigeration system 29
Figure II. 5 Diagram of a vapor compression refrigeration cycle (Pressure 'P' - enthalpy 'h') 30
Figure II. 6 Solar thermoelectric refrigeration system 30
Figure II. 7 Solar Rankine cooling schematic: (a) separate cycles, (b) integrated cycle. 32
Figure II. 8 Schematic diagram of a solar ejector cooling system 33
Figure II. 9 Complete process of a desiccant dehumidification system 34

Figure II. 10 Principle of the liquid desiccation cooling 34
Figure II. 11 Principle of the solid desiccation cooling 35
Figure II. 12 Schematic diagram of desiccant cooling system 36
Figure II. 13 Schematic diagram of the solar adsorption cooling system 37
Figure II. 14 Schematic diagram of a solar-driven absorption refrigeration system with thermal energy storage 39
Figure II. 15 Solar cooling by absorption system 40
Figure II. 16 Absorption refrigeration machine 40
Figure II. 17 Diagram of a single effect solar absorption cooling system with solar collector and thermal storage. 43
Figure II. 18 Diagram of double-effect solar absorption (P,T) 44
Figure II. 19 Schematic of a half-effect solar absorption cycle 44
Figure II. 20 Diagram of triple-effect solar absorption cycle 45
Figure II. 21 Influence the Temperature of generator (Tg) on the COP for absorption systems. 45
Figure II. 22 System installation of solar absorption cooling with thermal storage and solar collector 47
Figure II. 23 Percentage of use of the different technologies 48
Figure II. 24 Schematic of the solar adsorption refrigeration system. 51
Figure II. 25 Layout of vapour absorption system using waste heat 52
Figure II. 26 Pressure and temperature analysis of absorption system 52
Figure II. 27 Experimental vapour absorption refrigeration system, geometry of shell and helical coil solution heat exchanger 53
Figure II. 28 System absorption refrigeration developing 53
Figure II. 29 Schema of LiBr- Al2O3-H2O absorption cooling system powered by solar energy 54
Figure II. 30 Layout of single effect absorption refrigeration (ABR). 55
Figure II. 31 Schematic diagram of the experimental set-up 56
Figure II. 32 Schematic of the experimental apparatus 57
Figure II. 33 Picture of the prototype of ammonia-water absorption chiller 58
Figure II. 34 Architecture of the absorption chiller 58

Figure III. 1 Basic schematic of a solar absorption refrigeration machine single-effect. 61
Figure III. 2 Generator 62

Figure III. 3 Condenser 63
Figure III. 4 Expansion valve 63
Figure III. 5 Evaporator 64
Figure III. 6 Absorber 65
Figure III. 7 Solution pump 65
Figure III. 8 Plate heat exchanger 66
Figure III. 9 Merkel Diagram (H–x diagram) for NH_3/H_2O 71
Figure III. 10 Oldham diagram (P,T) for NH3/H2O 72

Figure IV. 1 Algorithmic procedure for the calculation and optimization of COP 77
Figure IV. 2 Engineering equation solver software (EES) 78
Figure IV. 3 COP variation with generator temperature for different refrigerant mass concentrations at Pb=1 bar, Ph=7bar 79
Figure IV. 4 COP variation with evaporator temperature for different refrigerant mass concentrations at Pb=1 bar, Ph=7 bar 80
Figure IV. 5 COP variation with generator temperature for different refrigerant mass concentrations at Pb=1.4 bar, Ph=7bar 81
Figure IV. 6 COP variation with evaporator temperature for different refrigerant mass concentrations at Pb=1.4 bar, Ph=7 bar 82
Figure IV. 7 COP variation with generator temperature for different refrigerant mass concentrations at Pb=1.7 bar, Ph=7bar 83
Figure IV. 8 COP variation with evaporator temperature for different refrigerant mass concentrations at Pb=1.7 bar, Ph=7 bar 84
Figure IV. 9 COP variation with generator temperature for different refrigerant mass concentrations at Pb=1 bar, Ph=8bar 85
Figure IV. 10 COP variation with evaporator temperature for different refrigerant mass concentrations at Pb=1 bar, Ph=8 bar 86
Figure IV. 11 COP variation with generator temperature for different refrigerant mass concentrations at Pb=1.4 bar, Ph=8bar 87
Figure IV. 12 COP variation with evaporator temperature for different refrigerant mass concentrations at Pb=1.4 bar, Ph=8 bar 88
Figure IV. 13 COP variation with generator temperature for different refrigerant mass concentrations at Pb=1.7 bar, Ph=8bar 89

Figure IV. 14 COP variation with evaporator temperature for different refrigerant mass concentrations at Pb=1.7 bar, Ph=8 bar.....90
Figure IV. 15 COP variation with generator temperature for different refrigerant mass concentrations at Pb=1 bar, Ph=10 bar.....91
Figure IV. 16 COP variation with evaporator temperature for different refrigerant mass concentrations at Pb=1 bar, Ph=10 bar.....92
Figure IV. 17 COP variation with generator temperature for different refrigerant mass concentrations at Pb=1.4 bar, Ph=10 bar.....93
Figure IV. 18 COP variation with evaporator temperature for different refrigerant mass concentrations at Pb=1.4 bar, Ph=10 bar.....94
Figure IV. 19 COP variation with generator temperature for different refrigerant mass concentrations at Pb=1.7 bar, Ph=10 bar.....95
Figure IV. 20 COP variation with evaporator temperature for different refrigerant mass concentrations at Pb=1.7 bar, Ph=10 bar.....96
Figure IV. 21 Effect of High Pressure (Ph) on Maximum COP — x = 25%.....97
Figure IV. 22 Effect of Ammonia Mass Concentration on COP 97

List of tables

Table I. 1 Sun's azimuth orientation. 13

Table II. 1 Comparison of working pairs in absorption refrigeration systems 41
Table II. 2 Characteristics of new binary and ternary mixtures used in absorption refrigeration systems 42
Table II. 3 Comparison of different market available small capacity absorption chillers 49
Table II. 4 Comparative technical characteristics of commercially available small-capacity sorption refrigeration units 50

Table III. 1 Presentation of the different study parameters 73

Table IV. 1 Best COP values for different pressures and concentrations for Ph=7 bar 85
Table IV. 2 Best COP values for different pressures and concentrations for Ph=8 bar 91
Table IV. 3 Best COP values for different pressures and concentrations for Ph=10 bar 96

Nomenclature

COP	coefficient of performance [-]
P	pressure [bar]
Ex	efficiency of heat exchanger [-]
h	enthalpy [kJ/kg]
$\dot{m}$	mass flow rate [kg/s]
Q	h eat transfer rate [KW]
T	temperature [°C]
W	work of pump [KW]
x	mass concentration [%]
z	Altitude [m]
L	Longitude [m]

Subscripts

a	absorber
c	condenser
ev	evaporator
g	generator
h	high
b	low
m	ambient
In	inlet condition
out	outlet condition

Greek nomenclature

δ	solar declination [rad]
ω	solar hour angle [rad]
λ	Longitude of the location [rad]
χ	Azimuth [rad]
γ_s	solar altitude [rad]
φ	Latitude [rad]

Abbreviations

SEARS	single-effect absorption refrigeration systems
H2O	water
LiBr	lithium bromide
NH_3	ammoniac
LiCl	lithium chloride
$CaCl_2$	calcium chloride
$LiNO_3$	Lithium nitrate
NaSCN	Sodium thiocyanate

TSV	True solar time
TU	Universal time
TL	Local time
PV	Photovoltaic
PTC	Parabolic trough collectors
PDR	Parabolic dish reflectors
FC	Fresnel collectors
AC	alternating current
DC	direct current
VCR	vapor compression refrigeration

General introduction

General introduction

1. Global energy demand and environmental challenges

The sustained rise in worldwide energy demand, propelled by rapid industrialization, urban expansion, and population growth, has significantly increased electricity consumption worldwide. Among all sectors, cooling and refrigeration represent one of the fastest-growing energy demands due to rising thermal comfort requirements, food preservation needs, medical storage, and industrial applications[1, 2].

Conventional vapour compression refrigeration systems dominate the cooling market because of their technological maturity and high reliability. However, these systems rely mainly on fossil-fuel-based power generation, thereby increasing greenhouse gas emissions and intensifying climate change [1, 3]. Furthermore, many synthetic refrigerants employed in such systems are characterized by elevated global warming potential and, in certain cases, ozone depletion potential [4]. Although international environmental frameworks have been established to mitigate these impacts, the environmental footprint of cooling technologies continues to represent a significant challenge. [5]

Consequently, enhancing the performance of low-energy and environmentally responsible cooling systems has emerged as a strategic objective worldwide, driven by the challenges of climate change mitigation and sustainable energy management.

2. Solar energy as a strategic renewable resource

The progressive transition away from fossil fuel dependency has intensified interest in renewable energy technologies. Solar energy, in particular, represents a highly promising option due to its global distribution, sustainability, and minimal environmental impact. It may be utilized through photovoltaic conversion to generate electricity or through solar thermal processes to supply heat for heating and cooling applications.

Countries located in high solar irradiation regions benefit from exceptional solar potential. Algeria, characterized by vast desert areas and high annual solar radiation levels, offers highly favourable conditions for solar energy exploitation. The integration of solar technologies in such regions can significantly reduce dependence on conventional energy sources while supporting sustainable development[6].

Harnessing solar thermal resources to drive cooling systems constitutes a strategic approach to sustainable refrigeration, particularly in hot-climate regions where peak cooling requirements naturally coincide with high solar radiation levels.

3. Solar refrigeration technologies

Solar refrigeration systems are generally classified into two main categories:

- **Photovoltaic-driven refrigeration systems**, where solar radiation is converted into electricity to operate conventional compression cycles.
- **Solar thermal-driven refrigeration systems**, where solar heat is directly used to drive thermodynamic cycles.

Although photovoltaic systems are simple to integrate, solar thermal refrigeration systems offer higher direct energy utilization efficiency for medium and large-scale applications. By eliminating multiple energy conversion stages, thermal systems can improve overall system performance. [7, 8]

Among solar thermal refrigeration technologies, absorption and adsorption systems are the most widely studied. These systems operate using heat energy instead of mechanical compression, making them suitable for integration with solar collectors.

4. Absorption refrigeration technology

Absorption refrigeration systems replace the mechanical compressor of conventional systems with a thermally driven absorption–desorption process. This configuration enables the utilization of low- to medium-temperature heat sources, including solar thermal collectors, to drive the cooling process.

Two main working pairs are commonly used: NH_3–H_2O and H_2O/LiBr. The ammonia–water (NH_3–H_2O) working pair is particularly suitable for refrigeration applications because ammonia acts as the refrigerant and enables sub-zero temperature production. This makes it appropriate for food preservation, cold storage, and industrial refrigeration.[9]

Additionally, ammonia is considered a natural refrigerant due to its null ozone depletion potential and negligible global warming impact, further highlighting its ecological benefits over synthetic alternatives. Despite these environmental advantages, absorption refrigeration systems generally achieve lower coefficients of performance (COP) than conventional vapor compression units [10], with their performance being highly sensitive to key operating conditions, including:

- Generator temperature
- Evaporator temperature
- Condenser and absorber pressures
- Ammonia concentration

Thermodynamic irreversibility associated with heat and mass transfer processes further affect system efficiency.

5. Research problem and scientific motivation

Although numerous studies have investigated solar absorption refrigeration systems, several limitations remain. Many models rely on simplified assumptions, limited parametric ranges, or insufficient analysis of the combined influence of concentration, temperature, and pressure levels on system performance.
The energetic performance of (SEARS) single-effect absorption refrigeration systems is strongly dictated by the choice of thermodynamic operating parameters. Identifying the optimal operating conditions is therefore essential to enhance system competitiveness and enable effective implementation, especially in high solar irradiance regions like Algeria.

A detailed thermodynamic modelling approach combined with systematic parametric analysis is necessary to better understand system behaviour and minimize thermodynamic losses.

6. Objectives of the thesis

The main objective of this thesis is to contribute to the improvement of the energetic performance of solar-driven SEARS using the NH_3–H_2O working pair.

To achieve this objective, the work focuses on:

- Formulating a detailed thermodynamic equilibrium model that rigorously applies mass and energy balance principles.
- Implementing the model computationally to simulate system performance.
- Analysing the influence of ammonia concentration, temperature levels, and pressure conditions on COP.
- Identifying optimal thermodynamic operating regions that maximize system efficiency.

Through this investigation, the study aims to provide theoretical insights and practical guidance for the design and optimization of solar absorption refrigeration systems in high solar irradiation regions.

7. Manuscript Structure

The manuscript is organized as follows:

- **Chapter I** presents the assessment of solar resources, including solar geometry, radiation components, and evaluation of solar potential in Algeria.
- **Chapter II** provides an overview of refrigeration technologies, with particular emphasis on thermally driven and absorption systems.
- **Chapter III** details the thermodynamic modelling of the SEARS using the NH_3–H_2O working pair, including modelling assumptions and governing equations.
- **Chapter IV** presents the simulation results, parametric analysis, and discussion of system performance under different operating conditions, highlighting optimal efficiency regions.

Chapter I

Solar Resource Assessment

Chapter 1 Solar resource assessment

I.1. Introduction

Developing efficient solar-driven refrigeration systems requires an in-depth assessment of the available solar energy, accounting for its temporal fluctuations and spatial distribution [11]. Since these systems operate by harnessing thermal energy from solar collectors, their operational performance, reliability, and economic feasibility are closely tied to the solar radiation characteristics at the installation site. Therefore, accurate solar resource assessment is an essential initial stage in the design and optimization of solar thermal refrigeration systems [12].

Solar radiation reaching the Earth's surface is governed by complex astronomical and atmospheric phenomena. The apparent motion of the Sun, resulting from the Earth's rotation and revolution around the Sun, determines the variation of solar angles throughout the day and across seasons [13]. Parameters such as solar declination, hour angle, solar altitude, and azimuth directly influence the amount of energy incident on horizontal and inclined surfaces. Consequently, solar geometry analysis provides the theoretical framework necessary for evaluating solar irradiance under different operating conditions [14].

In addition to astronomical factors, atmospheric effects including absorption, scattering, and reflection modify the extra-terrestrial radiation before it reaches the ground. The global solar radiation at a given site is made up of direct, diffuse, and reflected components, each playing a significant role in the thermal performance of solar collectors. Accurate modelling and simulation of solar-powered systems require an understanding of these elements. [15]

For countries characterized by strong solar resources, such as Algeria, solar energy constitutes a strategic and sustainable alternative to decrease reliance on conventional fossil energy sources while limiting related environmental effects. Owing to its location within the global sunbelt, Algeria benefits from substantial annual solar irradiation, especially in the southern regions. This significant solar potential makes the country particularly well suited for solar thermal technologies, including absorption refrigeration systems.

This chapter presents the fundamental principles required for solar resource evaluation. it first introduces the general characteristics of the sun and the earth–sun geometrical relationships. Then, it describes the main astronomical parameters used in solar position calculations. An overview of Algeria's solar potential follows an examination of the various components of solar radiation. Finally, a general categorization of solar thermal collectors is presented to establish the technological basis for the solar refrigeration system studied in this work.

I.2. Sun

I.2.1 Fundamental Properties of the Sun

The Sun, located at the center of the solar system, is the main source of energy driving Earth's climate and renewable energy systems [16]. It belongs to the G-type main-sequence category (G2V) and formed around 4.6 billion years ago. Energy is generated in its core through thermonuclear fusion, where hydrogen nuclei combine to form helium, releasing large amounts of energy in accordance with the mass–energy principle [17]. The Sun has a radius of approximately 6.96×10^8 meters and a mass of about 1.99×10^{30} kilograms, accounting for nearly the entire mass of the solar system [1]. The average Earth–Sun distance, or astronomical unit (AU), is about 1.496×10^{11} meters, with minor seasonal variations due to the elliptical orbit of the Earth [12].

Solar radiation covers a wide range of wavelengths, extending from ultraviolet to infrared. The majority of the energy is concentrated in the visible and near-infrared regions, which are especially important for applications related to solar thermal systems and photovoltaic energy conversion [18].

The mean solar irradiance received at the top of the earth's atmosphere on a plane normal to the Sun's rays is defined as the solar constant, whose internationally accepted value is approximately 1361 W/m² [19][5]. This parameter serves as a fundamental reference for the modelling, simulation, and performance evaluation of solar energy systems.

From an engineering standpoint, the apparent movement of the Sun with respect to the Earth, caused by the planet's rotation and its orbital motion, determines the temporal and spatial variation of solar irradiance received at the Earth's surface [12, 16, 17]. Consequently, an accurate description of solar geometry and solar radiation characteristics is crucial for the proper design and simulation of solar thermal technologies, including solar-powered absorption refrigeration systems [13].

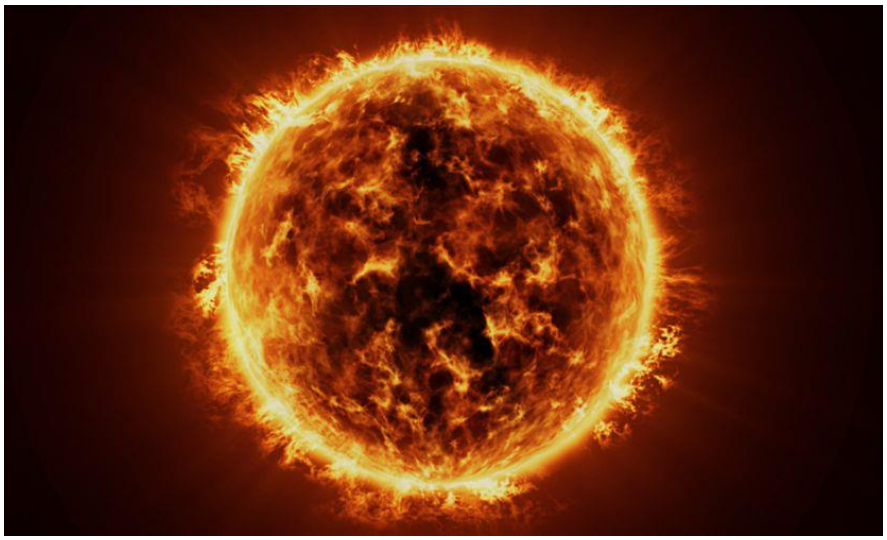


Figure I. 1 Sun

I.2.2. Earth motion

The apparent motion of the sun relative to the earth is primarily the result of two fundamental movements of the earth: rotation about its own axis and revolution around the sun. These motions govern the temporal and spatial distribution of solar radiation received at the earth's surface and are therefore of major importance in solar energy analysis and modelling [16].

The earth performs a complete rotation about its axis in roughly 24 hours, leading to the periodic succession of daytime and night-time. This rotational motion defines the hour angle, which represents the angular displacement of the sun with respect to the local meridian of an observer and has a direct influence on the instantaneous solar irradiance received by a surface[18]. As a result, the sun's position varies continuously during the day, affecting both the angle of solar incidence and the amount of energy available for solar thermal systems [17].

In addition to its rotation, the earth moves along an elliptical orbit around the sun, completing one revolution in about 365.25 days. The interaction between this orbital motion and the inclination of the earth's rotational axis, which is approximately 23.45° with respect to the orbital plane (the ecliptic), produces seasonal variations in the amount of solar radiation reaching the earth's surface [16]. This axial inclination results in changes in the solar declination angle during the year, which consequently affects both the length of the day and the solar elevation at a specific location [12].

The earth sun distance varies slightly during the year due to orbital eccentricity, reaching a minimum at perihelion and a maximum at aphelion. Although this variation has a relatively small effect compared to axial tilt, it still induces measurable fluctuations in the extra-terrestrial solar irradiance [18, 19].

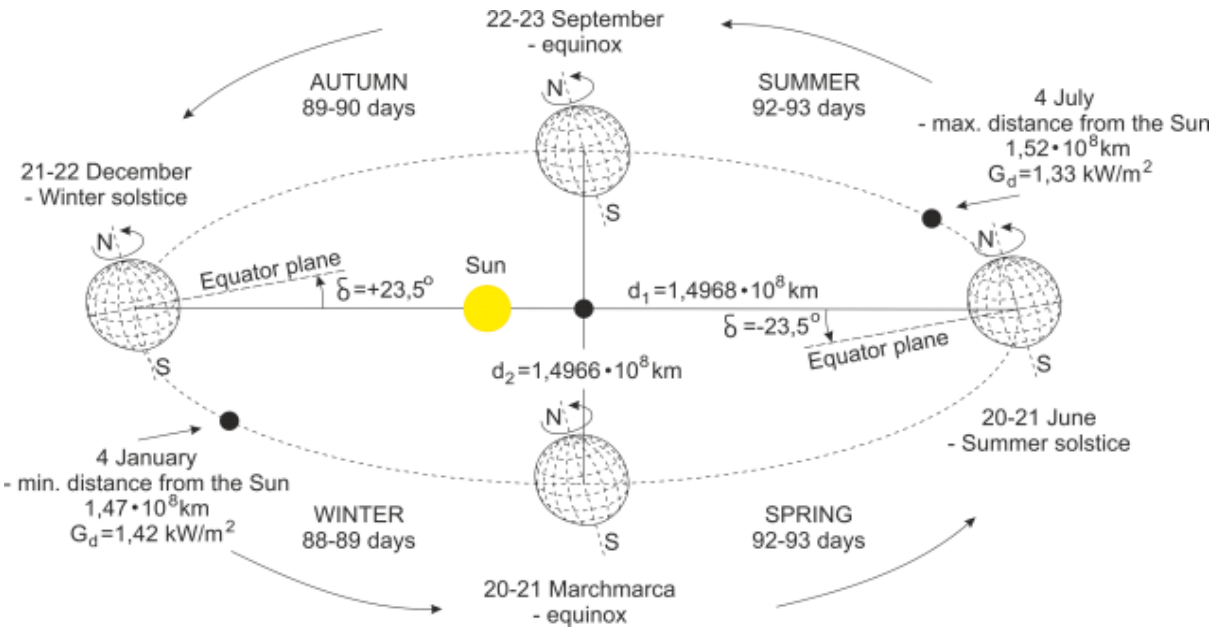


Figure I. 2 Orbital Motion of the Earth Relative to the Sun [20]

Understanding earth motion parameters such as declination angle, hour angle, and earth–sun distance correction factor is essential for accurate solar geometry calculations. These parameters form the basis for the modelling of solar irradiance and irradiation on horizontal and inclined surfaces, which is critical for the design and optimization systems of solar thermal, including solar-driven absorption refrigeration technologies [16, 17].

I.2.3. Apparent solar path

The apparent motion of the Sun illustrates its path across the sky from the perspective of a stationary observer on Earth. This apparent trajectory results from the interplay of Earth's rotation, its revolution around the Sun, and the approximately 23.45° inclination of its axis relative to the orbital plane [21].

On a daily basis, the Sun appears to rise in the east, reach its maximum elevation at solar noon, and set in the west. This daily trajectory corresponds to a circular arc whose position and inclination depend on the observer's latitude and the solar declination angle [22]. The angular displacement of the Sun along this path during the day is quantified by the hour angle, which increases by 15° per hour due to the Earth's rotation [23].

Over the course of a year, the apparent solar path varies significantly as a consequence of seasonal changes in solar declination. During the summer solstice, the Sun follows a higher and longer path across the sky, resulting in increased day length and higher solar elevations. Conversely, during the winter solstice, the solar path is lower and shorter, leading to reduced solar irradiation [21, 24]. At the equinoxes, the solar path is symmetric, and day and night durations are approximately equal.

The apparent solar path is commonly represented using solar path diagrams, which plot the Sun's position in terms of solar altitude and azimuth angles for different days of the year and times of day [22]. Such diagrams are indispensable in solar engineering, providing a means to visualize and quantify the solar resource incident on surfaces with varying orientations, whether horizontal or inclined.

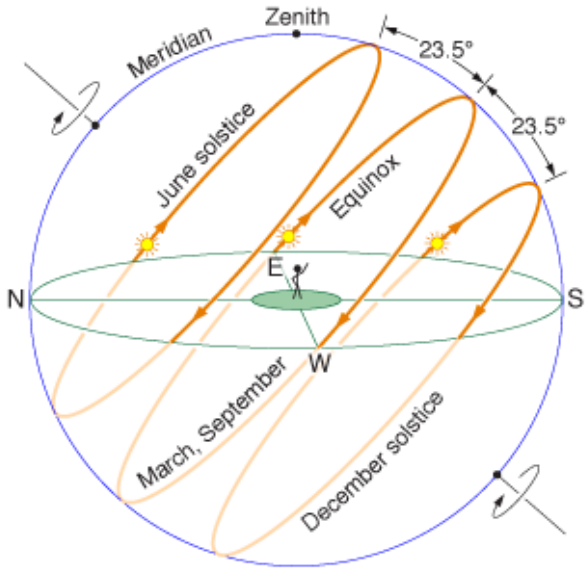


Figure I. 3 Determining the position of the sun [25]

I.2.4. Celestial Sphere

An imaginary sphere with a huge radius that is centred on Earth is called the celestial sphere, used to represent the apparent positions and motions of celestial bodies such as the sun. it provides a simplified geometric framework for defining solar angles and describing the apparent daily and seasonal motion of the sun as observed from a fixed point on earth [27].

On the celestial sphere, the projection of the earth's equator forms the celestial equator, while the extension of the earth's rotational axis defines the celestial poles. The apparent rotation of the sun around these poles is a consequence of the earth's rotation. The ecliptic, corresponding to the apparent annual path of the sun, is inclined by about 23.45° with respect to the celestial equator due to the tilt of the earth's axis.

This concept is widely used in solar geometry and solar energy engineering to determine solar position parameters such as declination, hour angle, altitude, and azimuth, which are essential for estimating solar irradiance on inclined surfaces [28].

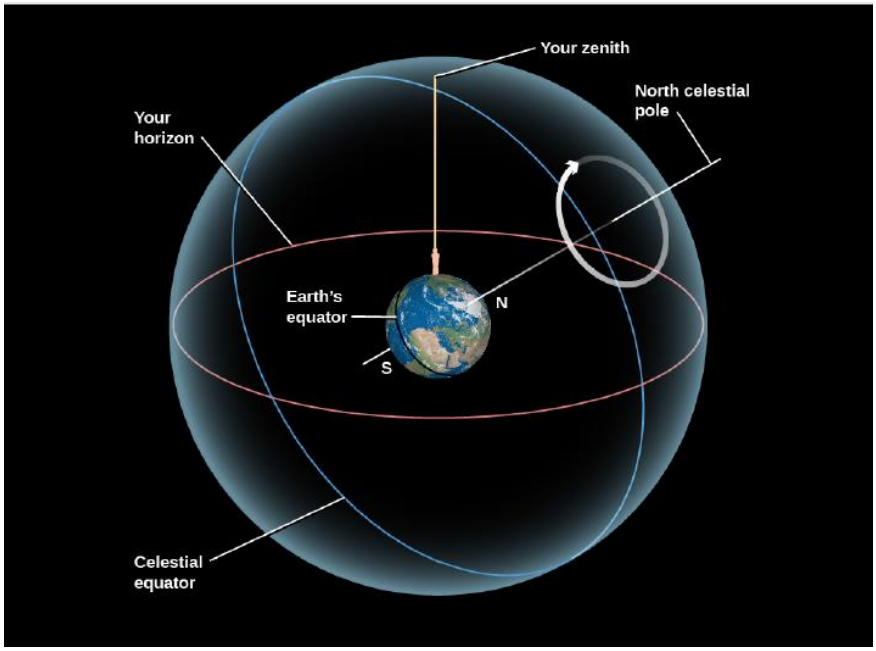


Figure I. 4 Circles on the Celestial Sphere [28]

I.3. Astronomical data

At any specific site, the solar position varies continuously with time throughout the day and across the year. This position can be described using two main coordinate frameworks: one defined with respect to the earth's equatorial plane (equatorial coordinate system), and another defined relative to the local horizontal plane of the observer (horizontal coordinate system).

I.3.1 Equatorial coordinates

The movement of the sun is tracked in relation to the Earth's equatorial plane using two angles (δ, ω).

I.3.1.1 Solar declination

The solar declination (δ) is the angle between the line connecting the centers of the Earth and the Sun and the Earth's equatorial plane. It represents the Sun's angular displacement north or south of the celestial equator and varies systematically over the year due to the axial tilt of the Earth. The tilt causes the Sun's apparent position on the celestial sphere to oscillate between approximately +23.45° at the northern summer solstice and −23.45° at the northern winter solstice, with zero declination at the equinoxes when the Sun lies on the celestial equator [14, 29, 30].

In solar energy and atmospheric science, the declination angle is essential for calculating the Sun's position relative to an observer, as it directly influences the solar altitude and azimuth and thus the instantaneous solar irradiance received on a surface. In most engineering applications, the solar declination is approximated by a sinusoidal function of the day number (n) of the year:

$$\delta = 23.45 \times \sin((\frac{360}{365}) \times (284 + n)) \quad \text{(I.1)}$$

Where n is the ordinal day of the year (January 1 = 1, December 31 = 365) [29, 30].This simple empirical formula captures the main annual variation and is widely used in solar geometry models for evaluating solar resource availability and solar thermal system design. More complex expressions derived from spherical astronomy can further refine the declination calculation when higher accuracy is required for precise position algorithms [14].

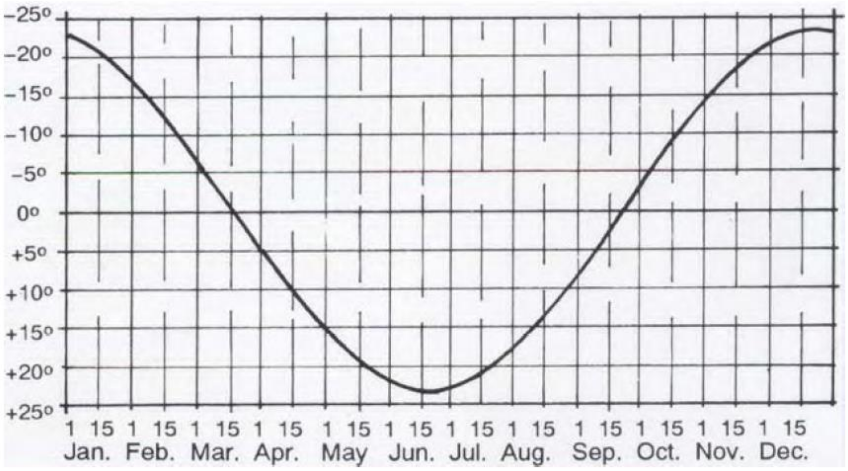


Figure I. 5 Annual variation of declination [31]

I.3.1.2 Hour angle of the sun

This angle corresponds to the projection of the Sun's direction onto the local meridian of the considered site (**Figure I.7**). The solar hour angle changes continuously throughout the day [32]. Its value can be determined using the formulation proposed by M. Capderou in the Solar Atlas of Algeria [33]:

$$\omega = 15(TSV - 12) \tag{I.2}$$

With:

$$TSV = TL - TU + \left(\frac{\Delta t + \Delta\lambda}{60}\right) = TL - \left(TU - \frac{\lambda}{15}\right) + \frac{\Delta\lambda}{60} \tag{I.3}$$

$$\Delta t = 9.87 \times \sin\left(\frac{360}{365}(N - 81)\right) - 7.3 \times \cos\left(\frac{360}{365}(N - 81)\right) - 1.5 \times \sin\left(\frac{360}{365}(N - 81)\right) \tag{I.4}$$

TSV: True solar time (time marked so that the sun is at its zenith at noon)
TU: Universal time: the time difference relative to the Greenwich meridian.
For Algeria: TU = +1.
TL: Local time: time shown on a watch.
Δt: correction of the equation of time.
λ: Longitude of the location.
ω > 0: afternoon; ω < 0: morning; ω = 0: noon TSV.

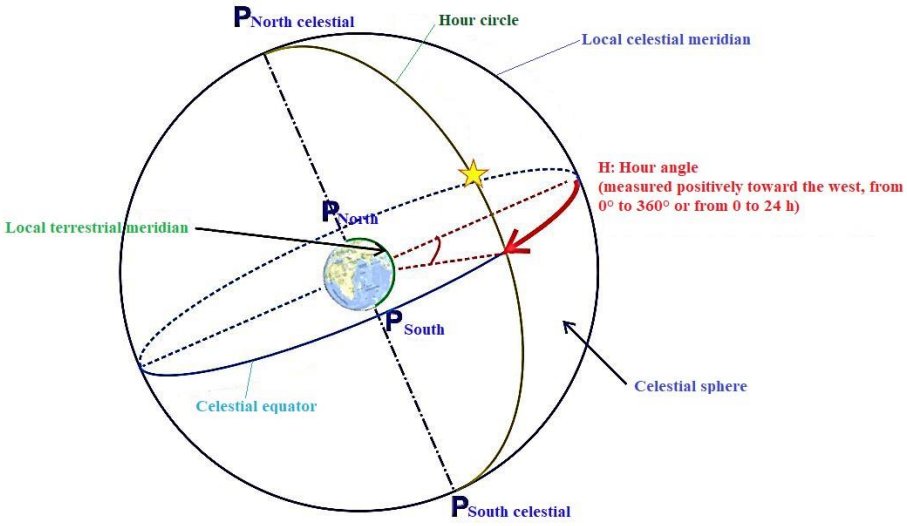


Figure I. 6 Variation in the hour angle as a true solar time [34]

I.3.1.3 Solar time

Solar time is directly associated with the rotation of the Earth around its axis. Mean solar time (MST) is defined using the concept of the mean solar day, which represents the average time separating two consecutive transits of the Sun across the local meridian of a specific location. By convention, the duration of this mean solar day is taken as 24 hours.
In contrast, true solar time (TST) represents the hour angle of the Sun at a given place and time and depends on both the Earth's rotational and orbital motions. It reflects the natural alternation of day and night, and the duration of the true solar day varies between 23 h 59 min 39 s and 24 h 00 min 30 s. [35]

I.3.2. Horizontal coordinates of the sun

At any given instant, the solar position is characterized by two angular parameters: the solar azimuth angle (χ) and the solar elevation angle (γ_s). For the city of Tlemcen, the corresponding geographical coordinates are: latitude $\varphi = 35.0°$ N, longitude $\lambda = -1.5°$ E, and an altitude of z = 247 m. [36]

I.3.2.1 Sun azimuth (χ)

The solar azimuth angle (χ) is defined as the angle between the projection of the Sun's direction onto the horizontal plane and the local south direction. In the Solar Atlas of Algeria, M. Capderou proposed an analytical expression to determine the solar azimuth, given by Equation (I.5). [35, 36]

$$\cos(x) = \frac{\cos(\delta).\cos(\omega).\sin(\varphi) - \sin(\delta).\cos(\varphi)}{\cos(\gamma_s)} \quad \text{(I.5)}$$

With:
δ: Solar declination.
ω: Hour angle.

γs: Sun's altitude.
φ: Latitude of the location.
The sun's azimuth orientations are given in **Table I.1**:
Table I. 1 Sun's azimuth orientation.

	Angle	**Orientations**
x	-90	East
	0	South
	+90	West
	180	North

I.3.2.2 Solar altitude angle

The solar altitude angle (γ_s) is defined as the angle between the Sun's direction and the local horizontal plane (Figure I. 8). A value of (γ_s = 0°) corresponds to sunrise or sunset. When (γ_s < 0°), the Sun is below the horizon and nighttime conditions prevail, whereas (γ_s > 0°) indicates daytime. The solar altitude ranges from (+90°), when the Sun is at the zenith, to (-90°), corresponding to the nadir [37]. This parameter can be calculated using a well-established analytical expression:

$$\sin(\gamma_s) = \cos(\varphi).\cos(\delta).\cos(\omega) + \sin(\varphi).\sin(\delta) \quad \text{(I.6)}$$

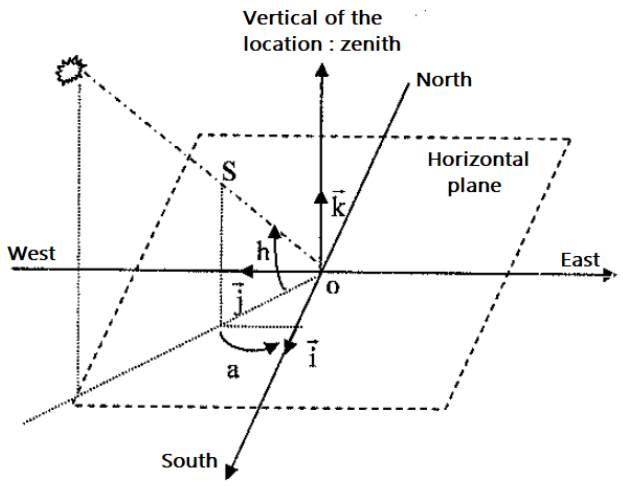


Figure I. 7 Horizontal reference point

I.3.3 Geographical coordinates [38]

I.3.3.1 Latitude of location (φ)

Latitude refers to the angular distance between a point on the Earth's surface and the equatorial plane. Its value ranges from 0° at the equator to 90° toward the poles in the Northern Hemisphere and is usually expressed in degrees.

I.3.3.2 Longitude (L)

Longitude is defined as the angular distance of a location from the Greenwich meridian. It is expressed in degrees and specifies the east–west position of a point on the Earth's surface.

I.3.3.3 Altitude (z)

Altitude corresponds to the vertical elevation of a site above a reference surface, generally taken as mean sea level (0 m). This parameter is expressed in metres and influences atmospheric and solar radiation characteristics.

I.4 Solar radiation

In practical applications, solar radiation must often be evaluated on surfaces with arbitrary orientation. The total radiation incident on such a surface is composed of three main components (Fig.9):

- Direct solar radiation,

- Diffuse radiation originating from the sky,

- Reflected diffuse radiation, resulting from the reflection of global solar radiation by the surrounding ground. [15]

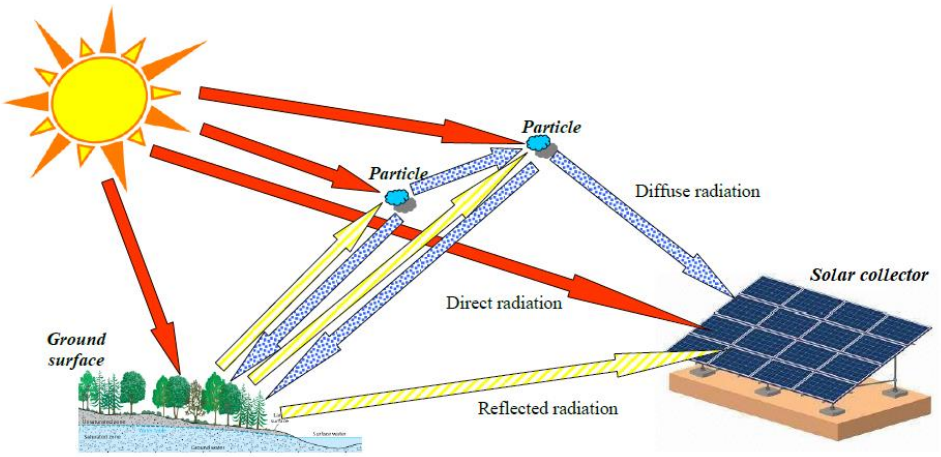


Figure I. 8 Solar radiation [39]

The Sun emits electromagnetic radiation over a broad spectral range extending approximately from 0.22 to 10 µm. The spectral composition of solar radiation reaching the Earth's surface is presented in Figure I.10. The associated energy distribution can be roughly classified into three main regions [20]: approximately 9% in the ultraviolet range (wavelengths shorter than 0.4 µm), 47% within the visible spectrum (0.4–0.8 µm), and nearly 44% in the infrared region (wavelengths longer than 0.8 µm).

The mean solar power received at the upper boundary of the earth's atmosphere, commonly referred to as the solar constant, is approximately 1.37 kW/m², with a variation of about ±3 %

due to the elliptical nature of the Earth's orbit around the Sun. As solar radiation passes through the atmosphere, a portion of this energy is absorbed and scattered, so that the irradiance reaching the Earth's surface seldom exceeds 1200 W/m². Furthermore, the Earth's rotation and axial tilt lead to spatial and temporal variations in the available solar energy, depending on latitude, time of day, and season. Atmospheric conditions such as cloud cover, fog, aerosols, and other meteorological factors introduce additional hourly and daily fluctuations, reducing or enhancing the received radiation and contributing to its diffuse component. [40]

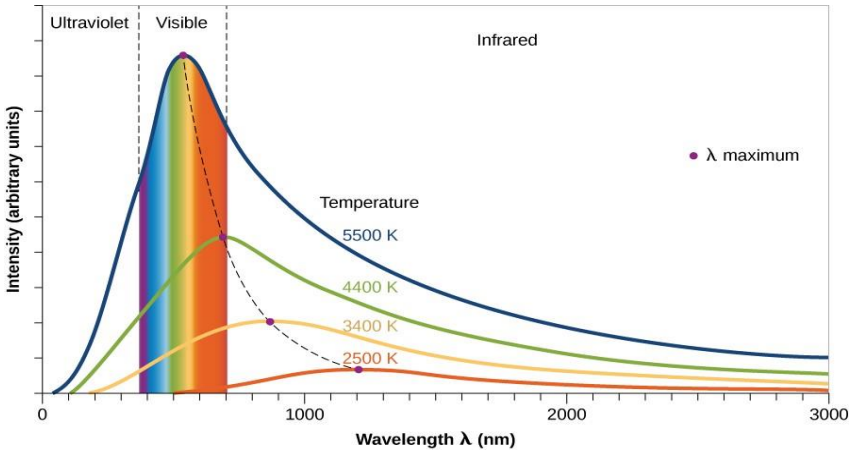


Figure I. 9 Spectral analysis of solar radiation [28]

I.4.1. Direct radiation

Direct solar radiation is the portion of solar energy that reaches the Earth's surface without being scattered or deviated by atmospheric constituents such as gases or particles. It is typically measured with a Pyrheliometer (Figure I.11), positioned so that its sensor surface is perpendicular to the Sun's rays.



Figure I. 10 Pyrheliometer [39]

I.4.2. Diffuse radiation

Diffuse solar radiation is the portion of sunlight that has been scattered and deviated from its original path due to interactions with atmospheric particles. It is measured using a device called a Pyranometer (Figure I.12).



Figure I. 11 Pyrometer [41]

I.4.3. Global radiation

Global solar radiation is the total radiation received on a horizontal surface from the Sun, including both direct and diffuse components. It is measured using a Pyranometer (Figure I.13), a device that directly senses the incoming thermal flux on its surface, expressed in watts per square meter (W/m²). [36]



Figure I. 12 Pyranometer

I.5 Solar Resource in Algeria

The solar resource of a region consists of data describing the temporal variation of available solar radiation over a given period. It is essential for simulating the performance of solar energy systems and accurately sizing them to meet the intended energy demand [42].

With a total area of 2,381,741 km², Algeria is the largest country in the Mediterranean region, according to the German Aerospace Agency [40]. The country possesses the highest solar potential in the entire Mediterranean basin, estimated at 169,000 TWh/year for thermal solar

energy and 13.9 TWh/year for photovoltaic solar energy [42]. This solar potential is roughly equivalent to ten major natural gas fields, such as those discovered at Hassi R'Mel.
Algeria also offers significant long-term opportunities for investment in solar thermal power plants, being recognized among the sunniest countries in the world [40].

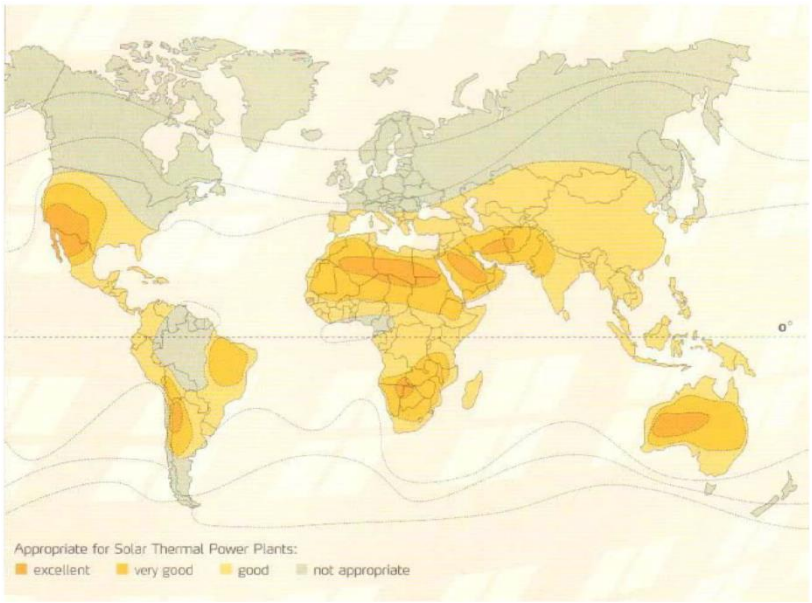


Figure I. 13 Global regions with high potential for Solar Power**.** [43]

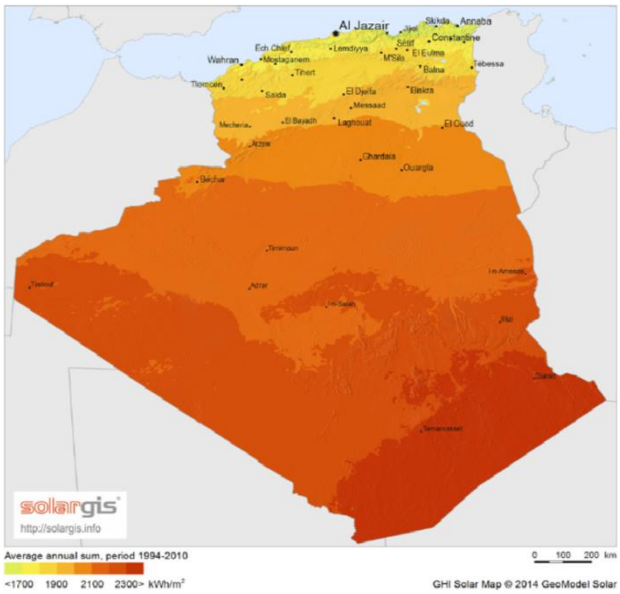


Figure I. 14 Algeria global horizontal irradiation [44]

I.6. General of solar thermal collectors

Solar thermal collectors, which are essential parts of solar water heating and cooling systems, are in charge of absorbing solar radiation and turning it into thermal energy. Typically, they are made up of layers of insulation, a transparent cover, a heat transfer fluid, and an absorber. Heat produced by the absorber is transferred to a working fluid, like water or antifreeze solutions. By preventing heat loss and shielding the system from outside influences, the glass cover increases

system efficiency. Depending on their temperature range and working principle, solar collectors are typically divided into two categories: stationary collectors and concentrating collectors. [45]

I.6.1. Stationary solar collectors

I.6.1.1 Flat plate collectors (FPC)

The most popular stationary collectors are flat plate collectors, particularly for low-temperature and residential applications. They use a flat absorber plate that is protected by thermal insulation and transparent glazing to absorb both direct and diffuse solar radiation. Operating temperatures typically fall between 40 and 60 °C.

FPC systems are appropriate for residential water heating because they are straightforward, long-lasting, and reasonably priced. Nano-fluids, sophisticated coatings, better absorber designs, and hybrid integration with PV/T systems and thermal storage units have all been the focus of recent research on increasing efficiency.

However, elements like flow rate, absorber design, ambient conditions, and insulation quality all have an impact on FPC performance. As a result, many optimization studies have been carried out utilizing energy and exergy analyses [46].

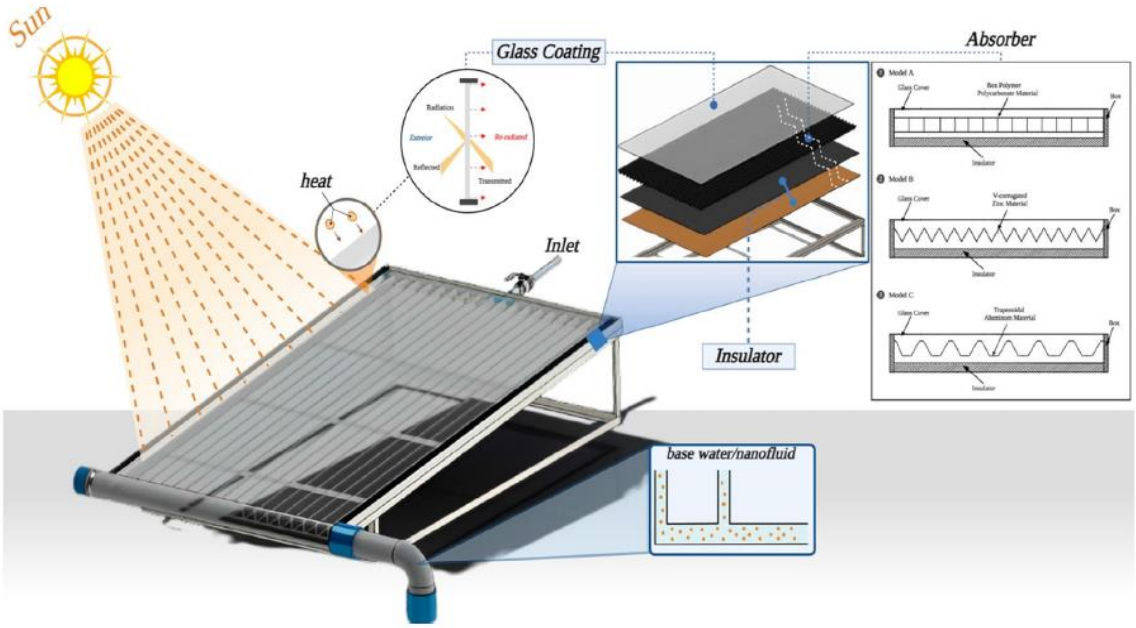


Figure I. 15 Schematic view of flat plate collectors (FPC) [45]

I.6.1.2 Evacuated tube collectors (ETC)

Glass tubes with an internal vacuum layer make up evacuated tube collectors, which drastically cut down on conductive and convective heat loss. Compared to FPC, this design allows ETC systems to reach higher temperatures (above 80 °C).

They are extensively utilized for solar cooling, desalination and heating in homes and businesses. The effects of tilt angle optimization, phase change materials, tube design, and Nano fluids on system performance have all been studied.

ETC systems are especially well-suited for applications in cold climates and high temperatures because of their low heat loss coefficient. [47]

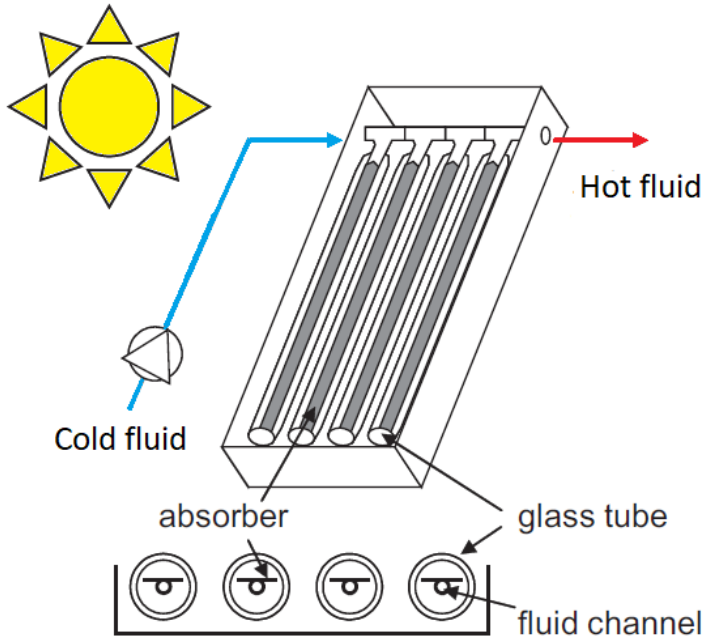


Figure I. 16 Schematic of evacuated tube collector

I.6.1.3 Solar air collectors (SAC)

Solar air collectors use air as the working fluid to transfer heat. They are commonly applied in space heating, drying processes, and desalination systems. SAC systems have a simpler structure and lower cost compared to water collectors, but generally lowers thermal efficiency.
Their performance depends on absorber design, airflow configuration, and heat transfer enhancement techniques. Recent studies have investigated perforated absorbers, micro-heat pipes, ribbed surfaces, and optimized geometries to improve efficiency.
Limitations include intermittent solar radiation, the need for auxiliary power for forced convection, and limited energy storage options. [48]

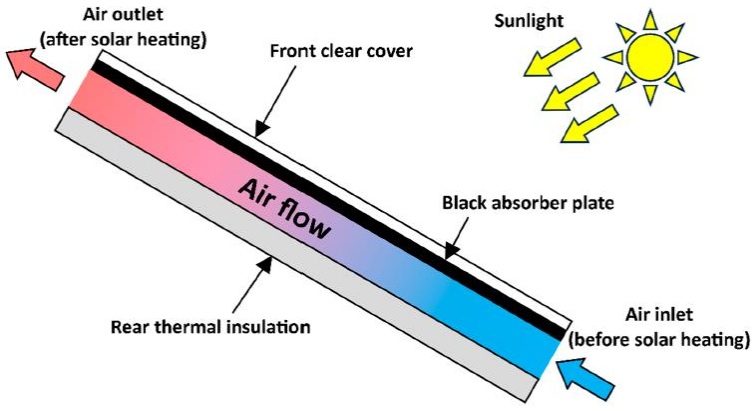


Figure I. 17 Schematic of solar air collector (plate version)

I.6.1.4 Unglazed collector

Unglazed collectors are simple and low-cost systems without a transparent cover. They are primarily employed in low-temperature uses, particularly for heating swimming pools. Due to high heat losses, their efficiency is lower than glazed collectors, and large surface areas are required. Nevertheless, they offer advantages in terms of cost, architectural integration, and electricity savings. Their performance is highly dependent on climatic conditions and material selection..[49]

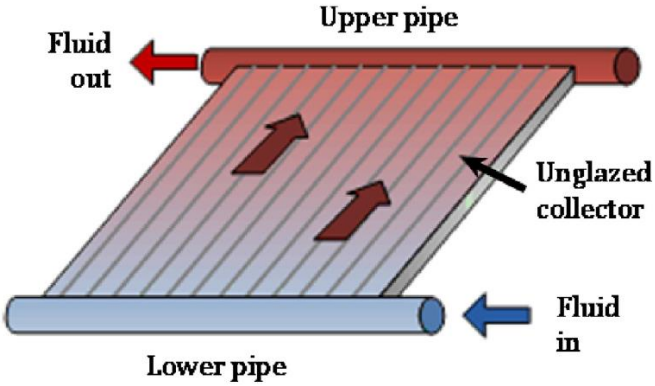


Figure I. 18 Unglazed solar collector

I.6.2. Concentrating solar collectors (CSC)

Concentrating collectors use optical devices to focus solar radiation onto a small receiver area, allowing very high operating temperatures (often above 200 °C). They consist of a concentrator and a receiver and are mainly used in power generation and industrial processes.

I.6.2.1. Parabolic trough collectors (PTC)

Parabolic trough collectors employ a curved parabolic mirror to focus incoming solar radiation onto a linear absorber tube positioned along the focal line. The heat transfer fluid flowing through this tube can attain temperatures of approximately 400–500 °C, which makes this technology appropriate for steam production and power generation applications.

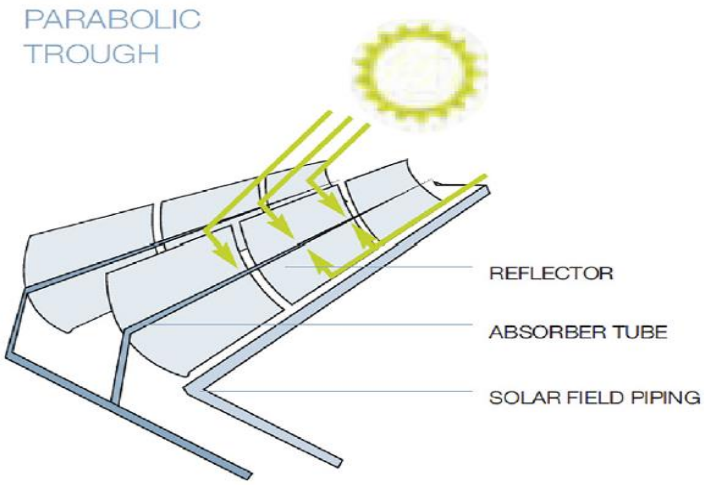


Figure I. 19 Schematic diagrams of parabolic trough collector (PTC)

PTC systems are among the most mature concentrating technologies. Research focuses on improving heat transfer, optical efficiency, nanofluids, and hybrid systems. [47]

I.6.2.2. Parabolic dish reflectors (PDR)

Parabolic dish collectors concentrate solar radiation onto a single focal point using two-axis tracking. They can achieve very high temperatures (up to 600 °C), making them suitable for power generation, industrial heating, and solar cooking.
PDR systems have high concentration ratios and efficiency, and recent studies investigated cavity receivers, nanofluids, optical modeling, and thermal storage integration. [47]

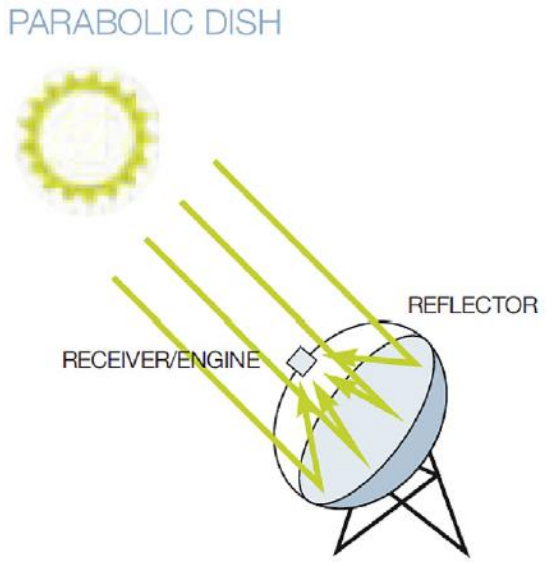


Figure I. 20 Schematic diagrams of parabolic dish reflectors (PDR)

I.6.2.3. Fresnel collectors (FC)

Fresnel collectors use segmented mirrors arranged on the ground to reflect sunlight onto a fixed receiver. They offer a simpler and lower-cost alternative to PTC, although with lower optical efficiency due to cosine losses.
They are promising for industrial heating and large-scale solar thermal plants, with ongoing research aimed at improving optical design and reducing costs. [45]

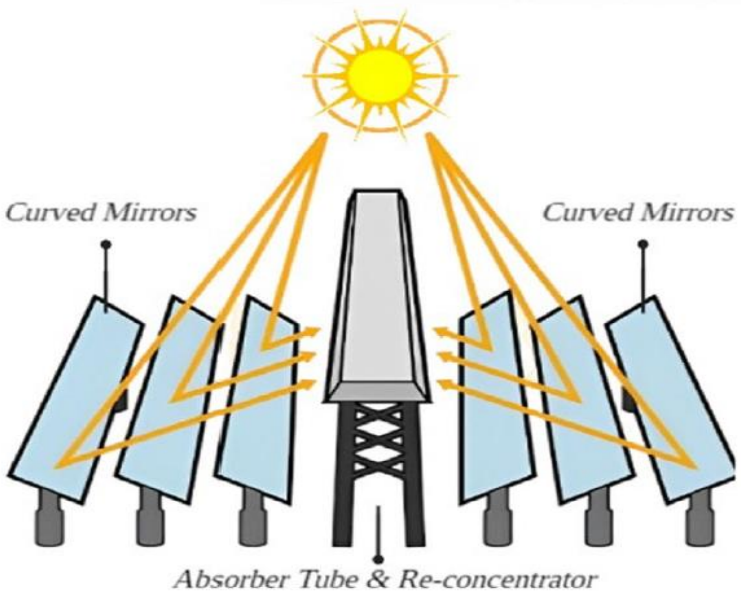


Figure I. 21 Schematic diagram of Fresnel collector (FC)

I.6.2.4. Heliostat field collectors (HFC)

Heliostat field systems consist of many mirrors (heliostats) that reflect solar radiation toward a central tower receiver. These systems can reach extremely high temperatures (up to 2000 °C) and are mainly used in solar power tower plants.
Research focuses on heliostat field optimization, tracking algorithms, high-temperature energy storage, and cost reduction strategies. [45]

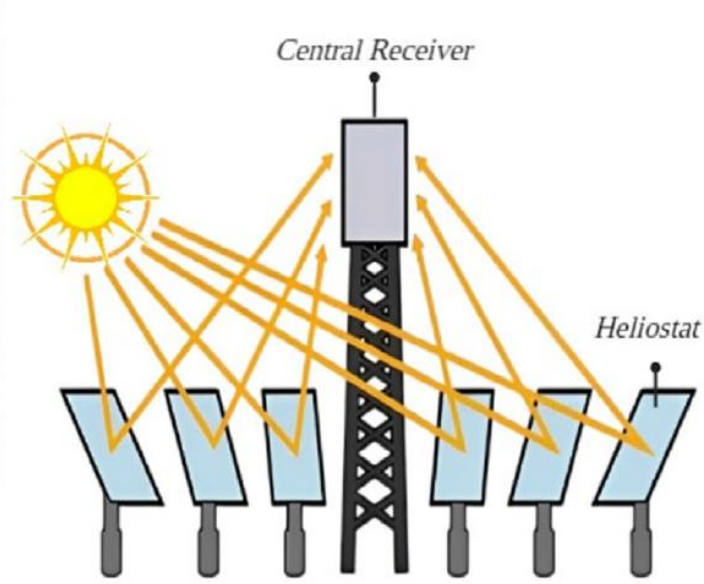


Figure I. 22 Schematic diagram of heliostat field collectors (HFC)

I.6.3. Future Research Trends

Future research on solar collectors aims to improve both optical and thermal performance. Optical improvements focus on reflector design and tracking accuracy, while thermal

enhancements include advanced absorber geometries, Nano fluids, and improved heat transfer mechanisms. The integration of thermal storage and hybrid systems is also a key research direction for increasing reliability and efficiency of solar thermal technologies.

I.7. Conclusion

This chapter presented the fundamental concepts related to the assessment of solar resources. The principal properties of the Sun and the geometric relationships between the Earth and the Sun were described to clarify the temporal and spatial variability of solar radiation. In addition, the key solar angles and the various components of solar radiation direct, diffuse, and reflected—were examined, since they have a direct impact on the efficiency and operation of solar thermal systems.

The significant solar potential of Algeria was highlighted, confirming its suitability for solar thermal and cooling applications.

In the next chapter, cooling technologies and their different types will be presented, with particular emphasis on thermally driven systems, in order to establish the theoretical background necessary for the study of solar absorption refrigeration systems.

Chapter II

Cooling and Refrigeration Technologies

Chapter 2 Cooling and refrigeration technologies

II.1. Introduction

Increasing cooling requirements across residential, commercial, and industrial sectors have intensified energy use and environmental burdens, largely due to the dependence of conventional refrigeration systems on fossil-fuel-based electricity. To mitigate these impacts and improve overall energy efficiency, the development of sustainable cooling technologies has become a central research priority. Solar energy, in particular, offers a highly attractive solution, especially in areas with high solar potential [50]. Solar cooling systems use either photovoltaic electricity or solar thermal energy and include different technologies such as electrically driven systems, thermo-mechanical cycles, and sorption-based systems like absorption, adsorption, and desiccant cooling.

This chapter presents a detailed overview of cooling technologies with a particular focus on solar-based refrigeration systems. The fundamentals of solar energy, classification of solar cooling technologies, working principles of sorption processes, and different absorption cycle configurations are presented. Furthermore, recent developments, market trends, and thermal energy storage concepts associated with solar cooling systems are discussed to establish the scientific and technological background for the subsequent chapters of this thesis.

II.2. Solar energy

Over the past few decades, solar energy has attracted considerable interest among researchers because of its versatility and broad range of applications. The increasing need for sustainable energy alternatives has encouraged the deployment of solar technologies in both residential and industrial sectors, including water heating, space conditioning, cooking, electricity production, and refrigeration systems. [51]. Solar energy is produced by the Sun through thermonuclear fusion reactions at its core. Most of the energy resources on Earth, whether direct or indirect, originate from this solar output, with the exception of nuclear, tidal, and geothermal sources. The Sun delivers an immense amount of energy to the Earth's surface, making it one of the most plentiful renewable resources [52].. The intensity of solar radiation outside the Earth's atmosphere is typically expressed by the solar constant, which has an average value of approximately 1368 W/m² [53].

II.3. Solar refrigeration

A solar cooling system is structured around three interconnected subsystems (**Figure II.1**). The first is the solar energy supply subsystem, which mainly consists of solar thermal collectors that capture solar radiation and convert it into usable heat, together with a thermal storage tank that ensures continuous operation under variable solar conditions. The second subsystem is the thermally driven cooling unit, which transforms the collected thermal energy into cooling capacity through processes such as absorption, adsorption, or desiccant cooling. The third subsystem corresponds to the cooling load, representing the space or application that utilizes the produced cooling energy, such as air conditioning for buildings or refrigeration for specific uses.

The overall configuration and performance of a solar cooling system depend strongly on the type of solar collectors employed, the selected cooling technology, and the intended end-use of the cooling output [54].

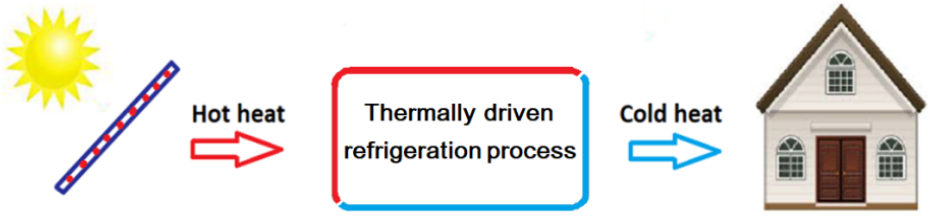


Figure II. 1 Schematic representation of a solar thermal cooling system

Solar thermal energy is commonly employed as the primary energy source for solar cooling and air-conditioning systems (SCACSs). Figure II.2 illustrates a general classification of solar cooling technologies, which can be grouped into two principal categories according to their mode of operation. The first category is based on photovoltaic (PV) systems, where the electricity produced by PV panels is used to operate conventional refrigeration or air-conditioning units. The second category relies on solar thermal technologies, in which the heat collected from solar radiation is directly used to drive cooling processes [50].

Solar thermal cooling technologies are further categorized according to the process used to convert heat into a cooling effect. These systems include ***thermo-mechanical cycles***, where thermal energy is transformed into mechanical work, and ***thermal sorption systems***, which directly use heat to generate cooling.
Thermal sorption cooling systems can be categorized into open-cycle and closed-cycle configurations based on their mode of operation. In open-cycle systems, the air supplied to the indoor environment is treated directly by regulating both temperature and humidity. Conversely, closed-cycle systems employ a circulating chilled-water loop, in which cooling is produced indirectly and then distributed to the conditioned spaces [55].

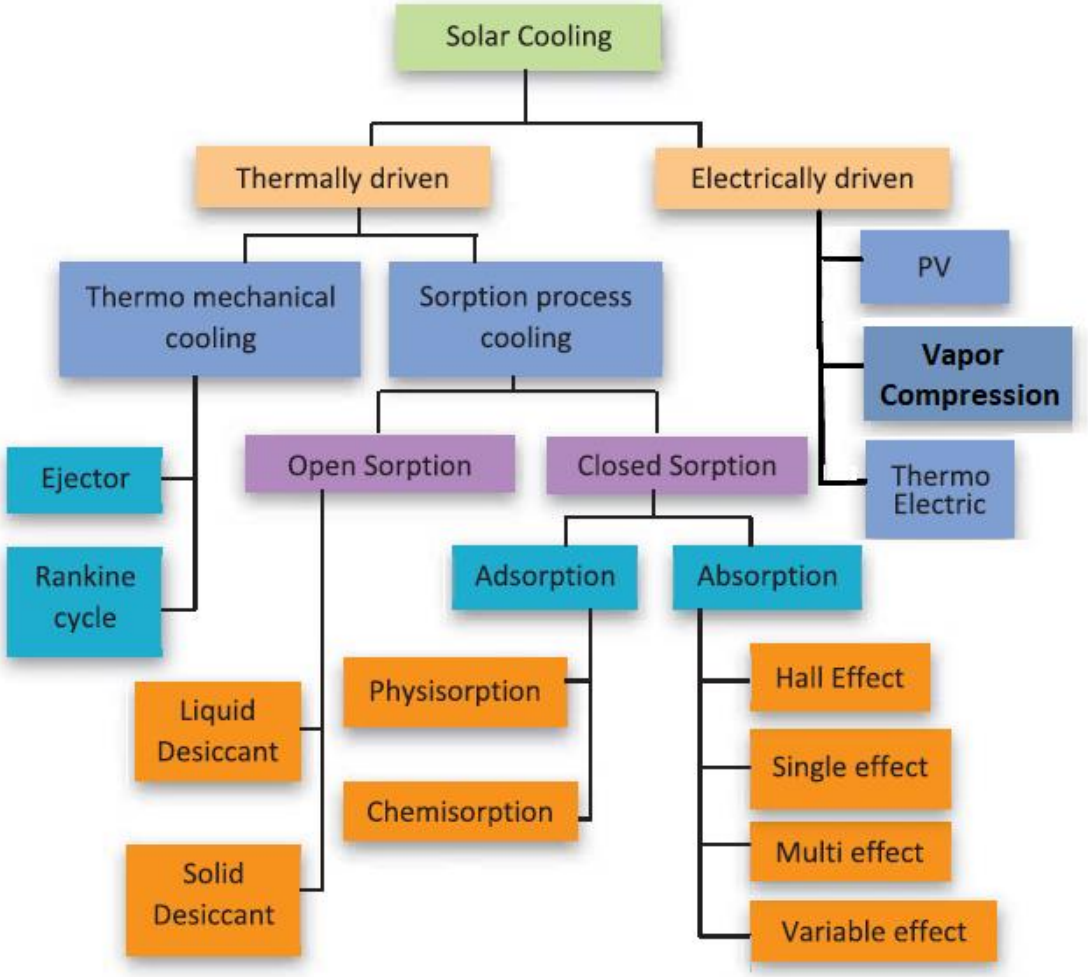


Figure II. 2 Classification of solar cooling systems [56]

II.4. Electrically driven

Solar-electric refrigeration systems are typically classified into photovoltaic and thermoelectric cooling technologies.

II.4.1. Photovoltaic (PV)

A solar electrical cooling system is composed primarily of photovoltaic (PV) panels coupled with an electrically driven refrigeration unit. In this configuration, solar radiation is first converted into electrical energy, which is then used to operate refrigeration technologies in a manner similar to conventional electrically powered cooling systems. [56]

Photovoltaic cells produce electricity by transforming incoming solar radiation into electrical current through the photovoltaic effect. Many solar electrical cooling systems are designed for stand-alone operation, particularly in remote or off-grid applications. PV modules are manufactured from various semiconductor materials, including single-crystalline silicon,

polycrystalline silicon, and thin-film technologies, with silicon-based materials dominating the current market **(Figure.II.3)**.

The conversion efficiency of PV technologies varies depending on the cell structure. Polycrystalline and thin-film PV modules typically exhibit efficiencies in the range of 10–17%, while single-crystalline PV cells can achieve efficiencies of approximately 15–20%, particularly when multi-junction architectures are employed. In comparison, conventional silicon wafer–based technologies generally present lower performance and higher production costs when compared with advanced thin-film solutions.

The electricity produced by photovoltaic panels can be used to operate several types of cooling technologies, such as thermoelectric refrigeration devices, Stirling-cycle cooling systems, and conventional vapour compression refrigeration units .[57]

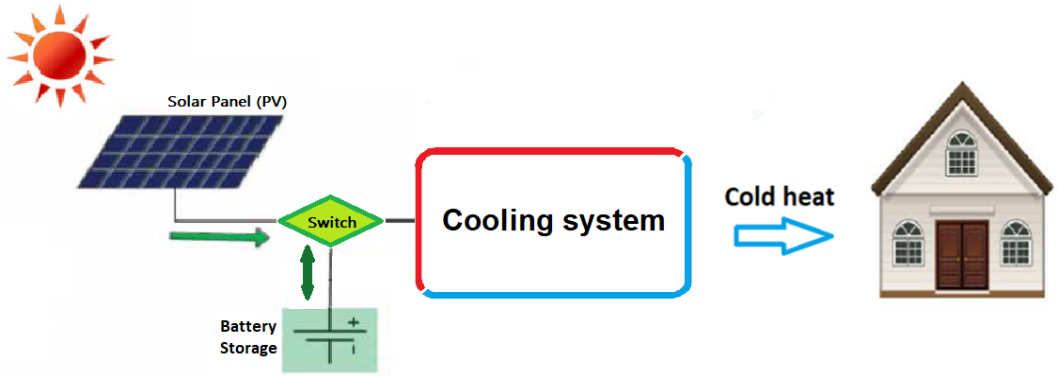


Figure II. 3 Solar photovoltaic (PV) cooling system

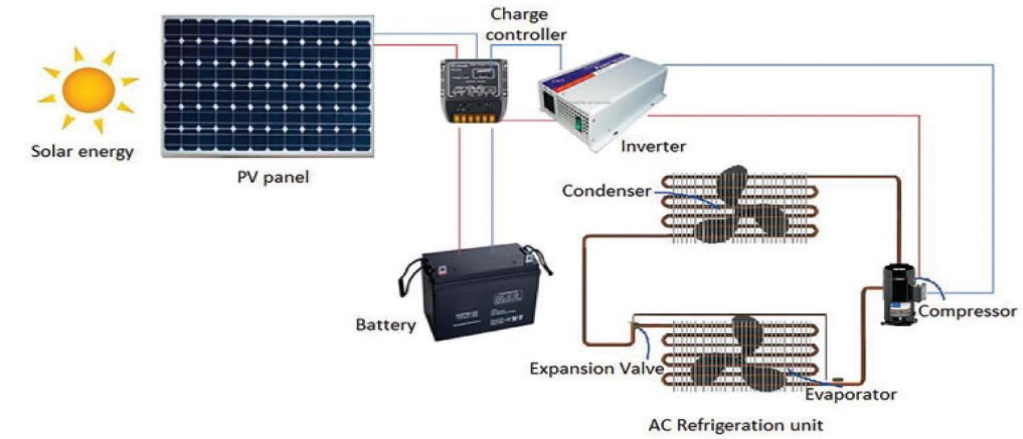
II.4.2. Vapour compression

Vapour-compression refrigeration systems represent the predominant technology for cooling applications. Worldwide cooling demand is expected to increase significantly, with projections indicating it may triple by 2050 [58].

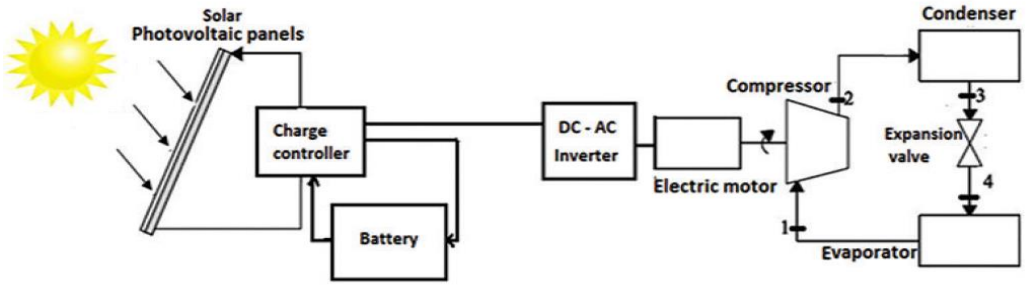
The conventional vapor compression cycle is widely used for cooling applications and is typically powered by electrical energy. Photovoltaic (PV) panels are primarily employed to convert solar radiation into electrical power, which is generally produced in the form of direct current (DC). However, most household and industrial electrical devices operate using alternating current (AC). As a result, a power conversion system is required. A complete photovoltaic refrigeration system therefore consists of several essential components, as illustrated in **Figure II.4** [59].

These include the PV panels, which generate electricity from solar energy; a battery system, used to store electrical energy and supply it as DC voltage; a charge controller, which protects the batteries from overcharging; an inverter, responsible for converting DC electricity into AC; and finally, a vapor compression refrigeration unit, which operates as a conventional compression system powered by the electricity delivered through the inverter [42].

Moreover, the COP of photovoltaic-driven air conditioning systems can reach values as high as 9, particularly under favorable operating conditions and high solar irradiance levels. Such elevated COP values highlight the strong potential of photovoltaic-assisted cooling technologies to significantly improve energy efficiency while reducing dependence on conventional electrical grids [60].



(a)



(b)

Figure II. 4 Illustration and schematic representation of a solar-powered vapour compression refrigeration system [61]

The vapor-compression refrigeration (VCR) cycle consists of four primary elements: a compressor, a condenser, an expansion device, and an evaporator. The compressor increases the pressure and temperature of the refrigerant in vapor form before directing it to the condenser. Within the condenser, the high-pressure vapor rejects heat to the surrounding environment and undergoes condensation, transforming into liquid refrigerant. The liquid then passes through the expansion valve, where a sharp reduction in pressure and temperature occurs prior to entering the evaporator. In the evaporator, the refrigerant absorbs thermal energy from the refrigerated space, leading to its evaporation and thereby producing the cooling effect. The resulting vapor is subsequently drawn back into the compressor, completing the thermodynamic cycle, as illustrated in **Figure II.5**. [62]

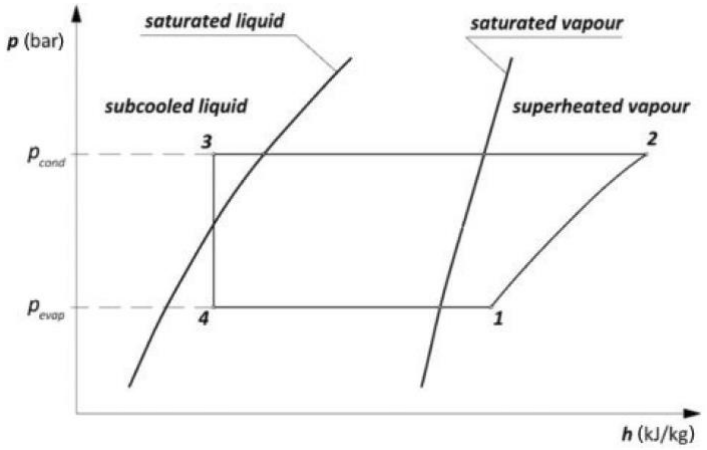


Figure II. 5 Diagram of a vapor compression refrigeration cycle (Pressure 'P' - enthalpy 'h') [61]

II.4.3. Thermo electric

Thermoelectric refrigeration devices operate through the Peltier phenomenon, whereby heating or cooling is generated at the interface of two different semiconductor materials when an electrical current passes through them [63]. When a direct current flows through coupled p-type and n-type semiconductor elements, thermal energy is extracted from one surface of the module and transported to the other surface, resulting in a temperature gradient (**Figure II.6**). The heat is subsequently dissipated to the environment from the hot side. Reversing the direction of the current reverses the heat flow path, enabling the system to function in either cooling or heating mode [64].

Thermoelectric coolers have no moving parts, no refrigerants, compact size, and high reliability, making them environmentally friendly and suitable for precise temperature control. However, their low COP and relatively high cost limit their widespread use compared to vapor compression systems. Consequently, thermoelectric cooling is mainly applied in specialized areas such as electronic device cooling, medical instruments, aerospace, and military applications [63].

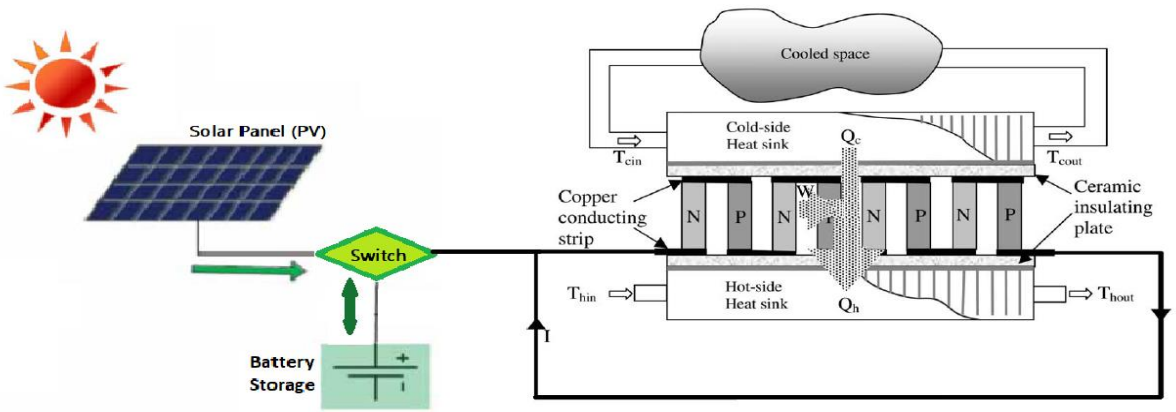


Figure II. 6 Solar thermoelectric refrigeration system

II.5. Thermally driven

II.5.1. Thermo-mechanical cooling

In recent years, solar thermo-mechanical cooling technologies have attracted growing interest because of their flexibility and operational benefits. By selecting suitable working fluids, these systems can provide low-temperature refrigeration. In addition, when the cooling load decreases, the system can produce electrical power by coupling the prime mover with an electric generator. They are also capable of maintaining reliable performance under off-design operating conditions and can utilize a wide range of heat source temperatures supplied by solar collectors.

II.5.1.1. Rankine cycle

The recovered thermal energy is used to drive a working fluid, which in turn powers a turbine to generate electricity. This electrical energy can then be utilized to operate a conventional vapor compression refrigeration cycle. Solar Rankine refrigeration systems were extensively investigated during the 1970s and 1980s; however, research activity in this field declined significantly over the subsequent two decades. Recent advancements in organic Rankine cycle (ORC) equipment, along with the development of eco-friendly refrigerants, have led to a resurgence of interest in solar thermo-mechanical cooling systems, improving both their practicality and operational efficiency [71].

The fundamental concept of solar Rankine refrigeration systems is to exploit solar thermal energy to produce mechanical work, which is then used to drive a classical vapor compression refrigeration cycle. Two main system configurations, illustrated in **Figure II.7**, have been proposed in the literature. In the first configuration (a), the Rankine cycle is separated from the refrigeration cycle, with the Rankine expander mechanically coupled to the compressor of the vapor compression system. The second configuration (b) represents an integrated cycle, employing a combined expander–compressor unit and a shared condenser for both the Rankine and refrigeration cycles [65].

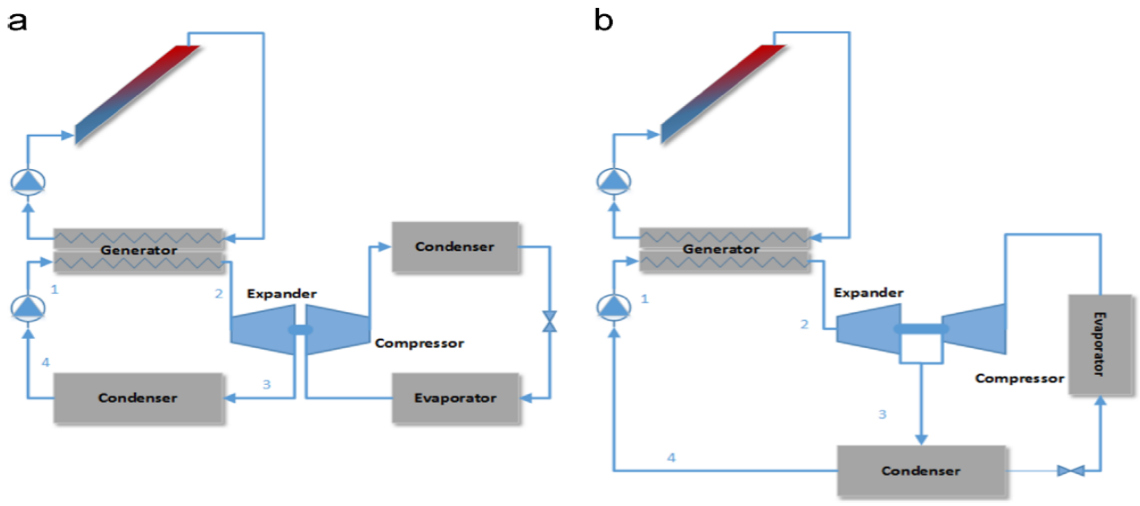


Figure II. 7 Solar Rankine cooling schematic: (a) separate cycles, (b) integrated cycle.

II.5.1.2. Ejector cycle

The solar ejector cooling system, shown in Figure II.8, operates in a manner comparable to a conventional vapor-compression refrigeration system, with the key difference that the mechanical compressor is substituted by a thermally activated ejector. The system comprises three primary loops: solar, power, and refrigeration. Solar energy heats the working fluid in the generator, producing high-pressure vapor that expands through the ejector nozzle. This expansion induces a pressure drop that entrains low-pressure vapor from the evaporator, and the two vapor streams mix before undergoing pressure recovery in the diffuser. The mixed flow then condenses as it releases heat to the environment. A portion of the condensed fluid is pumped back to the generator, while the remaining fluid passes through a throttling valve and enters the evaporator. Heat absorption in the evaporator completes the refrigeration cycle [65].

[65].

Although the COP of ejector cooling systems is generally lower than other thermally driven systems, their simple design and low maintenance make them attractive for building cooling applications. System performance mainly depends on ejector geometry, operating conditions, and working fluid properties, with the entrainment ratio being the key performance indicator [66, 67].

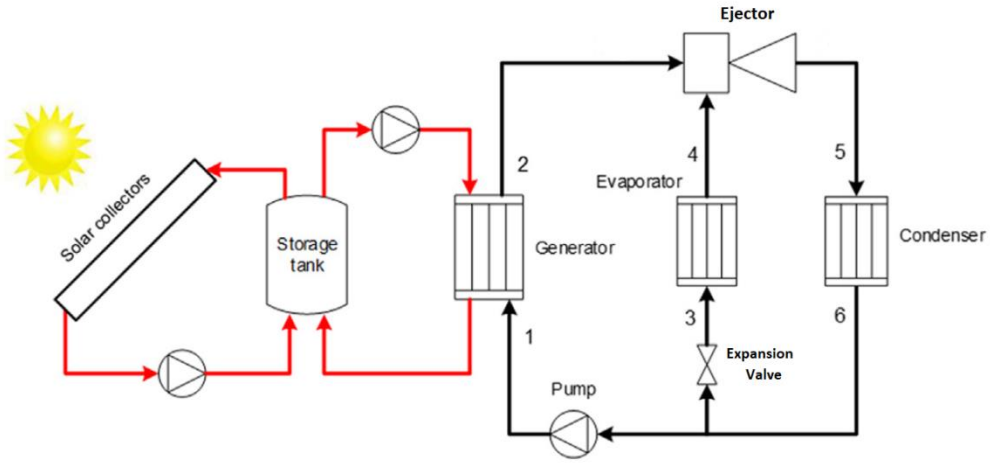


Figure II. 8 Schematic diagram of a solar ejector cooling system

II.5.2. Sorption process cooling

Sorption technology is widely applied in solar thermal cooling techniques, where the refrigeration effect is obtained through physical or chemical interactions between two working substances: a *sorbent (sorbant)* and a *refrigerant*, also called the *sorbate (sorbat)***.** The sorbate, characterized by a low boiling temperature, acts as the refrigerant and is responsible for producing the cooling effect through evaporation, while the sorbent either solid or liquid has the ability to attract, retain, and release the sorbate during the operating cycle [68].

A key advantage of sorption technology lies in its capability to directly convert thermal energy, such as solar heat, into cooling power, thereby significantly reducing or eliminating the need for mechanical compression and electrical energy consumption. Based on their operating principles and system configuration, sorption cooling technologies are generally classified into ***closed sorption systems***, in which the working pair circulates within a sealed loop (adsorption or absorption systems), and ***open sorption systems***, where the sorbent interacts directly with ambient air, as in desiccant-based cooling processes [66].

II.5.2.1. Open sorption systems

Open-cycle thermal refrigeration is based on solid or liquid desiccant systems used for air dehumidification. The process involves two main stages: sorption, where moisture is transferred from humid air to the desiccant due to vapor pressure differences, releasing latent heat; and desorption (regeneration), in which the absorbed moisture is removed by heating the desiccant. After cooling, the material is ready for a new cycle. These systems provide cooling combined with air dehumidification [36].
The primary distinction between solid and liquid desiccant systems lies in the way they interact with moisture. Solid desiccants, such as silica gel, primarily capture water vapor through physical adsorption, without undergoing chemical reactions. In contrast, liquid desiccant materials generally absorb moisture via chemical or physicochemical processes, as illustrated in **Figure II.9.**

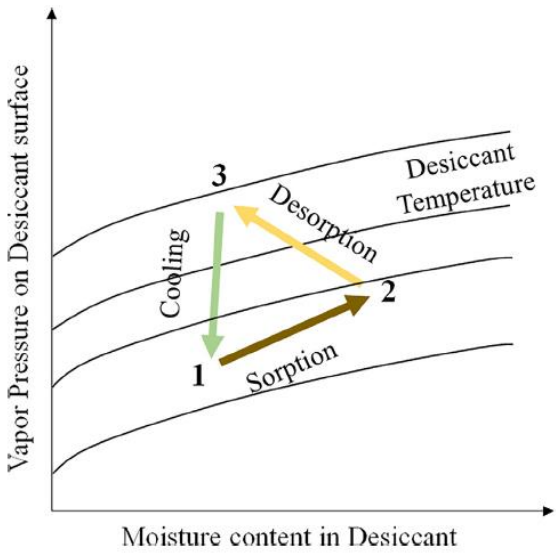


Figure II. 9 Complete process of a desiccant dehumidification system [69]

II.5.2.1.1. Liquid desiccant

Liquid desiccant systems commonly employ materials such as lithium chloride (LiCl), calcium chloride ($CaCl_2$), and lithium bromide (LiBr). A typical liquid desiccant cooling system, illustrated in **Figure II.10**, mainly consists of a conditioner and a regenerator. The conditioner treats the process air by spraying the liquid desiccant directly into the air stream, where it absorbs moisture. The solution then collects in a sump, from which it is pumped and recirculated.

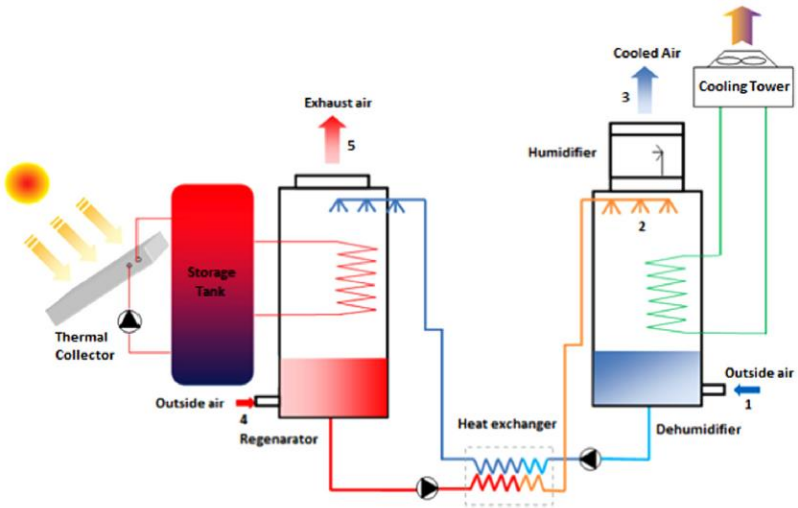


Figure II. 10 Principle of the liquid desiccation cooling

During moisture absorption, the desiccant temperature rises, its vapor pressure increases, and its concentration decreases due to water uptake. A fraction of the diluted solution is continuously diverted to the regenerator. In the regenerator, the desiccant is heated to raise its vapor pressure above that of the air, allowing moisture to be released into the regeneration air. The regeneration air exits the regenerator in a hot and humid state, while the desiccant returns more concentrated and is cooled before reuse [70].

II.5.2.1.2. Sorption solid

A solid sorption system generally consists of a slender coating of hygroscopic material such as silica gel deposited on a structural support. Most configurations adopt a rotary wheel arrangement, as illustrated in **Figure II.11**. The wheel gradually moves between two air streams: the supply (process) air and the regeneration air, and is functionally divided into two separate zones. As the process air flows through the first zone, water vapor is captured because the vapor pressure within the desiccant is lower than that of the incoming air.
The second zone is dedicated to regeneration, where heated air passes through the material, promoting the release of the retained moisture and restoring the drying capability of the desiccant. During dehumidification, the temperature of the treated air increases. This temperature rise is associated with the adsorption phenomenon, which involves the release of thermal energy corresponding to both the phase change of the absorbed water vapor and the interaction between the moisture and the desiccant surface [71].

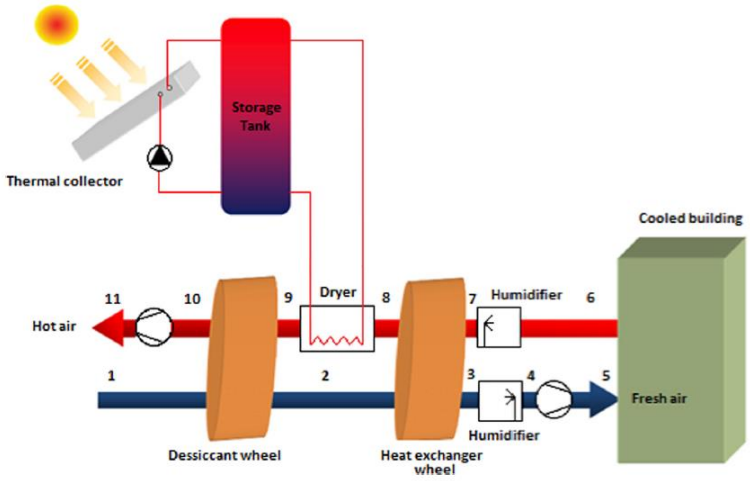


Figure II. 11 Principle of the solid desiccation cooling

II.5.2.1.3 Desiccant cooling

This system decreases the moisture content of ambient air by utilizing thermal energy supplied by solar collectors to drive the dehumidification process. The treated air is subsequently cooled through the air-handling unit, as shown in the following **Figure II.12.**

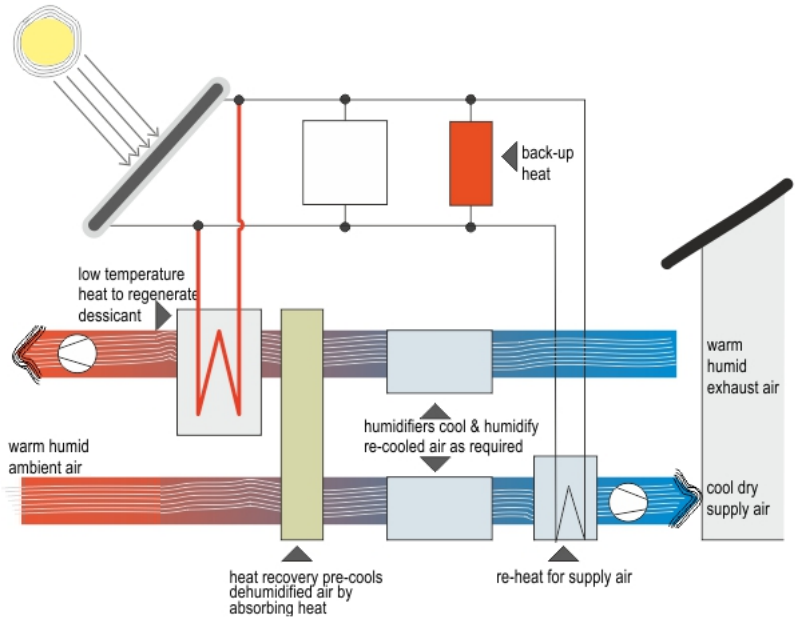


Figure II. 12 Schematic diagram of desiccant cooling system [72]

II.5.2.2. Closed sorption systems

Closed sorption cycles are divided in two categories Adsorption and Absorption:

II.5.2.2.1 Adsorption system

Adsorption refrigeration systems are based on the interaction between a solid adsorbent and a refrigerant, driven by thermal energy. These systems began to attract attention in refrigeration and heat pump applications in the early 1990s due to their ability to operate using low-grade heat sources, such as solar energy [73]. Depending on the nature of the interaction, adsorption can be classified as physical or chemical [74]. Adsorption is an exothermic process (**Figure II.13)**, while desorption is endothermic, and these thermal effects are exploited to generate cooling. Fixed-bed adsorption systems offer simple and reliable operation without moving parts, but their intermittent nature often reduces the system COP, making multi-bed configurations necessary for continuous cooling [75].

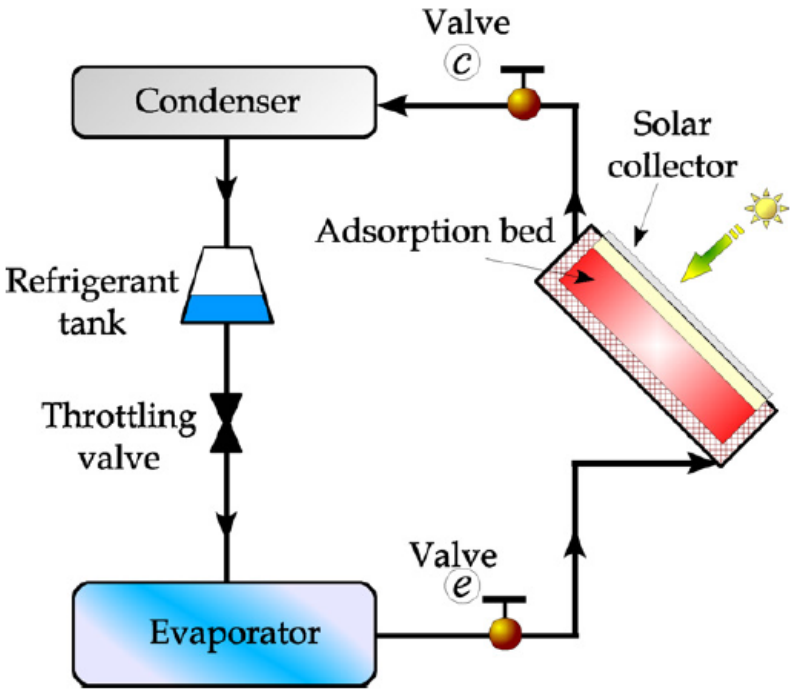


Figure II. 13 Schematic diagram of the solar adsorption cooling system [73]

A. Basic solar adsorption refrigeration cycle

The basic solar adsorption refrigeration cycle is a closed and intermittent cycle driven solely by thermal energy collected from solar collectors. It consists of an adsorber–collector, condenser, receiver, expansion valve, and evaporator [74]. The cycle includes four main thermodynamic stages: isosteric heating, desorption–condensation, isosteric cooling, and adsorption–evaporation. During the daytime, solar heat regenerates the adsorbent by desorbing the refrigerant, while cooling is produced during the nighttime adsorption phase through refrigerant evaporation. The achievable COP typically ranges between 0.3 and 0.7, depending on the driving temperature and operating conditions. [76]

The thermal COP of an adsorption refrigeration cycle is defined as the ratio between the useful cooling effect and the heat supplied to regenerate the adsorbent, as expressed in Eq. (7):

$$COP = \frac{Qe}{Qd} \tag{II.7}$$

Where Qe represents the cooling capacity, and $= Qd1 + Qd2$, corresponds to the total heat input required for adsorbent regeneration and desorption.

Similarly, the solar coefficient of performance is given by Eq. (8):

$$COP = \frac{Qe}{Qs} \tag{II.8}$$

Where: Qs denotes the solar thermal energy incident on the collector surface.

Adsorption refrigeration technology has been applied in various fields, including thermal refrigeration, separation processes, and purification systems.

B. Working pairs

The choice of the adsorbent–refrigerant working pair strongly influences the performance of adsorption systems. Common adsorbents include silica gel, activated carbon, and zeolite, while typical refrigerants are water, methanol, and ammonia [74]. Silica-gel/water pairs are suitable for solar applications due to their low regeneration temperature but require vacuum operation. Activated carbon/ammonia and carbon/methanol pairs provide higher adsorption capacities and are widely used for refrigeration and ice-making, although they involve safety and thermal conductivity limitations. Zeolite/water pairs require higher regeneration temperatures and are more appropriate for air-conditioning applications [77]. Current research focuses on developing advanced and composite adsorbents to improve heat and mass transfer performance [75].

C. Physical adsorption

Physical adsorption results from relatively weak interactions, like Van der Waals forces, between the refrigerant molecules and the surface of the porous adsorbent. This process is reversible and non-specific, allowing regeneration by heating the adsorbent [73]. Typical physical adsorption systems use silica-gel/water or activated-carbon/methanol and ammonia working pairs. These systems operate at relatively low driving temperatures and are well suited for solar cooling applications, although their cooling capacity and COP remain moderate [74].

D. Chemical adsorption

Chemical adsorption involves the formation of strong ionic or covalent bonds between the refrigerant and the adsorbent, leading to a greater heat release than that observed in physical adsorption. However, the process is more difficult to reverse and requires higher regeneration temperatures. Metal salts such as calcium chloride and lithium chloride are commonly used chemical adsorbents, often with ammonia or methanol as refrigerants [74]. Composite chemical adsorbents have shown promising improvements in COP and cooling capacity, but system complexity and cost remain important challenges [75].

E. Solar adsorption cooling systems

Solar adsorption cooling systems utilize solar thermal energy to drive adsorption refrigeration cycles and are particularly attractive for regions with high solar potential [74]. Experimental studies have reported COP values generally ranging from 0.05 to 0.3 for conventional systems, with higher values achieved using advanced adsorbents and optimized configurations. Applications include air-conditioning, refrigeration, ice production, and cold storage [74, 75]. On-going research aims to enhance system performance through multi-bed operation, heat and mass recovery techniques, and improved adsorbent materials [75].

II.5.2.2.2 Absorption system

In 1859, French engineer Ferdinand Carré patented the first absorption refrigeration system, utilizing ammonia as the refrigerant and water as the absorbent [78].

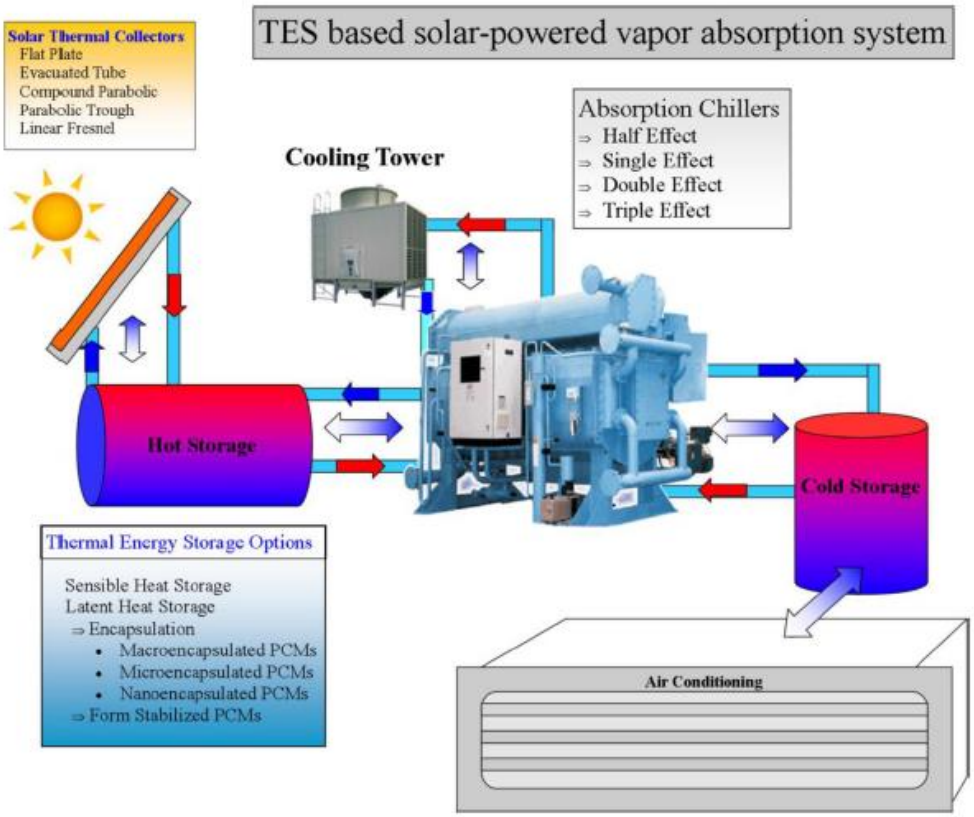


Figure II. 14 Schematic diagram of a solar-driven absorption refrigeration system with thermal energy storage [79]

A. Absorption Principle

Absorption refrigeration relies on the natural tendency of certain substances to interact across different phases, forming a solution or mixture. This behaviour is highly dependent on temperature and pressure: at low temperature and pressure, the liquid absorbent takes up the refrigerant vapour, while at higher temperature and pressure, it releases it (**Figures II.15** and **II.16**). This principle allows the refrigerant to move from the evaporator to the condenser using a pump, rather than a conventional mechanical compressor, which consumes more energy [51].

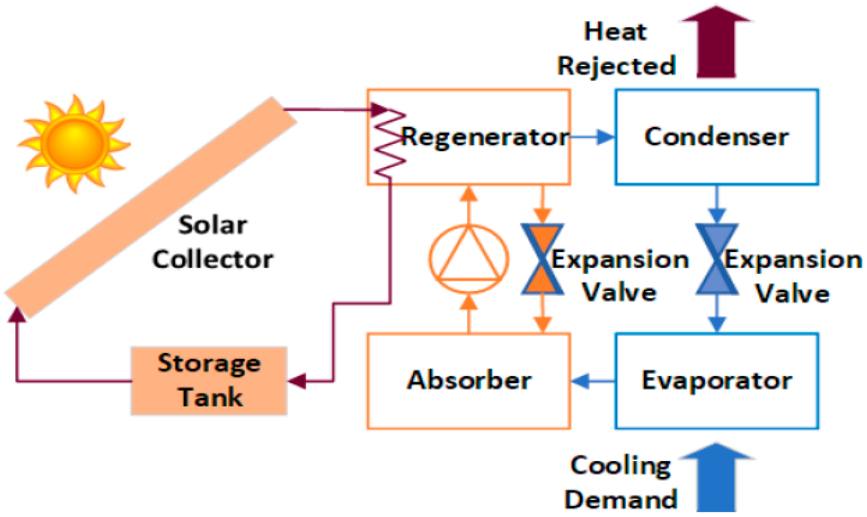


Figure II. 15 Solar cooling by absorption system [80]



Figure II. 16 Absorption refrigeration machine [81]

B. Working Pairs

In the 1950s, the lithium bromide–water (H_2O–LiBr) working pair was introduced in absorption refrigeration technology. Although many working pairs have been investigated in the literature, the H_2O–LiBr and NH_3–H_2O pairs remain the most widely used. The H_2O–LiBr pair, which employs a non-volatile absorbent (lithium bromide salt), is mainly used in air-conditioning applications, while the NH_3–H_2O pair, based on a volatile absorbent, is commonly used in refrigeration systems and requires an additional rectifier to ensure a pure refrigerant flow [82].

The NH_3–H_2O pair is widely applied in refrigeration and industrial systems because it is not limited by evaporation or absorption temperature, although ammonia is toxic and therefore used mainly in large-capacity installations (**Table II.1**) [83].
In contrast, the H_2O/LiBr pair is primarily used in air-conditioning applications, but its operation is restricted by water freezing at low temperatures and lithium bromide crystallization at high concentrations [10].

Table II. 1 Comparison of working pairs in absorption refrigeration systems [84]

Parameter	**Ammonia / Water (NH_3/H_2O)**	**Water / Lithium Bromide (H_2O/LiBr)**
Freezing point of the refrigerant	−77.75 °C / 6.103 Pa	0 °C / 6 × 10^3 Pa
Vapour from the generator	-Vapour containing traces of water	-Pure vapour (100% water)
Temperature range	−60 °C to +20 °C	+4.5 °C to +20 °C
Application domain	-Air conditioning and refrigeration; -Food industry; -Chemical industry	-Air conditioning; -Water cooling for chemical industry
Cost [€/ton]	400 € (60 000.00 DA)	6000 € (900 000.00 DA)
Main advantages	-No solid phase; -High refrigerant–absorbent affinity; -Low viscosity; -Environmentally friendly; -Good compactness; -Favourable operating pressure	-Pure vapour; -High refrigerant–absorbent affinity; -Low viscosity; -Environmentally friendly
Main disadvantages	-Toxicity and corrosiveness; -Need for rectification	-Possible crystallization; -Vacuum operation; -Poor compactness; -Corrosiveness

Several alternative working pairs have been proposed, such as $NH_3/LiNO_3$, $LiCl/H_2O$, $NH_3/CaCl_2$, NH_3/NaSCN, methanol/TEGDME, and TFE/TEGDME. Studies have shown that $NH_3/LiNO_3$ and NH_3/NaSCN can provide better performance than NH_3/H_2O at temperatures below the freezing point of water, while NH_3/H_2O performs better at higher temperatures. However, NH_3/NaSCN systems may suffer from crystallization problems at low temperatures, limiting their operating range. [85]
Table II.2 presents a comparison of selected ammonia-based working fluids used in absorption refrigeration systems. The table summarizes their main advantages, including operational and thermodynamic benefits, as well as their primary disadvantages, such as viscosity issues, crystallization risks, and generator temperature requirements. This comparison helps identify

suitable working pairs for different application conditions and highlights the trade-offs involved in selecting the optimal fluid. [84, 86]

Table II. 2 Characteristics of new binary and ternary mixtures used in absorption refrigeration systems

Working Fluid	Advantages	Disadvantages
NH_3 – $LiNO_3$ (Lithium Nitrate)	No rectification required; No crystallization; Favourable operating pressure; soluble with ammonia; Non-corrosive; Lower generator temperature compared to NH_3-H_2O pair; Better overall performance.	High viscosity → higher circulation rate than NH_3-H_2O → requires a more powerful pump.
NH_3 – NaSCN (Sodium Thiocyanate)	No rectification required; Favourable operating pressure; soluble with ammonia; Non-corrosive; Better overall performance.	High viscosity → higher circulation rate than NH_3-H_2O → requires a more powerful pump; risk of crystallization at evaporator temperatures below −10 °C.
NH_3 – H_2O – $LiNO_3$ (20–25% water in absorbent)	Better overall performance; Higher heat transfer coefficients; Lower viscosity compared to binary mixtures; Low vapour pressure; Very low rectification requirement.	Higher generator temperature compared to binary mixtures.

C. Performance and solar suitability

For the same operating temperature, LiBr–H_2O absorption systems generally exhibit higher coefficients of performance (COP) than H_2O–NH_3 systems due to the higher latent heat of vaporization of water compared to ammonia. Furthermore, the H_2O–NH_3 pair is> less suitable for solar applications because it requires high generator temperatures (125–170 °C), which can only be achieved using medium-concentration parabolic solar collectors. Due to maintenance constraints, such systems are not typically suitable for residential applications [87].

D. System configuration

As show in **Figure II.14**, an absorption refrigeration system includes the same refrigeration-side components as a vapour compression system, namely a condenser, an expansion valve, and an evaporator. However, the mechanical compressor is replaced by a thermal compressor composed of a generator, an absorber, a throttling valve, and a solution pump [51].

II.6. Types of absorption cycles

According to the thermodynamic operating cycle and the method of solution regeneration, absorption refrigeration systems can be classified into three main types: single-effect, half-effect, and multi-effect cycles, including double-effect and triple-effect solar absorption configurations [7].

II.6.1. Single effect absorption cycle

The single effect absorption cycle is the simplest and most commonly used configuration in solar absorption cooling systems. In this cycle, solar collectors provide the thermal energy required to drive the generator, while a storage tank and an auxiliary heater ensure continuous operation when solar radiation is insufficient (**Figure II.17**). Most commercial solar absorption chillers operate with the LiBr–H_2O working pair and achieve a COP between 0.6 and 0.8. Typical driving temperatures range from 80 to 100 °C for water-cooled systems, whereas air-cooled systems require slightly higher temperatures.

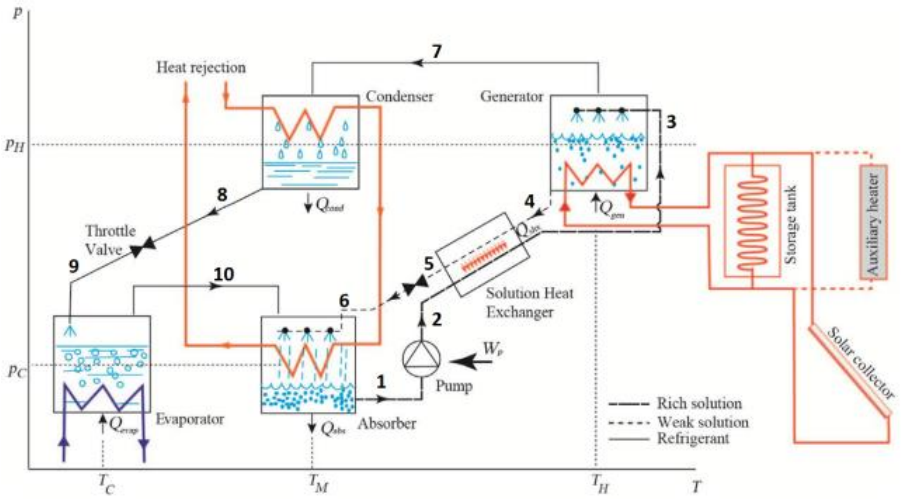


Figure II. 17 Diagram of a single effect solar absorption cooling system with solar collector and thermal storage.

II.6.2. Double-effect absorption cycle

The double-effect absorption cycle is an advanced configuration designed to improve system efficiency by adding an additional generator stage operating at a higher temperature. In this system, the heat released from the high-temperature generator is reused to drive a second low-temperature generator, leading to a significant increase in COP, typically between 1.1 and 1.2. However, this cycle requires high driving temperatures (140–180 °C), which are usually supplied by concentrating solar collectors such as parabolic trough or linear Fresnel collectors. Due to their complexity and cost, double-effect systems are mainly used in large-capacity applications.

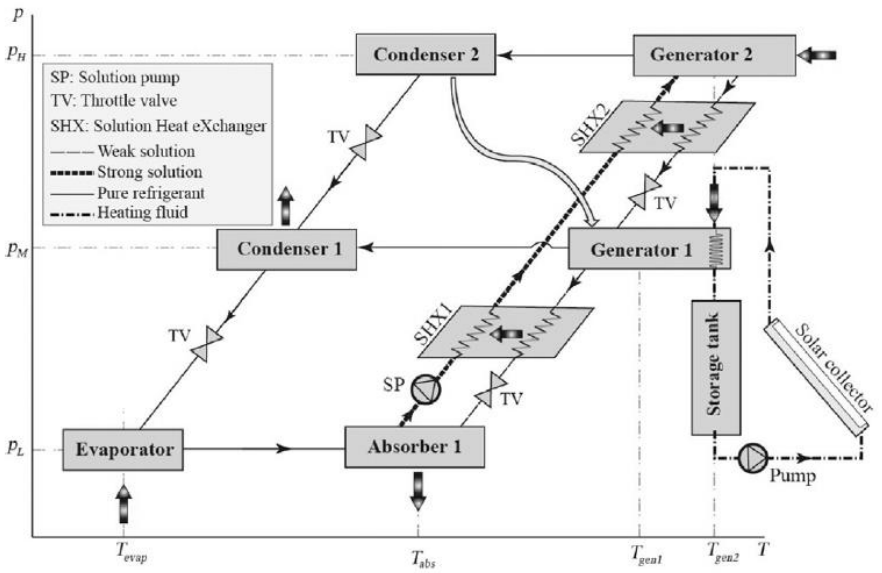


Figure II. 18 Diagram of double-effect solar absorption (P,T)

II.63. Half-effect solar absorption cycle

The half-effect absorption cycle, known also as the two-stage or double-lift cycle, operates at relatively low driving temperatures compared to single- and double-effect systems. Its COP is approximately half that of the single-effect cycle, but it offers the advantage of using low-temperature solar heat sources. Despite this benefit, half-effect systems require larger heat exchanger surfaces and solar collector areas to achieve the same cooling capacity. Experimental studies have reported COP values around 0.36 with generator temperatures between 55 and 75 °C, indicating its suitability for low-grade thermal energy applications.

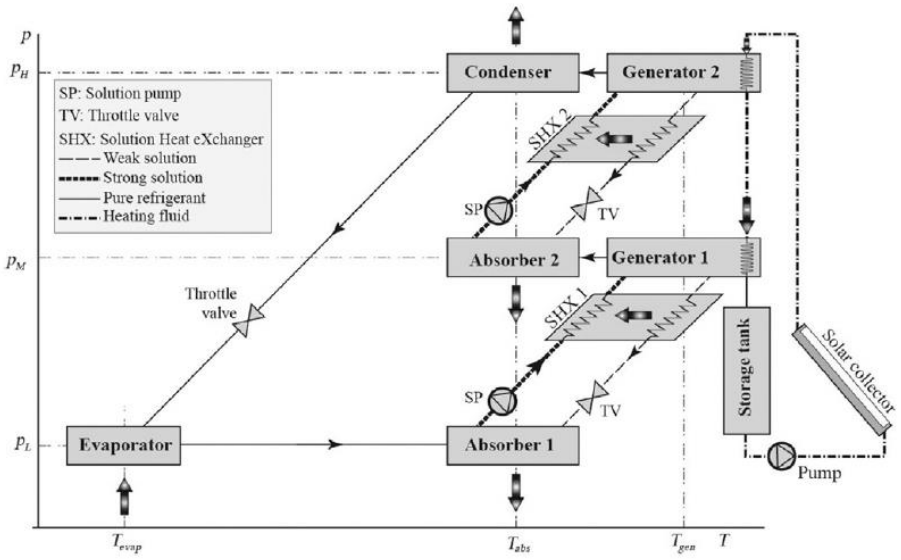


Figure II. 19 Schematic of a half-effect solar absorption cycle

II.6.4. Triple-effect solar absorption cycle

Triple-effect cycles involve three generators and three condensers or two cascaded loops, enabling COPs up to 1.7–1.8 theoretically. These systems are costlier and require high temperature sources (>200 °C), careful material selection, and corrosion prevention. The selection of configuration depends on solar availability, cooling requirements, performance, and cost [51].

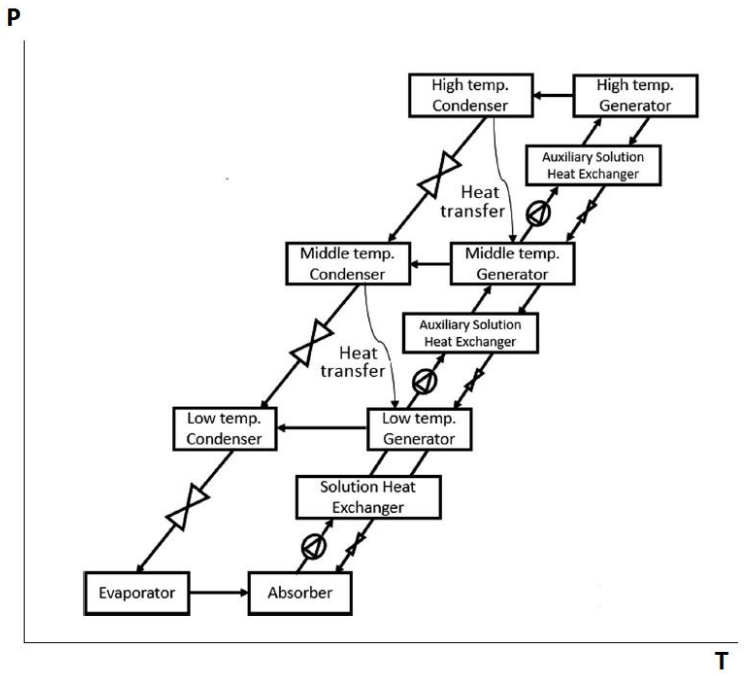


Figure II. 20 Diagram of triple-effect solar absorption cycle [81]

Figure II.21 show the differences in the effect of generator, evaporator, and condenser temperatures on the COP of single-, double-, and triple-effect absorption cooling systems using the H_2O/LiBr working pair. [88]

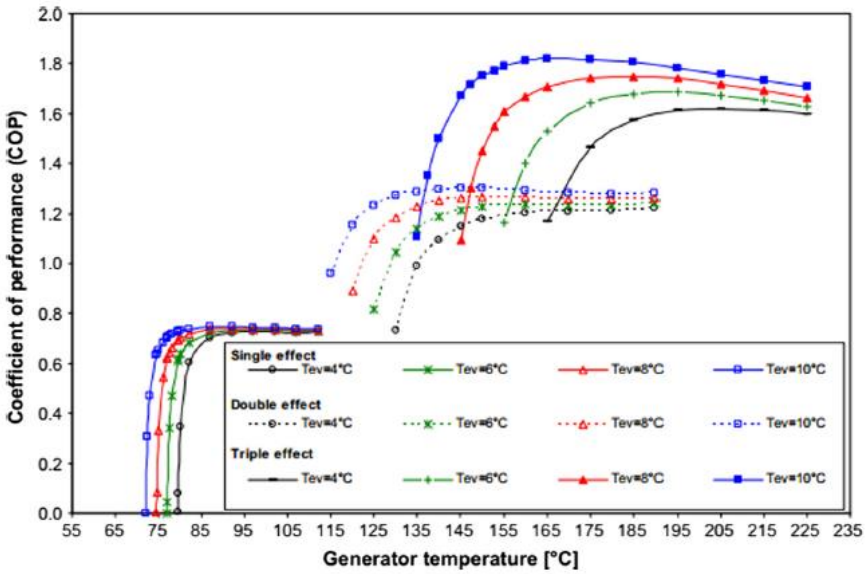


Figure II. 21 Influence the Temperature of generator (Tg) on the COP for absorption systems. **[88]**

II.7. Difference between absorption and adsorption

II.7.1. Absorption

Absorption is a bulk phenomenon in which a substance (absorbate) penetrates into the interior of another substance (absorbent), forming a homogeneous mixture or solution. The absorbed molecules become part of the volume of the absorbing medium. Absorption can be either a physical process, such as a gas dissolving in a liquid, or a chemical process involving a reaction between the two substances. For example, the dissolution of air in water represents physical absorption, while the absorption of lithium bromide (LiBr) in water involves chemical interactions between the solute and solvent.

II.7.2. Adsorption

Adsorption is a surface process where molecules of a substance (adsorbate) gather on the exterior of a solid or liquid material (adsorbent) without entering its interior. This process increases the concentration of molecules at the surface. Adsorption can occur through weak physical interactions, such as Van der Waals forces (physisorption), or through strong chemical bonds, such as ionic or covalent bonds (chemisorption). Unlike absorption, adsorption is confined to the surface of the material. [57]

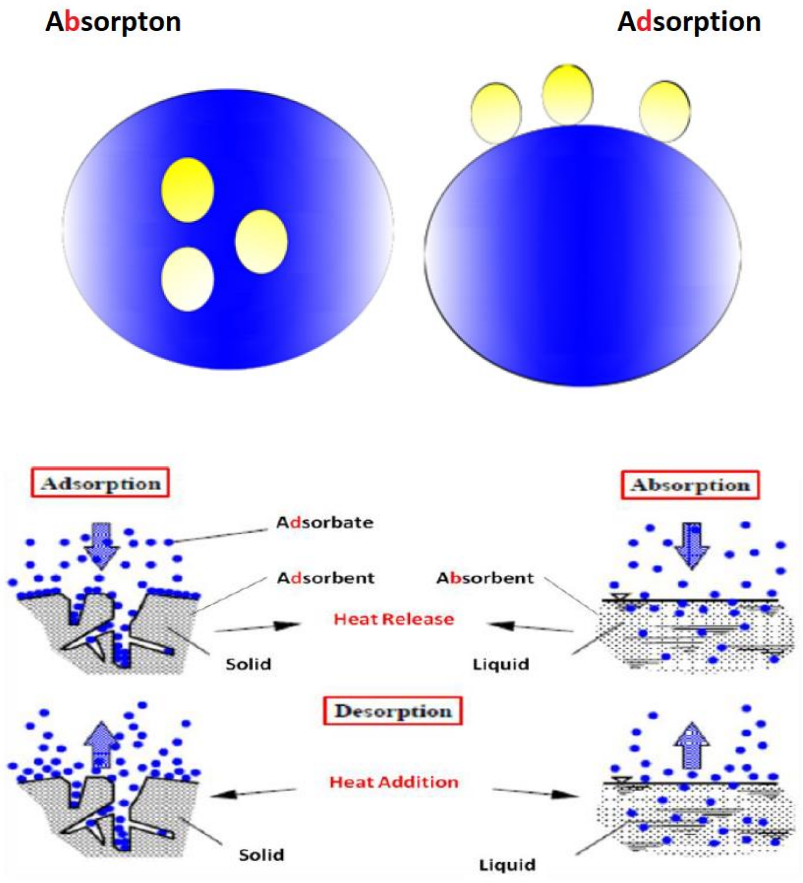


Figure .II.22. Difference between Absorption and Adsorption.

II.8. Thermal energy storage

The absorption refrigeration system is composed of three main parts: the solar collector, the thermal energy storage unit, and the absorption refrigeration system (**Figure II.22**) [90]. These components operate together to convert solar heat into cooling energy.

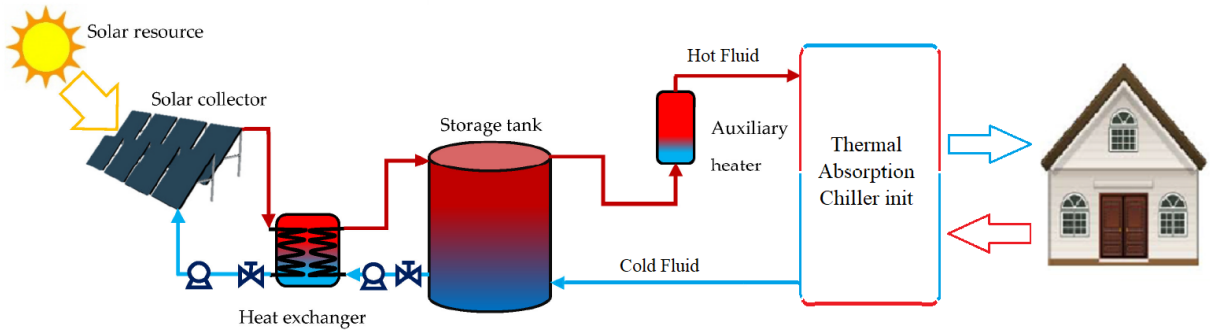


Figure II. 22 System installation of solar absorption cooling with thermal storage and solar collector [91]

The system functions by capturing solar radiation using solar collectors, where sunlight is transformed into thermal energy through absorption and greenhouse effects [36] [92]. This thermal energy is mainly supplied to the generator of the absorption cycle, reducing the dependence on conventional heating sources. When the solar heat production exceeds the system demand, the surplus energy is stored in a thermal storage tank for later use. During periods of low solar availability, such as cloudy conditions or night-time operation, an auxiliary heater is used to compensate for the lack of solar input [54].

Most commercial solar cooling systems currently operate according to this principle and commonly use evacuated-tube or flat-plate solar collectors to generate the required heat. Due to the intermittent nature of solar energy, thermal energy storage is essential to ensure continuous operation and to improve the overall system performance.

Thermal energy storage can be classified into three main categories: sensible heat storage, which is simple and efficient but depends on temperature variation; latent heat storage, which allows energy storage at nearly constant temperature but still requires further technological development; and thermochemical storage, which is mainly in the research stage. In practice, tanks filled with heat transfer fluids are widely used for thermal storage; however, their performance can be affected by thermal losses and fluid mixing phenomena [93].

II.9 Market distribution of solar cooling technologies

Figure II.23 presents the market distribution of solar cooling technologies based on sorption processes. The results indicate that absorption cooling systems dominate the market, representing about 82% of the installed systems, followed by adsorption systems with approximately 11%. Desiccant cooling systems are mainly used in large-scale applications and represent only a small fraction of total installations. This distribution highlights the technological maturity and widespread commercial adoption of absorption-based solar cooling systems compared to other sorption technologies.

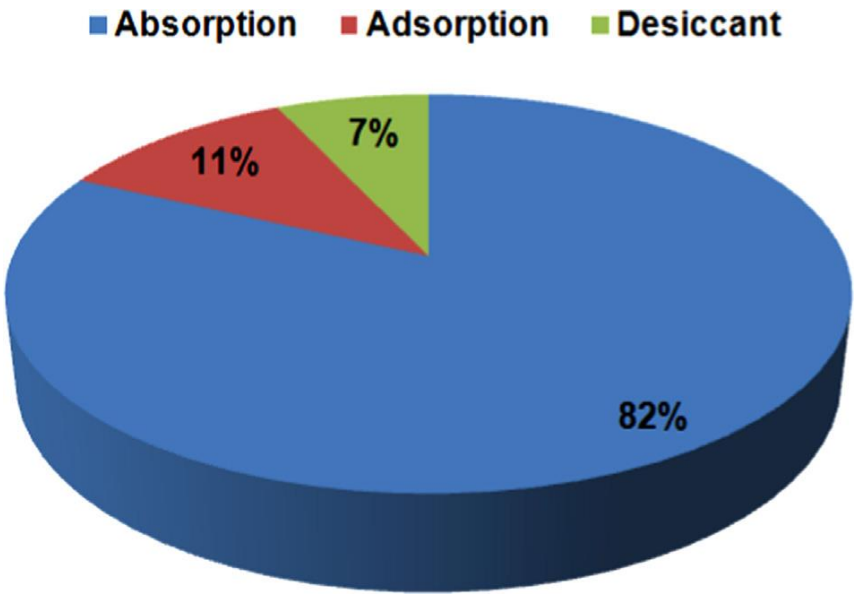


Figure II. 23 Percentage of use of the different technologies

II.9.1. Market overview of small-scale chillers [94]

Several manufacturers have developed small-capacity absorption system for solar cooling applications. Yazaki (Japan) has produced water–lithium bromide absorption chillers since 1977, with cooling capacities ranging from 35 to 105 kW, and the 35 kW unit is currently the most widely used in solar cooling systems. More recently, a 17.5 kW LiBr chiller has been introduced in Europe, such as the chillii® WFC 18 by SolarNext.

EAW (Germany) provides LiBr absorption system with capacities between 15 and 200 kW, designed for solar and combined heat and power (CHP) applications. Sonnenklima (Germany) has tested a 10 kW LiBr chiller (Suninverse 10) under various European climatic conditions.

Rotartica (Spain) is developing a low-capacity LiBr chiller (around 4–5 kW), achieving COP values of about 0.42. Its rotating absorber allows operation with dry re-cooling, which is particularly advantageous for small-scale systems. The technical characteristics of these chillers are summarized in **Table.II.2.**

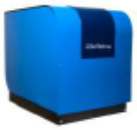
Table II. 3 Comparison of different market available small capacity absorption chillers

Company	Yazaki	EAW	Sonnenklima	Rotortica
Product name	WFC-SC5, chillii® WFC18	Wegracal SE15	suninverse 10	Solar 045
Technology	Absorption	Absorption	Absorption	Absorption
Working pair	H_2O/LiBr	H_2O/LiBr	H_2O/LiBr	H_2O/LiBr
	 (source: Yazaki)	 (source: Schüco)	 (source: Sonnenklima)	 (source: Rotartica)
Selling price €	20 000 (3 000 000 DA)	25 000 (3 750 000 DA)	22 500 (3 375 000 DA)	9 500 (1 425 000 DA)
Cooling capacity [kW]	17.6	15	10	4.5
Heating temperature [°C]	88 / 83	90 / 80	75 / 65	90 / 85
Recooling temperature [°C]	31 / 35	30 / 35	27 / 35	30 / 35
Cold water temperature [°C]	12.5 / 7	17 / 11	18 / 15	13 / 10
COP	0.70	0.71	0.77	0.67
Dimensions (WxDxH) [m x m x m]	0.60 x 0.80 x 1.94	1.75 x 0.76 x 1.75	1.13 x 0.80 x 1.96	1.09 x 0.76 x 1.15
Weight [kg]	420	660	550	290
Power [W]	72	300	120	1,200 (incl. ventilator)

In conventional absorption chillers, crystallization is usually avoided due to operational difficulties; however, Climatewell (Sweden) deliberately exploits this phenomenon using highly concentrated lithium chloride solutions to enhance internal thermal storage. Approximately 88 kWh of thermal energy is required to separate water from the salt solution and induce crystallization. Climatewell chillers with cooling capacities between 7 and 10 kW have been tested in Spain since 2005.

Since 2006, SolarNext (Germany) has distributed a 10 kW ammonia–water absorption chiller (chillii® PSC10), manufactured by Pink (Austria) and equipped with an innovative membrane pump. The system operates at driving temperatures between 75 and 85°C, depending on cooling conditions.

Table II. 4 Comparative technical characteristics of commercially available small-capacity sorption refrigeration units

Company	Climatewell	SolarNext	SorTech	SJTU
Product name	Climatewell 10	chillii® PSC10	ACS 08 chillii® STC8	SWAC-10
Technology	Absorption	Absorption	Adsorption	Adsorption
Working pair	H_2O/LiCl	NH_3/H_2O	H_2O/Silica gel	H_2O/Silica gel
	 (source: Climatewell)	 (source: Pink/SolarNext)	 (source: SorTech)	 (source: SJTU)
Prix de vente €	15 500	--	--	--
Cooling capacity [kW]	10	10	7.5	10
Heating temperature [°C]	83 / -	85 / 78	75 / 67	85 / 79
Recooling temperature [°C]	30 / -	24 / 29	27 / 32	30 / 36
Cold water temperature [°C]	- / 15	12 / 6	18 / 15	15 / 10
COP	0.68	0.63	0.53	0.39
Dimensions (WxDxH) [m x m x m]	1.20 x 0.80 x 1.60	0.80 x 0.60 x 2.2	0.79 x 1.06 x 0.94	1.80 x 1.20 x 1.40
Weight [kg]	875	350	260	1,600
Power [W]	170	300	57	200

Adsorption chillers face challenges related to low heat transfer between the adsorbent material and the heat transfer fluid. To overcome this limitation, coated heat exchangers are used to achieve short cycle times. Currently, small-capacity adsorption chillers on the market include a 7.5 kW water–silica gel chiller developed by SorTech (Germany) and a 10 kW unit developed by Shanghai Jiao Tong University and manufactured by Jiangsu Shuangliang in China.

II.10. Literature review

Research on solar cooling technologies has generated a significant volume of scientific publications covering their theoretical, experimental, and practical aspects. Among these contributions, a number of specialized journals play a key role in disseminating advances in solar cooling.

Wang et al.[95] experimentally investigated a solar-powered adsorption refrigeration system with an active mass transfer enhancement method. The system used activated carbon–methanol as the working pair and operated on a basic adsorption cycle. A pressure reduction during desorption process was achieved using a micro vacuum pump. A prototype system was designed, built, and tested under different weather conditions. Comparative experiments were conducted between natural and enhancing desorption modes. The results showed that the enhanced system increased the desorbed refrigerant mass by about 20%. The COP of solar was improved by at least 16.4% under clear sky conditions and up to 27.5% under partly cloudy conditions. The study confirmed faster desorption, shorter cycle time, and improved overall system performance.

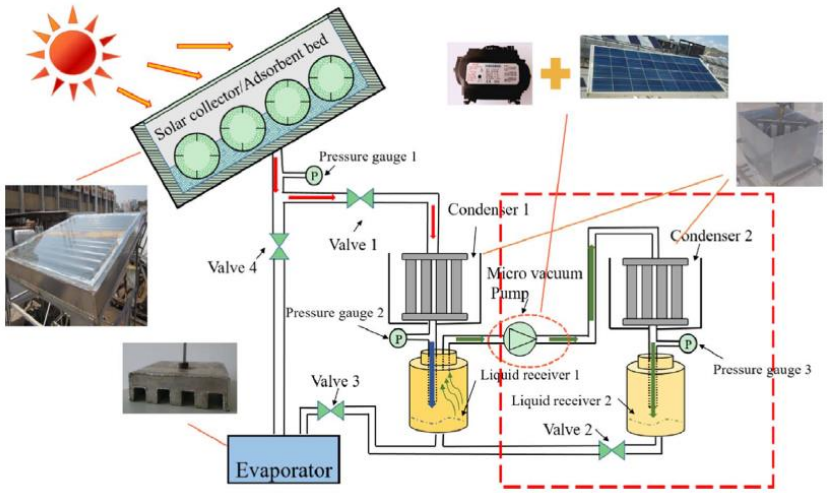


Figure II. 24 Schematic of the solar adsorption refrigeration system of Wang et al.

Kumar et al. [96] analysed a absorption single-effect refrigeration system driven by waste heat from steam turbine exhaust in a sugar industry using LiBr/H_2O binary . The exhaust steam, with an enthalpy of about 2500 kJ/kg, was used as the heat source for the generator. The system provided a cooling capacity of 1995 kW, which could be increased to 3675 kW at full boiler operation. A thermodynamic analysis based on the first law of thermodynamics was performed. The effects of cooling water inlet temperature, circulation ratio, and evaporator temperature on system performance were investigated. The results showed that lower cooling water inlet temperatures and lower circulation ratios improved system efficiency. The COP ranged between 0.6 and 0.8, with an optimal value of about 0.7 under favourable operating conditions. An increase in evaporator temperature and solution concentration led to a reduction in COP due to lower enthalpy of vaporization and higher absorber and generator loads. The electrical energy consumption was negligible compared to the supplied thermal energy. The study confirmed the technical and economic feasibility of waste-heat-driven absorption cooling in the sugar industry.

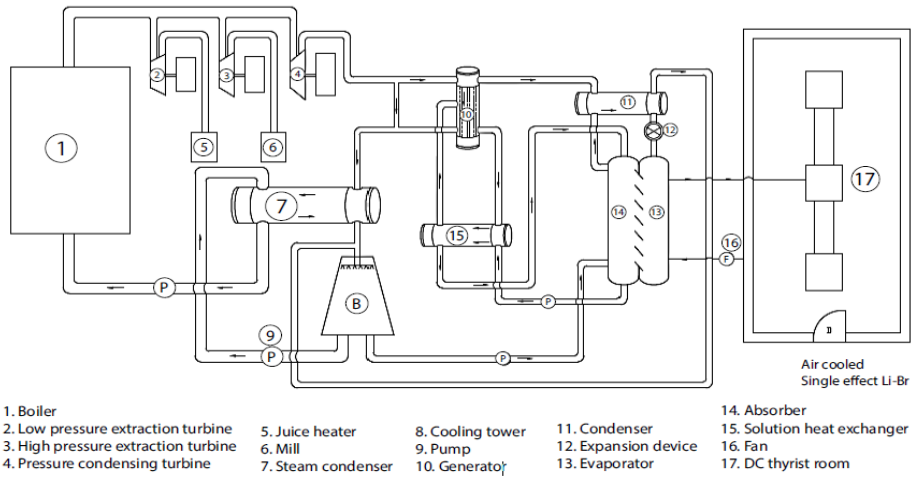


Figure II. 25 Layout of vapour absorption system using waste heat

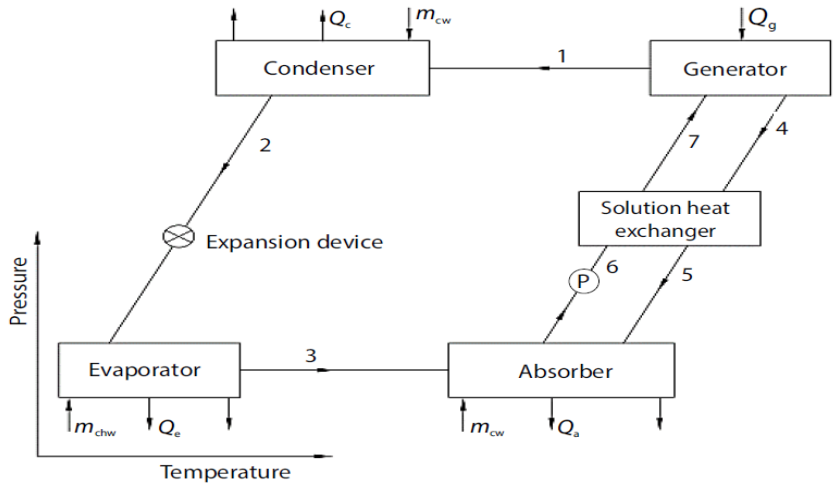


Figure II. 26 Pressure and temperature analysis of absorption system

Ramesh et al. [10] studied a shell-and-helical-coil solution heat exchanger (SHX) in an NH_3–H_2O vapor absorption refrigeration (VAR) system. They reported that the heat exchanger reached an effectiveness of 0.84–0.9, and integrating it into the system increased the COP by up to 60%, demonstrating its potential to improve heat recovery and overall efficiency.

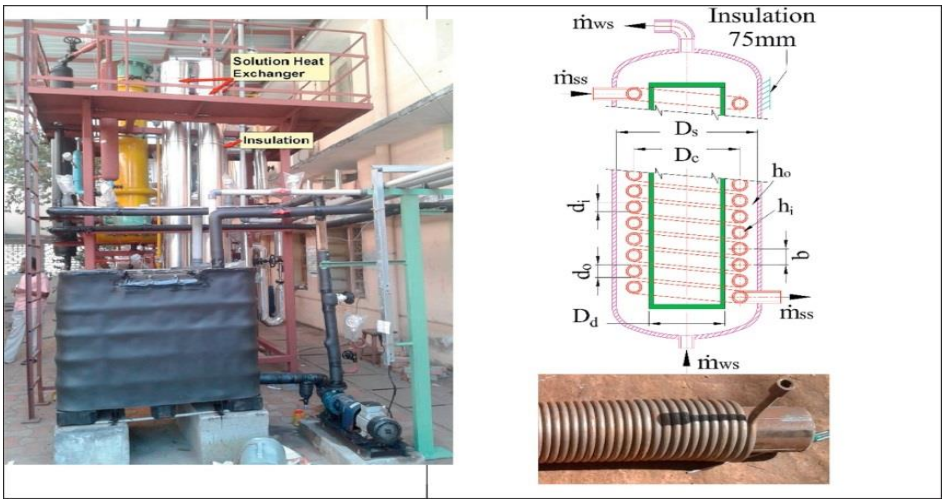


Figure II. 27 Experimental vapour absorption refrigeration system, geometry of shell and helical coil solution heat exchanger

Wang et al. [98] conducted a simulation study on an absorption refrigeration system using the NH_3–H_2O–LiBr ternary working pair based on a vapour–liquid equilibrium calculation model. A thermodynamic model was developed using the UNIQUAC activity coefficient model for the liquid phase and the Peng–Robinson equation of state for the vapour phase. The calculated equilibrium vapour pressure and liquid NH_3 concentration were validated against experimental data, with deviations between 0.5% and 9.6%. The simulated COP agreed well with experimental results, showing an absolute deviation of less than 0.02. The simulation demonstrated that adding LiBr reduced water evaporation losses and improved system performance. The effect of generator temperature and LiBr concentration on COP was analyzed. Results showed that COP increased with generator temperature and exhibited an optimal LiBr concentration under given conditions. The study confirmed that the proposed model is suitable for system design and optimization over extended temperature and pressure ranges.

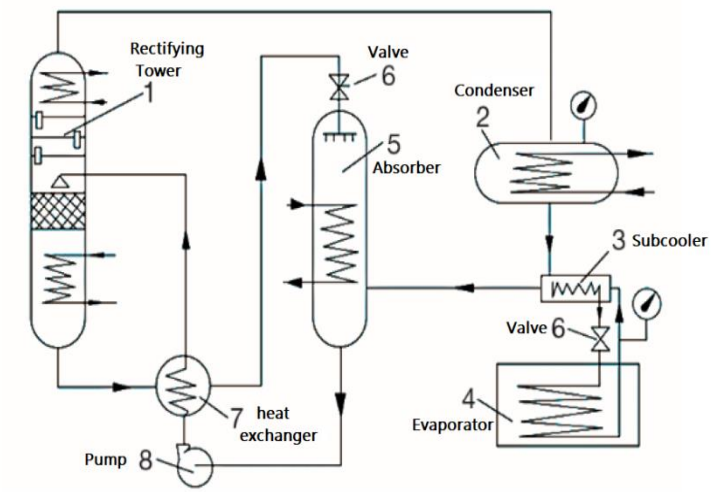


Figure II. 28 System absorption refrigeration developing by Wang et al.

Kilic and Ipek [99] performed a numerical thermodynamic analysis of a solar-driven absorption cooling system using LiBr–Al_2O_3–H_2O nanofluid as the working fluid. The required generator heat was supplied by a flat-plate solar collector, and system calculations were carried out using Engineering Equation Solver. The effects of generator temperature and Al_2O_3 nanoparticle concentration on system performance were investigated. The results showed that increasing both nanoparticle concentration and generator temperature enhanced the coefficient of performance. The COP increased from about 0.71 at 75 °C to a maximum value of 0.86 at 85 °C for 0.1% Al_2O_3 concentration. The improvement was attributed to increased thermal conductivity and heat transfer rates in the evaporator and absorber. However, higher nanoparticle concentrations were found to increase nanofluid viscosity and pressure drops. The study concluded that an optimal balance between maximum thermal conductivity and minimum viscosity is essential for efficient absorption cooling performance.

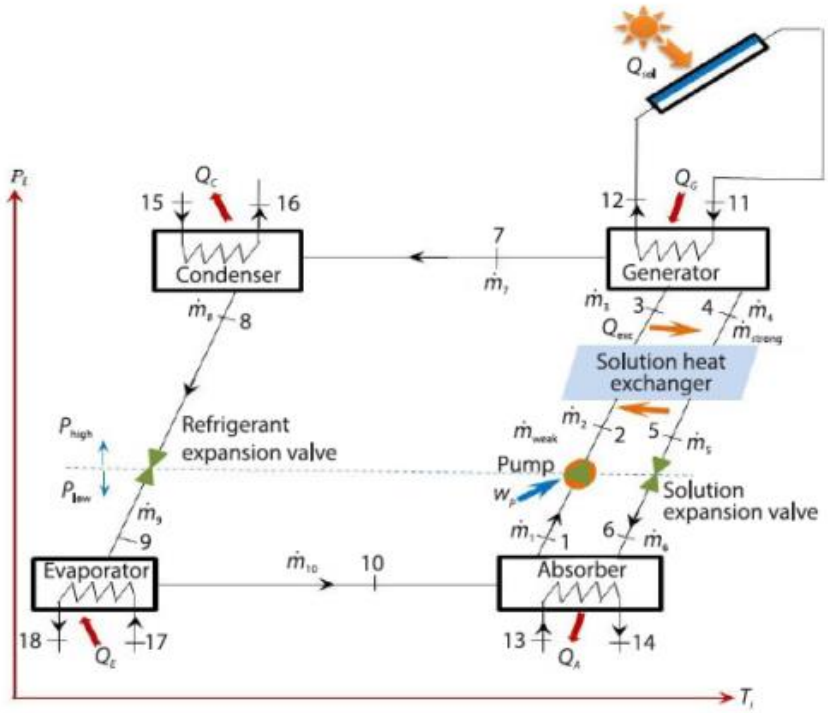


Figure II. 29 Schema of LiBr- Al2O3-H2O absorption cooling system powered by solar energy

Papadopoulos et al. [100] performed a systematic assessment of 75 working fluid mixtures, including 18 novel organic candidates, for single-effect absorption refrigeration systems. The mixtures were evaluated through a multi-criteria framework incorporating COP, exergy efficiency, operating pressures, rectification requirements, economic indicators, and safety, health and environmental (SHE) criteria. The results demonstrated that Prop/NMP and Meth/NMP mixtures outperformed conventional NH_3/H_2O and H_2O/LiBr systems in overall techno-economic performance. Cost reductions of up to 40% per ton of cooling and COP improvements up to 12.2% were reported, with performance comparable to or exceeding NH_3/H_2O. Prop/NMP was identified as a particularly attractive option due to its favorable balance

between COP, cost, and SHE characteristics. The economic assessment confirmed reduced capital and operating costs across different operating cases. The sustainability analysis indicated improved environmental and health profiles compared to acetaldehyde-based mixtures. The study concluded that Prop/NMP and Meth/NMP are promising alternatives for next-generation absorption refrigeration systems.

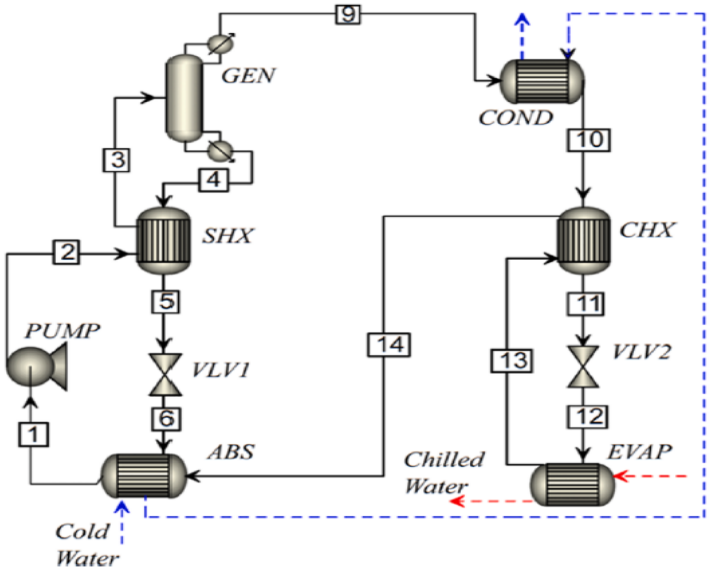


Figure II. 30 Layout of single effect absorption refrigeration (ABR) process of Papadopoulos et al.

Taboas et al. [101] performed a comprehensive study on a vertical brazed plate heat exchanger, which served as the generator in an NH_3–H_2O absorption chiller driven by a low-temperature heat source. The research examined a range of operating conditions, including pressures from 7 to 15 bar, ammonia concentrations of 0.42–0.62, heat fluxes between 20 and 50 kW/m², and mass flow rates from 70 to 140 kg/m²·s. The vapor quality was recorded up to 0.22. Results showed that the boiling heat transfer coefficient was mainly controlled by the solution mass flow, with higher flow rates enhancing heat transfer. Moreover, the pressure drop across the heat exchanger increased with both higher solution flow rates and higher vapor quality, reflecting their combined effect on performance. In contrast, heat flux had little influence on the heat transfer coefficient at elevated vapor qualities.

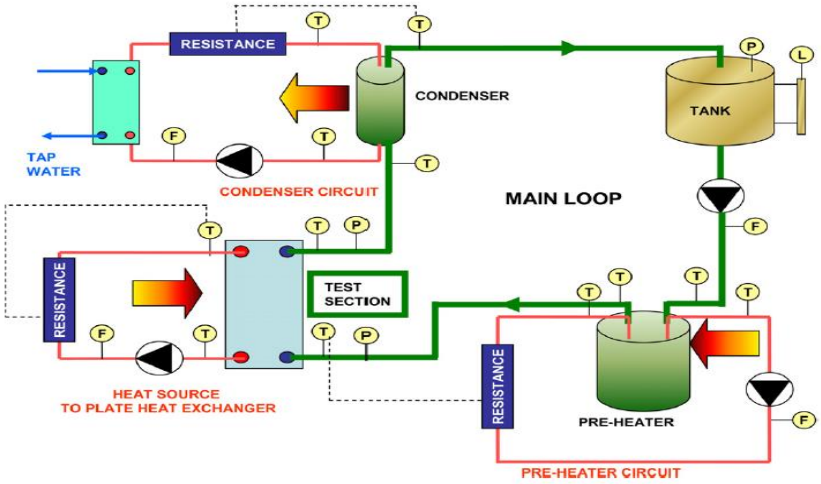


Figure II. 31 Schematic diagram of the experimental set-up of Taboas et al

Kang et al.[102] conducted experiments to study the interaction of heat and mass transfer during NH_3–H_2O falling film absorption in a plate heat exchanger equipped with offset strip fins. They investigated how liquid and vapor mass flow rates, inlet subcooling, and concentration differences affected absorption performance. The inlet ammonia concentration was varied from 5% to 15%, while the vapor concentration ranged between 64.7% and 79.7%. The results indicated rectification effects near the inlet and water desorption toward the absorber outlet. Both convective heat and mass transfer, represented by Nusselt and Sherwood numbers, increased when the inlet liquid temperature decreased and vapor temperature increased. Additionally, higher liquid and vapor Reynolds numbers improved overall heat and mass transfer. The study demonstrated that falling film absorption performance is strongly controlled by coupled heat and mass transfer processes."

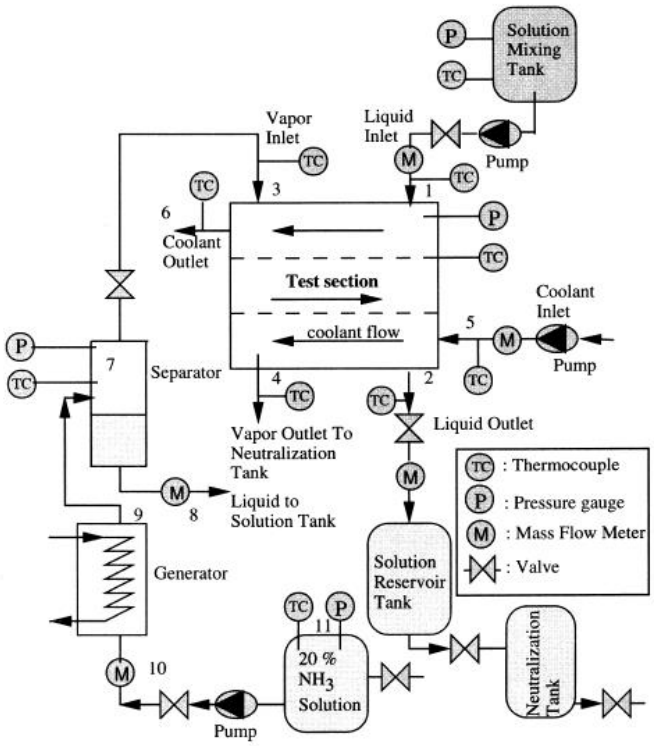


Figure II. 32 Schematic of the experimental apparatus of Kang et al

Triché et al.[103] conducted experimental and numerical investigations of heat and mass transfer in a falling film absorber used in an ammonia–water absorption chiller. The absorber was a plate heat exchanger operating with co-current vapour flow and counter-current coolant flow under real operating conditions. A fully instrumented 5 kW single-effect prototype chiller was employed to perform both global and local thermal analyses along the falling film. A one-dimensional numerical model was developed to describe coupled heat and mass transfer phenomena and was validated against experimental data. The comparison showed a maximum relative deviation of 15% between numerical and experimental results. The analysis revealed that mass transfer was governed by the falling film resistance, while liquid-side heat transfer resistance was negligible. A parametric study demonstrated that the coolant mass flow rate had a predominant effect on absorber performance compared to inlet condition variations. The study confirmed the critical role of absorber design and cooling conditions in improving absorption chiller efficiency.

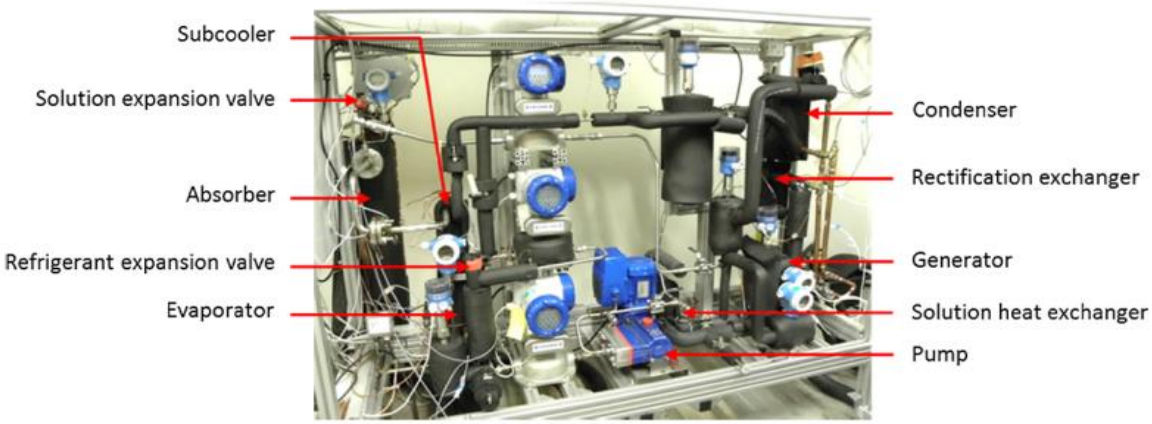


Figure II. 33 Picture of the prototype of ammonia-water absorption chiller

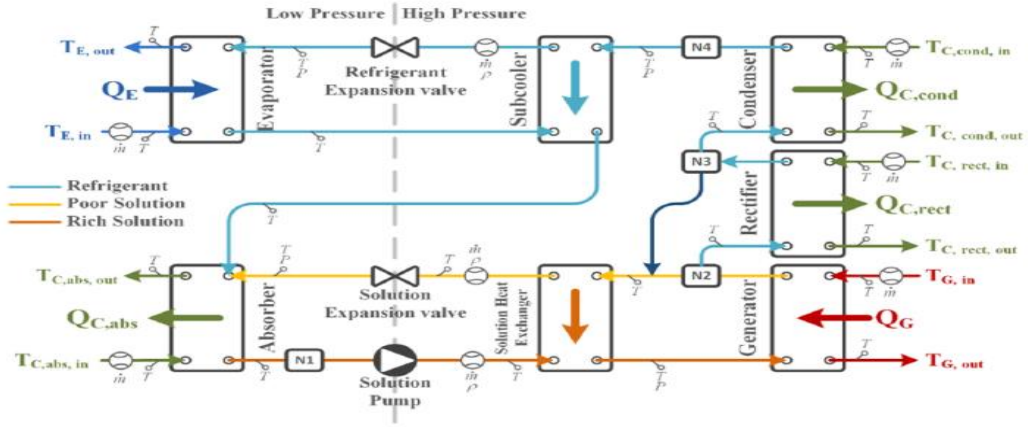


Figure II. 34 Architecture of the absorption chiller

As well as many studies such as: Emamifar [104], conducted a thermodynamic analysis of a hybrid absorption two-stage compression refrigeration system with a flash tank and an indirect sub cooler. The study found that the proposed system reduces electrical work and exergy destruction, leading to improved performance. Compared to a system without a subcooler, the proposed system enhances the overall COP by 7.86% and exergy efficiency by 11.21%. When compared to a simple cascade absorption compression system, the COP and exergy efficiency improvements are 11.42% and 16.48%, respectively. The results also highlight optimal intermediate pressure and the impact of temperature variations on performance. And PARK et al. [105] studied a hybrid absorption chiller combining single and double effect systems to better use waste hot water. They found that at full load, LiBr solution temperature and concentration increased slightly. The hybrid cycle COP was about 1.07, lower than the double effect system by 0.11. However, the hybrid's fuel COP (COPf) was higher at 1.28, and at 50% load, COPf reached 2.66. At loads below 50%, the system could operate without additional fuel, improving energy savings. And also J. Pirkandia et al. [106] analyzes a cooling, heating, and power cogeneration system based on a gas microturbine and a hot-water lithium bromide absorption chiller from an exergy and entropy perspective. The results show that the maximum electrical efficiency is achieved for a compressor pressure ratio of 5, with a cogeneration efficiency of approximately 48% and an exergy efficiency of 24%. Increasing the turbine inlet gas temperature enhances these

performances, while an increase in cooling capacity reduces the overall cogeneration efficiency without affecting exergy efficiency. The exergy analysis reveals that the combustion chamber is the component with the highest exergy losses and entropy generation. In a different research, Enoki et al. [107] studied a new Solution Transportation Absorption chiller using ammonia–water to move thermal energy over distances. They split the chiller to generator/condenser at the heat source and evaporator/absorber at the demand side. They tested generator temperatures between 100°C and 120°C with transport distances up to 500m. The STA system achieved a COP around 0.65, similar to conventional chillers. The generator temperature and transport distance had no significant effect on COP performance. In a separate study by Yıldırım and Yeşilata [108] investigated the optimization of a LiBr/H_2O absorption system powered by a low-temperature heat source, applying the Structural Bond Coefficients method. Their optimization decreased system irreversibility by 72.5%, although it increased initial investment costs; the additional expense could be recovered within 4.2 years. The study also suggested that integrating solar thermal collectors could further improve system efficiency, and that rising conventional energy prices may shorten the payback period. The research underlined the need to balance thermodynamic performance with economic feasibility. Similarly Kumar et al. [109] applied energy and exergy analyses to optimize an NH_3–H_2O absorption refrigeration system. They found that the generator temperature that maximizes the COP (0.54) is 99 °C, while the temperature that minimizes exergy destruction is 88 °C, 11 °C lower. Changes in evaporator and condenser temperatures affected the required cut-off temperature, with higher evaporator temperatures reducing it and higher condenser temperatures increasing it. These findings demonstrated the value of an exergy-based approach for system optimization.

From the literature reviewed, considerable research has focused on the use of ammonia as a refrigerant in absorption cooling systems. Previous studies have demonstrated that ammonia-based working pairs can significantly enhance the thermal performance and overall efficiency of solar absorption refrigeration systems.

II.11. Conclusion

The transition toward renewable energy sources has become a necessity in response to environmental pollution, the depletion of fossil fuel resources, and the increase in energy costs. Solar energy represents a promising solution for cooling applications, particularly in regions with high solar potential.

This chapter presented an overview of the main cooling technologies, including electrically driven systems, thermo-mechanical systems, and sorption-based technologies (adsorption, absorption, and desiccant cooling). These systems are used for refrigeration, air conditioning, and air treatment applications. Among these technologies, absorption systems stand out due to their ability to directly utilize solar thermal energy. In this chapter therefore provides the theoretical basis required for the thermodynamic analysis and modeling of the system studied in the following chapters.

Chapter III

Thermodynamic study of absorption refrigeration

Chapter 3 Thermodynamic study of absorption refrigeration

III.1. Introduction

Sorption refrigeration systems have attracted considerable attention as an alternative to conventional vapour compression systems due to their ability to operate using low-grade thermal energy sources, such as solar energy, industrial waste heat, and geothermal energy. In particular, solar-driven absorption chillers represent a promising solution for sustainable cooling applications in regions with high solar potential, such as Algeria. Among the various working pairs, the ammonia–water binary (NH_3/H_2O) is widely used because of its excellent thermodynamic properties, high latent heat of vaporization, and capability to produce low-temperature refrigeration.

In this study, a single-effect solar absorption refrigeration system using the ammonia–water working pair is selected.

This chapter presents a detailed thermodynamic study of the single-effect solar absorption refrigeration cycle using the NH_3/H_2O working pair. The objective is to establish a mathematical model based on mass and energy conservation principles, evaluate the system performance, and investigate the influence of operating parameters such as pressure and temperature on COP. The modelling is carried out under steady-state conditions using Engineering Equation Solver (EES), providing a reliable framework for predicting system behaviour and optimizing its performance for solar cooling applications.

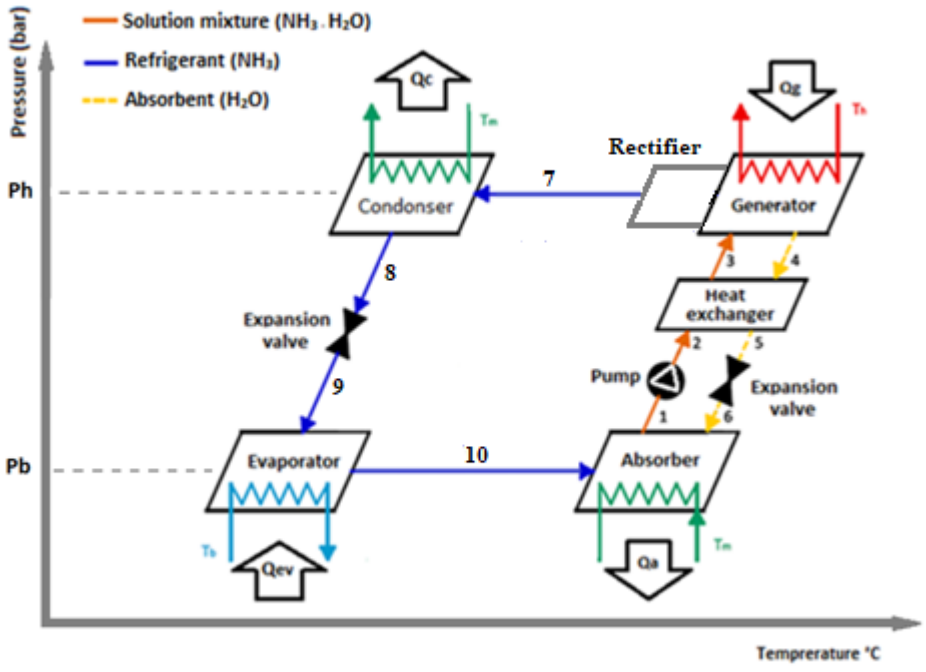


Figure III. 1 Basic schematic of a solar absorption refrigeration machine single-effect.

III.2. Description of the absorption cycle

The single-effect solar absorption refrigeration cycle using the NH_3/H_2O working pair is considered in this study due to its suitability for solar thermal applications and its ability to operate without mechanical compression [110, 111]. The system operates at two distinct pressure levels: a high-pressure level corresponding to the generator and condenser, and a low-pressure level corresponding to the evaporator and absorber, as illustrated in **Figure III.1.**

III.2.1. Generator

The cycle starts in the generator (Desorber), where the rich solution (ammonia dissolved in water) is heated by solar thermal energy supplied by solar collectors. The energy thermal input ***Qg*** raises the solution temperature, causing ammonia to desorb (separate) from the absorbent water due to its higher volatility.

As a result, two streams are produced:

- Ammonia-rich vapour leaving the generator toward the condenser, passing first through a finned-tube rectifier that condenses and returns residual water vapour to the generator, ensuring a nearly pure ammonia vapour reaches the condenser.
- Weak solution (low concentration of ammonia fluid) remaining in the generator and flowing toward the absorber.

This process is governed by mass and energy conservation laws, and the generator acts as the thermal equivalent of a compressor in conventional vapour compression systems.

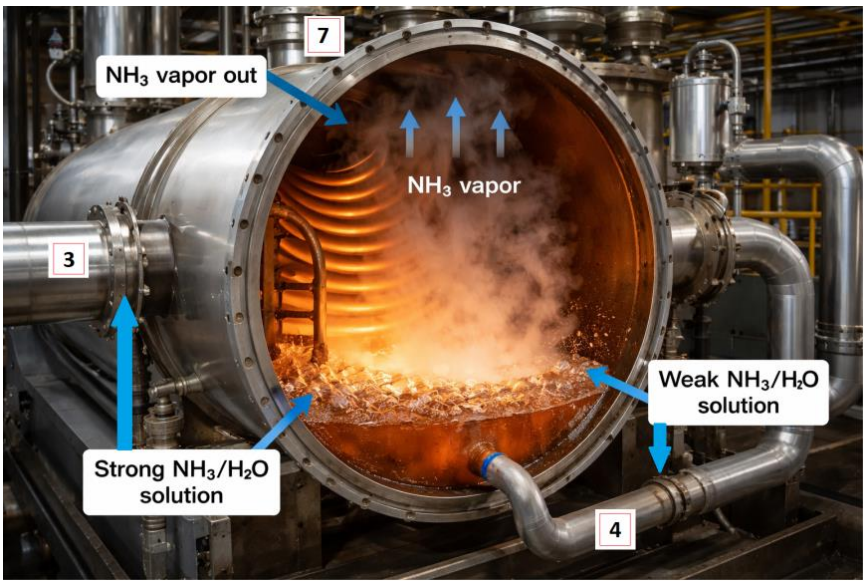


Figure III. 2 Generator

III.2.2. Condenser

The high-pressure (Ph) ammonia vapor enters the condenser, where it rejects heat ***Qc*** to the ambient environment (air or cooling water). During this process, the ammonia vapour condenses into a saturated or sub cooled liquid at high pressure.

The condenser ensures the transformation of vapour into liquid refrigerant, enabling the subsequent throttling process.

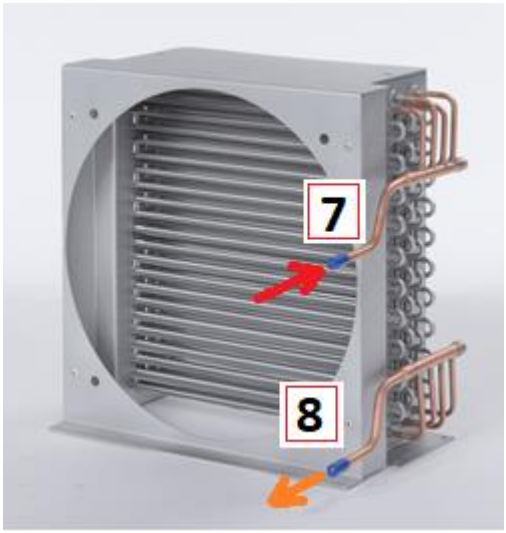


Figure III. 3 Condenser [112]

III.2.3. Expansion Valve

The condensed liquid ammonia passes through an expansion valve, where its pressure is reduced from the high-pressure level to the low-pressure level. This process is typically assumed to be isenthalpic (Joule–Thomson expansion).

The pressure drop leads to a significant temperature reduction, producing a low-temperature liquid–vapour mixture, which is suitable for cooling applications.

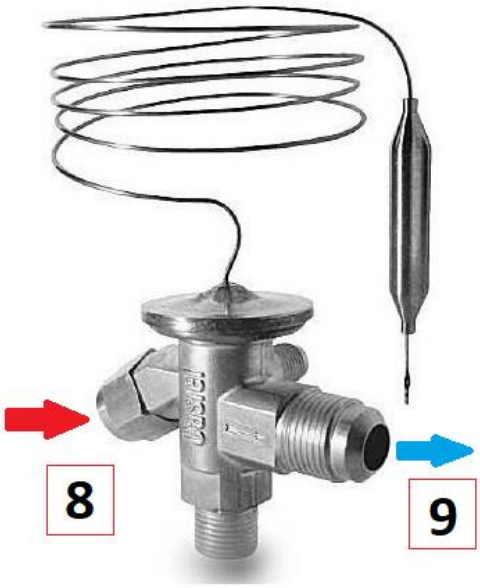


Figure III. 4 Expansion valve

III.2.4. Evaporator

In the evaporator, the low-pressure ammonia absorbs heat ***Qev*** from the refrigerated space or cooling load. The refrigerant evaporates completely, transforming into saturated or superheated vapour.
This is the cooling effect of the system, and it defines the refrigeration capacity of the cycle.

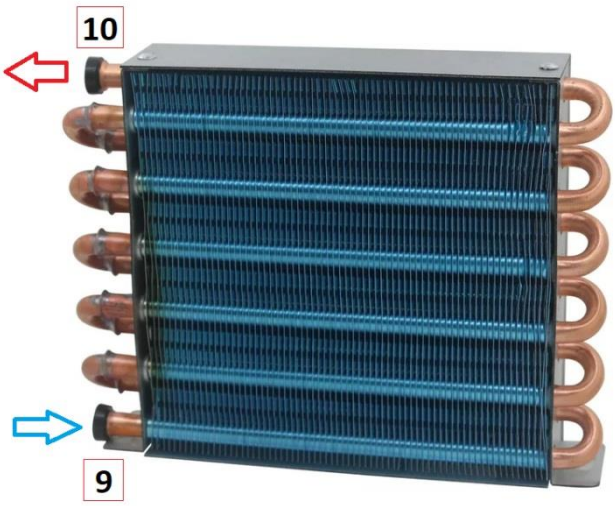


Figure III. 5 Evaporator [113]

III.2.5. Absorber

The low-pressure ammonia vapour flows into the absorber, where it comes into contact with the weak solution (water with low ammonia concentration) coming from the generator.
Ammonia is absorbed into the water, forming a rich solution. This absorption process is exothermic, releasing heat ***Qa***, which must be removed by cooling water or ambient air to maintain absorber performance.
The absorber plays a key role in maintaining low evaporator pressure and ensuring continuous refrigerant flow.

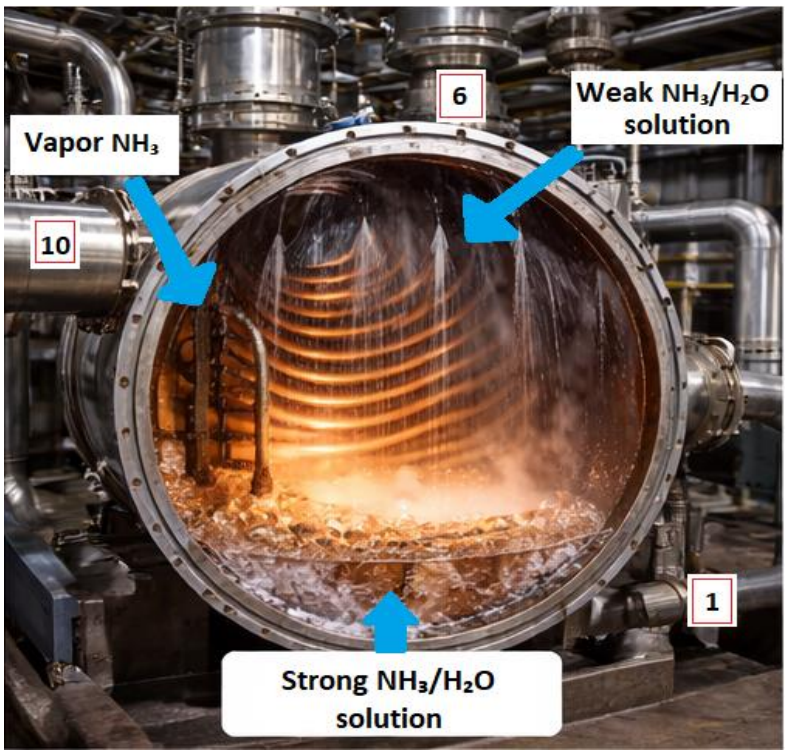


Figure III. 6 Absorber

III.2.6. Solution pump

The rich solution leaving the absorber is pumped to the generator pressure level using a solution pump. Since the working fluid is liquid, the pump requires very little mechanical work compared to a compressor in conventional systems. This is one of the main advantages of absorption systems.

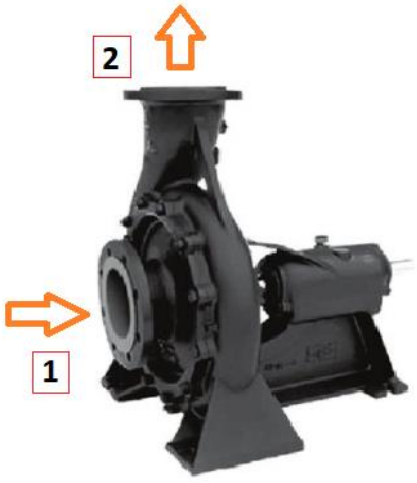


Figure III. 7 Solution pump [114]

III.2.7. Solution heat exchanger

Before entering the generator, the rich solution passes through a solution heat exchanger, where it is preheated by the hot weak solution leaving the generator. This internal heat recovery:

- Reduces the required solar heat input ***Qg***
- Improves the coefficient of performance ***(COP)***
- Enhances overall system efficiency.

Similarly, the weak solution is cooled before entering the absorber, improving absorption conditions.

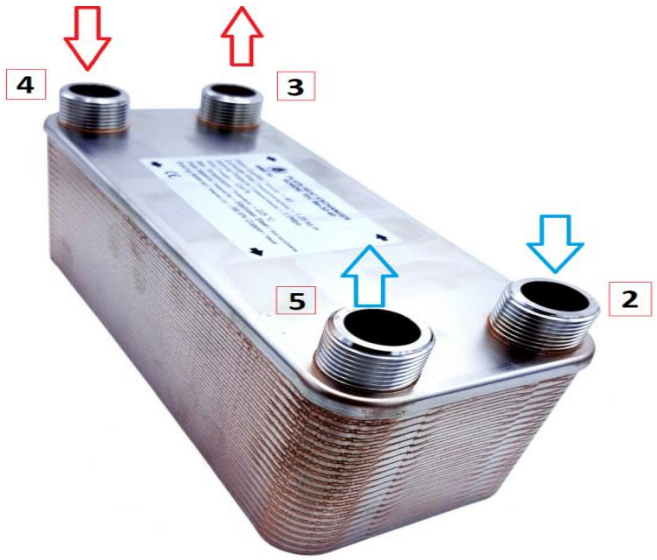


Figure III. 8 Plate heat exchanger [115]

III.2.8. Overall cycle operation

The absorption refrigeration cycle operates continuously as long as thermal energy is supplied to the generator. Solar energy acts as the primary driving force, replacing the mechanical compressor used in vapour compression refrigeration systems. The system thus offers advantages in terms of:

- Low electricity consumption
- Use of renewable energy
- Reduced greenhouse gas emissions
- Suitability for remote and off-grid applications

III.3. Thermodynamic study

The thermodynamic modelling of the different refrigeration cycles is based on the first law of thermodynamics applied to control volumes under steady-state and steady-flow conditions [116–118]. The general formulation of the mass and energy conservation equations for a control volume is presented below.

For a steady-state system, the mass conservation equation is expressed as:

$$\sum \dot{m}_{in} = \sum \dot{m}_{out} \quad \text{(III.1)}$$

This equation guarantees that, for every component of the absorption system, the total mass flow entering a control volume is equal to the mass flow leaving it.

For mixtures (NH_3/H_2O), a species mass balance can also be written as:

$$\sum \dot{m}_{in}\, x_{in} \;=\; \sum \dot{m}_{out}\, x_{out} \qquad \text{(III.2)}$$

Where:

$\dot{m}$: mass flow rate (kg/s).

x: mass fraction of ammonia in the solution.

The general steady-state energy conservation equation (First Law of Thermodynamics) for a control volume is given by:

$$\sum Q + \sum W \;= \sum \dot{m}_{out} h_{out} - \sum \dot{m}_{in} h_{in} \qquad \text{(III.3)}$$

Q : heat transfer rate (kW),

$\dot{W}$ work rate (kW),

h : specific enthalpy (kJ/kg),

The detailed mathematical relationships describing the single-effect cycle are given below:

III.3.1. Generator (Desorber)

- *Mass balance*

$$\dot{m}_3 = \dot{m}_4 + \dot{m}_7 \qquad \text{(III.4)}$$

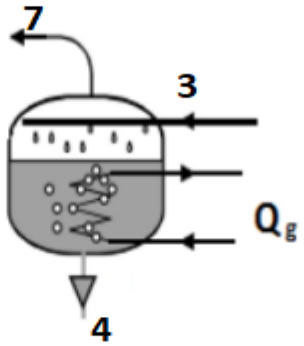
$$x_3 = x_r \qquad \text{(III.5)}$$

$$x_4 = x_p \qquad \text{(III.6)}$$

$$x_3 \dot{m}_3 = x_4 \dot{m}_4 \qquad \text{(III.7)}$$

- *Energy balance*

$$Q_g = \dot{m}_4\, h_4 + \dot{m}_7\, h_7 - \dot{m}_3\, h_3 \qquad \text{(III.8)}$$



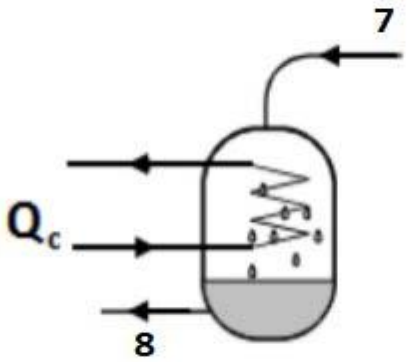
III.3.2. Condenser

- *Mass balance*

$$\dot{m}_7 = \dot{m}_8 \qquad \text{(III.9)}$$

- *Energy balance*

$$Q_c = \dot{m}_7\, h_7 - \dot{m}_8\, h_8 \qquad \text{(III.10)}$$



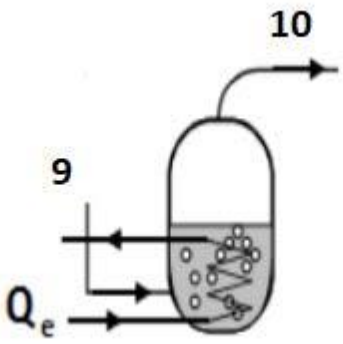
III.3.3. Evaporator

- *Mass balance*

$$\dot{m}_9 = \dot{m}_{10} \quad \text{(III.11)}$$

- *Energy balance*

$$Q_{ev} = \dot{m}_{10}\, h_{10} - \dot{m}_9\, h_9 \quad \text{(III.12)}$$



III.3.4. Absorber

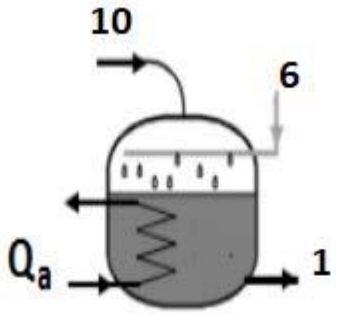
- *Mass balance*

$$x_1 \dot{m}_1 = x_6 \dot{m}_6 \quad \text{(III.13)}$$

$$\dot{m}_6 + \dot{m}_{10} = \dot{m}_1 \quad \text{(III.14)}$$

- *Energy balance*

$$Q_a = \dot{m}_{10}\, h_{10} + \dot{m}_6\, h_6 - \dot{m}_1\, h_1 \quad \text{(III.15)}$$



III.3.5. Heat exchanger

- *Mass balance*

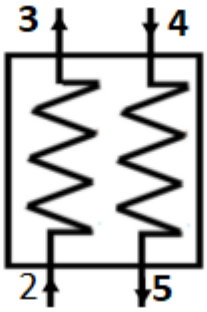
$$\dot{m}_3 = \dot{m}_2 \quad \text{(III.16)}$$

$$\dot{m}_5 = \dot{m}_4 \quad \text{(III.17)}$$

- *Energy balance*

$$Q_{ex} = \dot{m}_3\, h_3 - \dot{m}_2\, h_2 \quad \text{(III.18)}$$

$$Q_{ex} = \dot{m}_4\, h_4 - \dot{m}_5\, h_5 \quad \text{(III.19)}$$



III.3.6. Expansion valve

- *Mass balance*

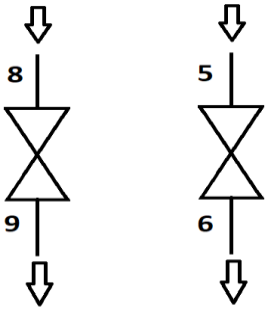
$$\dot{m}_8 = \dot{m}_9 \quad \text{(III.20)}$$

$$\dot{m}_5 = \dot{m}_6 \quad \text{(III.21)}$$

- *Energy balance*

$$Q_{8-9} = \dot{m}_9\, h_9 - \dot{m}_8\, h_8 \quad \text{(III.22)}$$

$$Q_{5-6} = \dot{m}_6\, h_6 - \dot{m}_5\, h_5 \quad \text{(III.23)}$$



III.3.7. Solution pump

The circulation pump delivers the refrigerant-rich solution to the high-pressure generator:

$$W = \dot{m}_1 \ (h_2 - \ h_1) \tag{III.24}$$



III.3.8. Coefficient of performance

The COP is a key indicator used to evaluate the efficiency of refrigeration systems. It is defined as the ratio between the useful cooling effect produced by the system and the energy required to operate it. In other words, COP expresses how effectively the supplied energy is converted into cooling capacity. A higher COP indicates better system performance and lower energy consumption. In solar-driven absorption refrigeration systems, the cooling effect corresponds to the heat removed from the refrigerated space at the evaporator, while the input energy is the thermal energy supplied to the generator to ensure the separation of the refrigerant from the absorbent solution during the regeneration process. Therefore, the COP provides a convenient parameter for comparing different refrigeration technologies operating under similar conditions and cycles. Mathematically, it is expressed as:

$$COP = \frac{Q_{ev}}{Q_g + W} \tag{III.26}$$

Q_a : Heat released by the absorber (kW).
Q_{ev}: Heat absorbed by the evaporator, representing the cooling capacity (kW).
Q_c : Heat released by the condenser (kW).
Q_g : Heat supplied to the generator (kW).
W: Mechanical work of the solution pump (kW).
The thermodynamic behaviour of the NH_3/H_2O absorption refrigeration system can be represented using Merkel diagram (**Fig.III.9**) and Oldham diagram (**Fig.III.10**), which describe the relationship between enthalpy, temperature, pressure, and ammonia concentration in the solution. These diagrams are widely used for detailed thermodynamic analysis of absorption cycles, allowing the determination of strong and weak solution concentrations as well as the

evaluation of heat transfer processes in the generator, absorber, condenser, and evaporator [119] [120, 121]

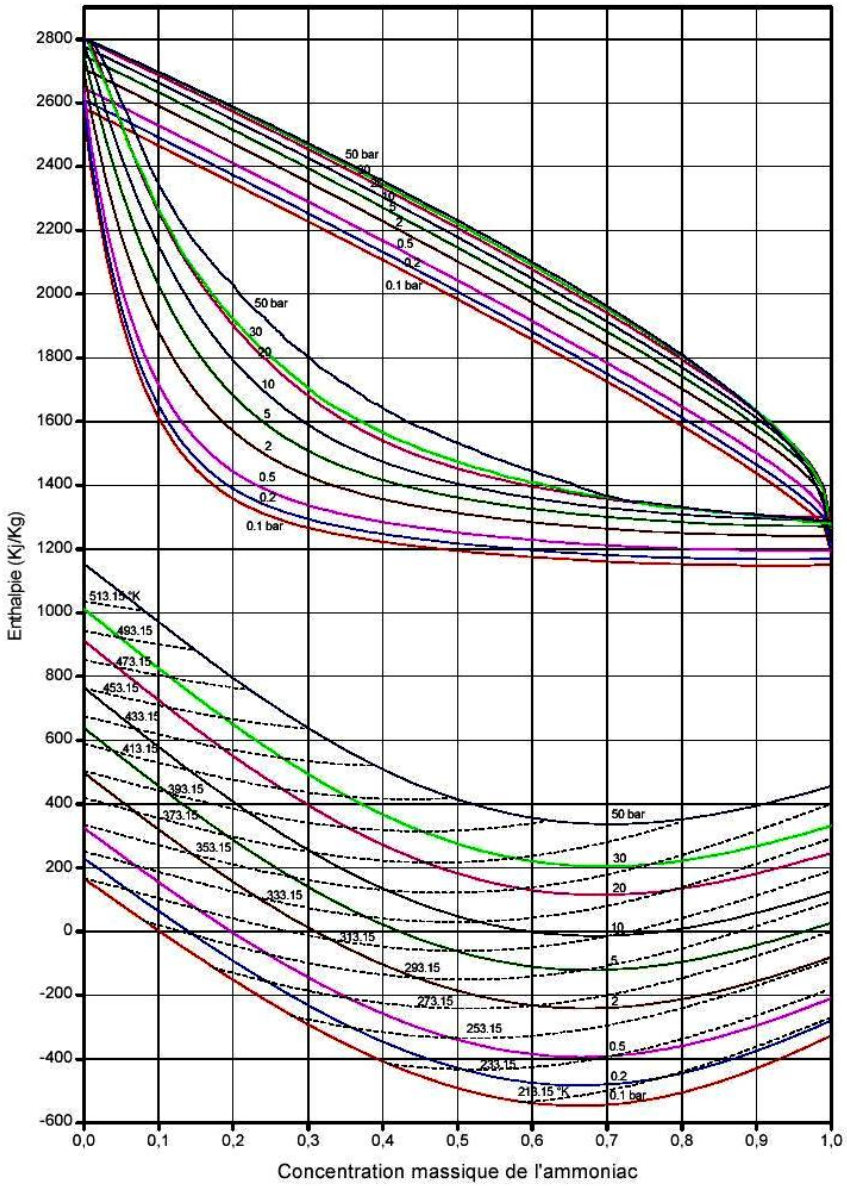


Figure III. 9 Merkel Diagram (H–x diagram) for NH_3/H_2O

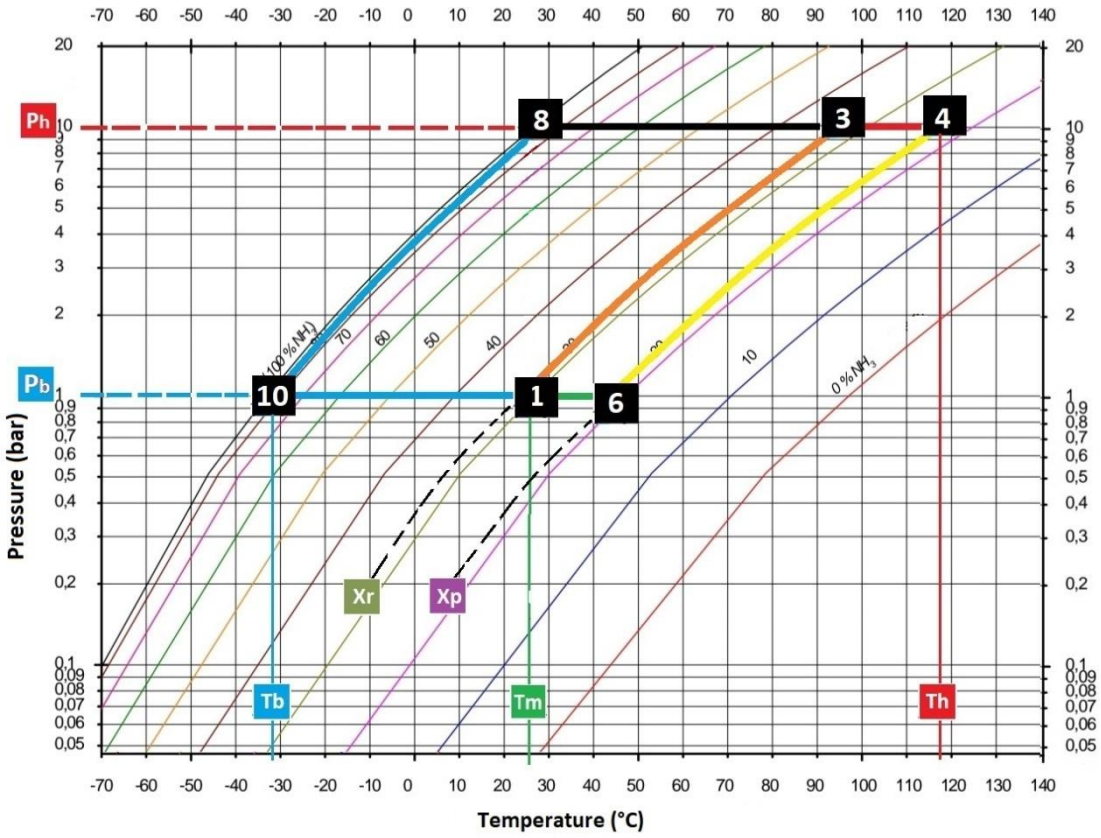


Figure III. 10 Oldham diagram (P,T) for NH3/H2O

In the present study, a simplified thermodynamic model based on mass and energy balance equations is adopted. The simulation of the absorption cycle is carried out using Engineering Equation Solver (EES), where thermodynamic properties are obtained from built-in correlations. The effects of operating temperature and pressure on the coefficient of performance (COP) are investigated. Therefore, the use of Oldham and Merkel diagrams is not explicitly implemented in the calculations but is considered as a theoretical reference framework for understanding the thermodynamic behaviour of the NH_3/H_2O working pair.

III.4. Working constraints

III.4.1. Hypotheses

To ensure consistency between the selected model and the actual system under study, several simplifying assumptions have been adopted:

- Heat losses to the external environment are neglected.
- The expansion process at the valve is assumed to be isenthalpic.
- Changes in kinetic and potential energy are considered negligible.
- The system is treated as adiabatic, implying no heat exchange with the surroundings a necessary condition for constructing a thermodynamic model that focuses on key performance indicators.

– Steady-state conditions are assumed, although the system inherently operates under dynamic influences such as variable solar radiation and ambient temperature, which are considered for more accurate performance assessment.

As part of this thermodynamic modelling, pressure losses in pipes and exchangers were neglected in order to simplify the analysis. This assumption is generally adopted in theoretical studies when the main objective is to evaluate the influence of thermodynamic parameters on COP.

III.4.2. Operating Parameters

Based on the available reference data [122] , the installation under investigation operates following a single-effect absorption refrigeration cycle. The working pair used is ammonia-water (NH_3-H_2O), where ammonia (NH_3) serves as the refrigerant and water (H_2O) as the absorbent (see **Fig.III.1.**). The system functions under the following **Table III.1** operating conditions:

Table III. 1 Presentation of the different study parameters

Parameters	
Low pressure.	1 ≤ Pb ≤ 1.7 bar
High pressure.	7 ≤ Ph ≤ 10 bar
Ambient temperature	Tm = 25°C
Heat exchanger efficiency	Ex = 0.83
Rich solution mass flow rate (NH_3/H_2O)	$\dot{m}_1 = 0.98 \approx 1$ (kg/s)
Refrigerant mass flow rate (NH_3)	$\dot{m}_7 = 0.45$ (kg/s)
Mass concentration of the mixture (NH_3/H_2O) at point 1 (rich solution)	x_r = 33%
NH_3 mass concentration at point 4	14% ≤ x_{NH_3} ≤ 25%

III.4.3. Binary working couple

The ammonia–water (NH_3–H_2O) binary working couple is one of the most widely used pairs in absorption refrigeration systems, particularly for solar-driven applications. Ammonia is considered a promising hydrogen and energy carrier due to its high hydrogen content, ease of storage, and absence of carbon emissions at the point of use, supporting efforts to reduce CO_2 emissions associated with the conventional Haber–Bosch process. [123]

As a refrigerant, ammonia exhibits a very low freezing point (−77.75 °C), allowing operation within a temperature range of −60 °C to +20 °C without risk of solidification [124]. It operates

at relatively moderate-to-high pressures compared to Water-based systems, thereby avoiding deep vacuum conditions and simplifying system design. Its high latent heat of vaporization enhances cooling capacity and energy efficiency while enabling lower refrigerant flow rates and more compact heat exchangers. [125].

The NH_3–H_2O pair is characterized by strong refrigerant–absorbent affinity, low viscosity, favorable operating pressure, good compactness, and compatibility with common metallic materials, which improves durability and reliability. This working pair is extensively employed in air conditioning and refrigeration applications, as well as in the food, chemical, and medical storage sectors, where reliable sub-zero cooling and efficient thermal performance are essential. [124–126].

However, despite these technical advantages, the extensive use of ammonia presents several challenges. Ammonia is relatively expensive, toxic, and requires strict safety measures during handling and operation. In addition, its availability and environmental considerations may limit large-scale implementation.

In this context, our study aims to reduce the ammonia mass concentration compared to previous studies, while simultaneously improving the coefficient of performance (COP).

Therefore, the present study seeks to develop a detailed thermodynamic model to evaluate the performance of a single-effect solar absorption refrigeration system, with particular attention to optimizing operating conditions and enhancing overall system efficiency.

III.5. Conclusion

In this chapter, a comprehensive thermodynamic analysis of a single-effect absorption refrigeration system using the NH_3/H_2O working pair has been presented. The cycle was described in detail, and mathematical models were developed for each component based on the first law of thermodynamics and mass conservation principles. The governing equations for the generator, condenser, evaporator, absorber, solution heat exchanger, expansion valves, and solution pump were established, enabling the evaluation of heat transfer rates and system performance indicators.

A simplified modelling approach was adopted to formulate the analytical expressions required for system performance evaluation. Although Oldham and Merkel diagrams provide a rigorous graphical representation of the thermodynamic behaviour of the NH_3/H_2O mixture, they were used in this study only as a theoretical reference. The complete set of equations derived in this chapter constitutes the basis for the numerical resolution and performance analysis presented in Chapter IV using Engineering Equation Solver (EES).

Chapter IV

Results and discussions

Chapter 4 Results and discussions

IV.1. Introduction

Research on solar absorption refrigeration systems is still evolving, aiming to compete with conventional vapour-compression systems, which remain the most widely used. Current studies focus on improving performance, reducing costs, and minimizing environmental impacts, while ensuring high energy efficiency.

In this context, particular attention is increasingly given to optimizing the working pair composition in order to enhance performance while limiting the amount of refrigerant used.

In this chapter, the results of a thermodynamic modelling study of a single-effect solar absorption refrigeration system using the NH_3/H_2O working pair are presented. Special emphasis is placed on variation the ammonia mass concentration compared to previous studies, while simultaneously improving the coefficient of performance (COP). A detailed performance analysis was carried out to examine how key operating parameters affect system efficiency, including generator temperature (Tg), evaporator temperature (Tev), low pressure (Pb), high pressure (Ph), and ammonia mass fraction (x_{NH_3}).

The influence of each parameter was examined individually while keeping all others constant. The main performance indicators considered are the coefficient of performance (COP), obtained using equation (III.26), and the refrigerant mass flow rate.

The effect of ammonia concentration on COP was analysed for values ranging from 14% to 25%, with the objective of identifying reduced concentration levels

that still ensure efficient operation. The influence of generator and evaporator temperatures was studied to determine optimal operating conditions. The impact of low- and high-pressure levels was evaluated to identify configurations that ensure thermodynamically stable and efficient operation.

An algorithmic calculation procedure, illustrated in **Figure IV.1**, was developed and implemented using Engineering Equation Solver (EES) to systematically assess the system performance and determine the optimal thermodynamic operating conditions. This approach ensures a comprehensive understanding of the interaction between pressure levels, concentration, and temperature on the overall efficiency of the absorption cycle.

Finally, the simulation results were compared with published experimental and theoretical data to validate the developed model and assess its predictive capability. This analysis allows the determination of optimal operating conditions and provides a better understanding of the system's behaviour under different operating scenarios.

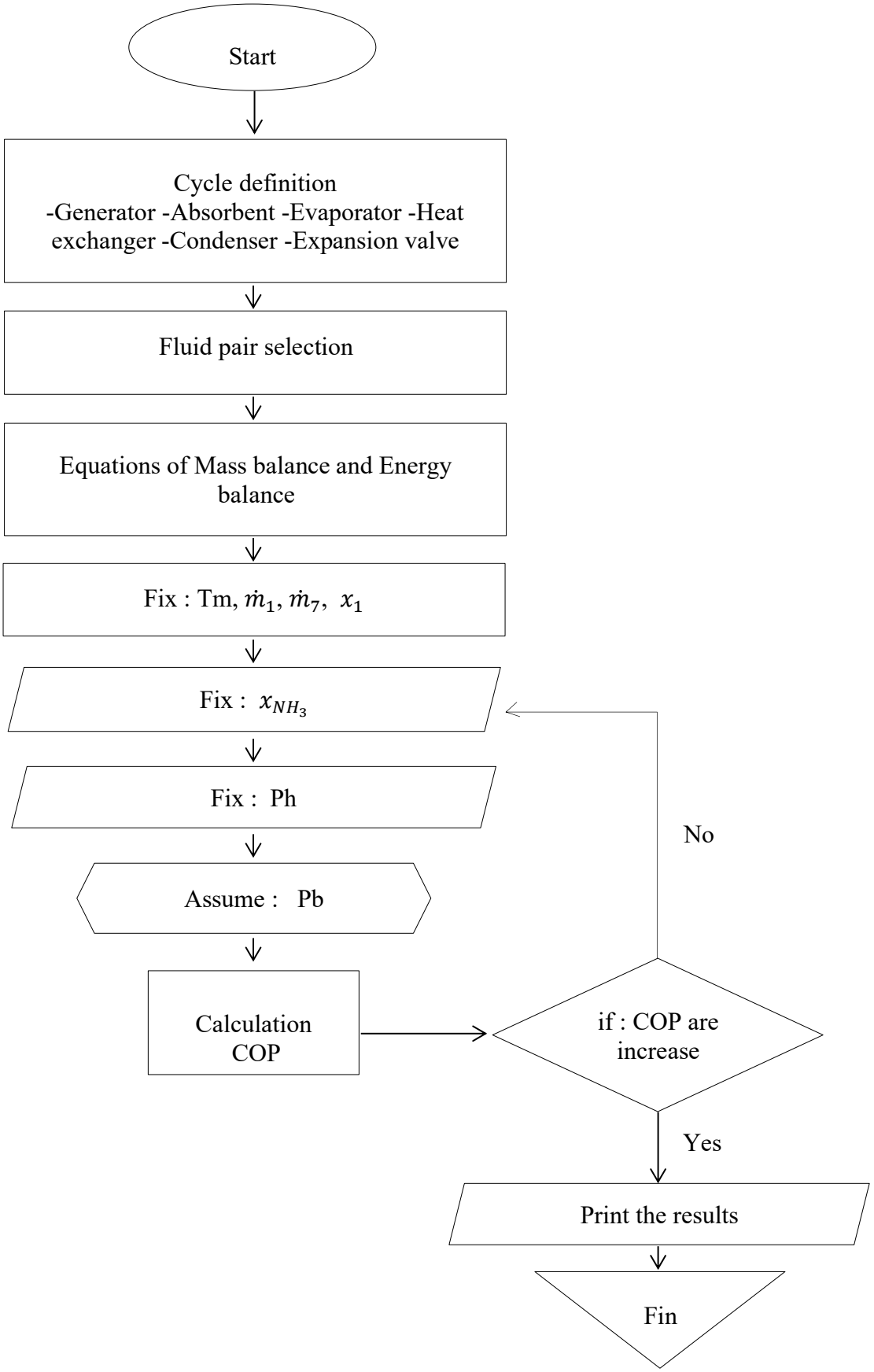


Figure IV. 1 Algorithmic procedure for the calculation and optimization of COP

IV.2. Model setup

To achieve a comprehensive understanding of the operating characteristics of a single-effect solar absorption system and to enhance overall system efficiency while reducing design complexity, implementation costs, and potential technical uncertainties, the development of a detailed mathematical model is indispensable. Numerous researchers have relied on simulation platforms such as TRNSYS [127], MATLAB [128], and TRANSOL [129, 130] for the modelling and analysis of cooling technologies.

In the present work, Engineering Equation Solver (EES) was selected due to its suitability for thermodynamic modelling and its strong capability in solving highly coupled nonlinear equations governing thermal systems [131, 132].

EES provides an efficient computational framework for the design and analysis of thermal systems, particularly those involving heat-driven refrigeration processes. It facilitates the evaluation of thermo physical properties, heat and mass transfer interactions, and system state variables under varying operating and environmental conditions. Through the application of EES, the performance of the absorption refrigeration system is simulated with high accuracy, enabling a detailed assessment of energetic behaviour and the identification of potential improvements in system operation.

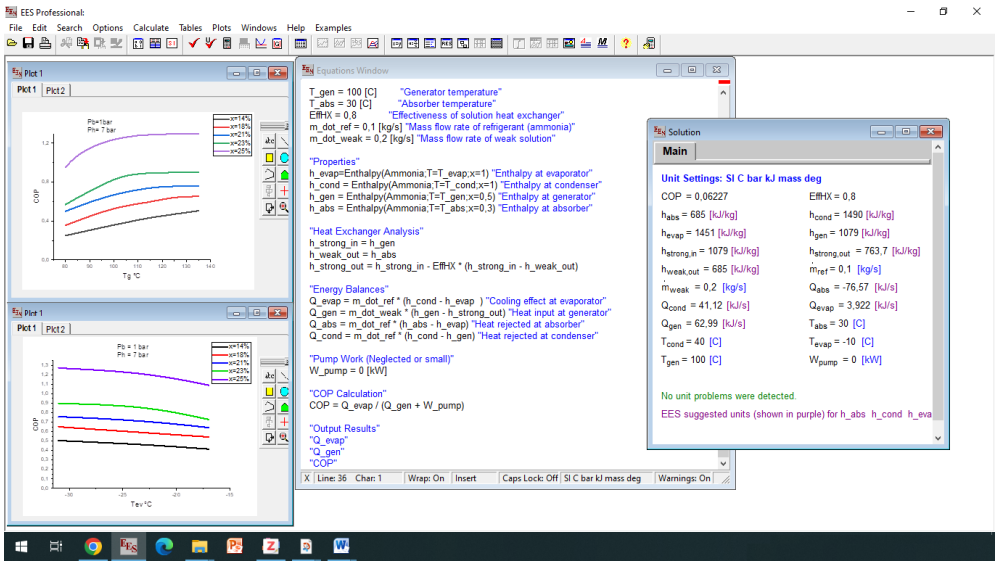


Figure IV. 2 Engineering equation solver software (EES)

IV.3. Results and discussion

The different results presented in this work are obtained from the numerical resolution of the governing mass and energy balance equations of the developed thermodynamic model described in **Chapter III**. The system of nonlinear equations was solved using Engineering Equation Solver (EES) software, which allows accurate evaluation of thermo physical properties of the NH_3/H_2O working pair and ensures reliable convergence of the solution.

The modelling results are used to analyse the thermal behaviour and performance of the single-effect absorption refrigeration system under various operating conditions. Particular attention is

given to the influence of key operating parameters such as ammonia concentration, generator temperature, evaporator temperature, absorber pressure, and condenser pressure on the system performance.

To ensure efficient operation of the NH_3/H_2O absorption machine, it is essential to carefully select the concentration of the binary mixture as well as the operating temperatures and pressures at the generator, evaporator, condenser, and absorber levels. These parameters directly affect the refrigerant mass flow rate, heat transfer rates, system irreversibility, and ultimately the coefficient of performance (COP). Therefore, a parametric study was carried out to determine the optimal operating range that maximizes the system performance while maintaining thermodynamic stability.

IV.4 Interpretations

The following explanation illustrates the variation of the coefficient of performance (COP) as a function of the generator temperature (Tg) and the evaporator temperature (Tev) for different ammonia concentrations (x_{NH_3}) under various pressure conditions.

IV.4.1. First study (Ph=7bar)

In this study, the low pressure (Pb = 1, 1.4 and 1.7 bar) was considered as a variable, while the high pressure (Ph = 7bar) was kept constant.

IV.4.1.1 For Pb = 1bar

The **Figure IV.3** illustrates the variation of the coefficient of performance (COP) as a function of the generator temperature (Tg) for a low-pressure of Pb=1bar and a high-pressure of Ph =7 bar.

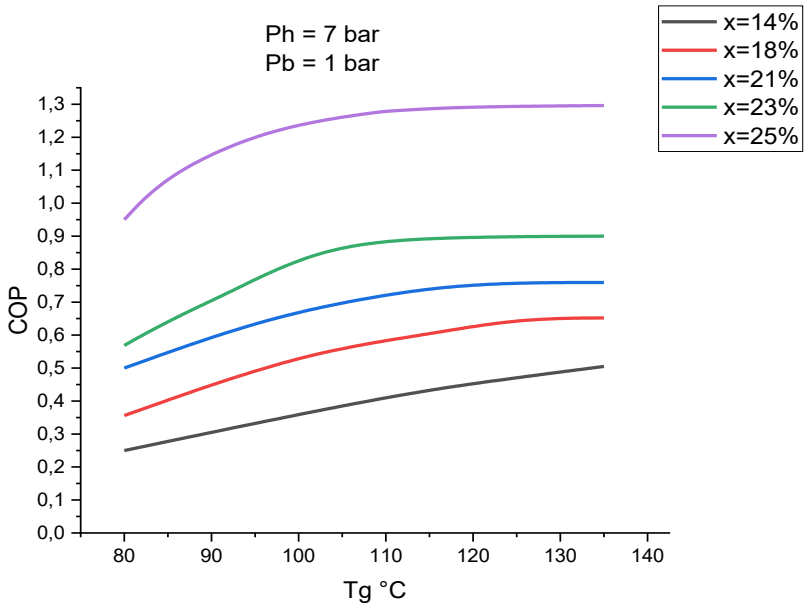


Figure IV. 3 COP variation with generator temperature for different refrigerant mass concentrations at Pb=1 bar, Ph=7bar

The COP start to increases from 0,25, 0,356, 0,504, 0,599 and 0,95 for the all ammonia concentrations (x_{NH_3}= 14%, 18%, 21%, 23% and 25%) respectively at Tg=80°C.
From the analysis of the figure, it is observed that for lower ammonia concentrations (14%, 18%, and 21%), the COP increases progressively as the generator temperature rises. In this range, the relationship between Tg and COP appears to be nearly proportional, indicating that increasing the generator temperature enhances the energy efficiency of the system. At Tg = 135; 125 and 120 °C, the corresponding COP values for x_{NH_3}= 14%, 18%, and 21% are 0.505, 0.652, and 0.7565, respectively.

However, as the ammonia concentration increases further (x = 23% and 25%), the system behaviour exhibits two distinct phases. In the first phase, the COP continues to increase with Tg, demonstrating that the absorption refrigeration cycle benefits from a higher generator temperature. However, in the second phase, a critical temperature threshold is reached, beyond which the COP no longer increases significantly and instead stabilizes.

This transition occurs at approximately Tg = 117 °C for x_{NH_3}= 23% and Tg = 114 °C for x_{NH_3} = 25%, where the system reaches an equilibrium state. At x_{NH_3}= 23%, the COP stabilizes at 0.8984, while for x_{NH_3}= 25%, the attained COP maximum values is 1.285.

Beyond this point, further increases in generator temperature do not provide substantial improvements in COP.

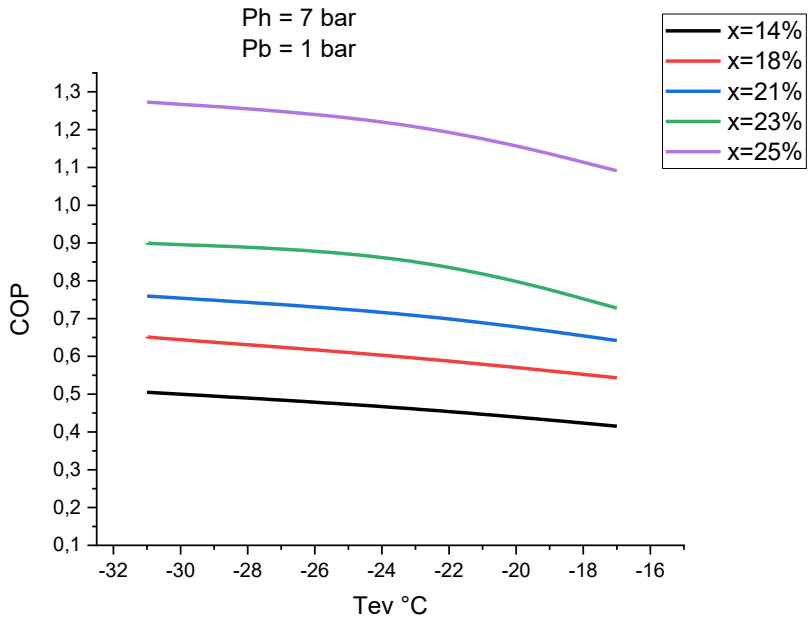


Figure IV. 4 COP variation with evaporator temperature for different refrigerant mass concentrations at Pb=1 bar, Ph=7 bar.

As for the **Figure IV.4**, illustrates the variation of the coefficient of performance (COP) as a function of the evaporator temperature (Tev) for different ammonia concentrations at an operating pressure of (Pb=1) bar.

The COP gradually decreases as Tev decreases, highlighting a decline in system efficiency at lower evaporation temperatures. This trend is expected since a lower Tev increases the energy demand of the absorption cycle, thereby reducing overall performance.

At (x=25%), the COP reaches its highest value, increasing from 1.098 at Tev= -17 °C to 1.285 at (Tev= -31°C), reinforcing the benefits of increased ammonia concentration. Similarly, at x_{NH_3} = 23%, the COP improves from 0.728 at Tev= -17 °C to 0.898 at Tev= -31°C.

Conversely, at lower ammonia concentrations, the COP remains significantly lower. For x=14%, the COP is only 0.415 at Tev=-17°C and 0.505 at Tev=-31°C, demonstrating reduced performance with a leaner ammonia solution. Similarly, at x_{NH_3} = 18%, the COP varies from 0.534 at Tev= -17°C to 0.652 at Tev = -31°C, while at x_{NH_3} =21%, it ranges from 0.642 to 0.759 for the same temperatures.

IV 4.1.2 For Pb = 1.4 bar

Figure IV.5 shows the influence of the generator temperature on the coefficient of performance (COP) of Pb = 1.4 bar for various ammonia mass fractions in the working solution. The results clearly indicate that both the generator temperature and the ammonia concentration strongly affect the system efficiency.

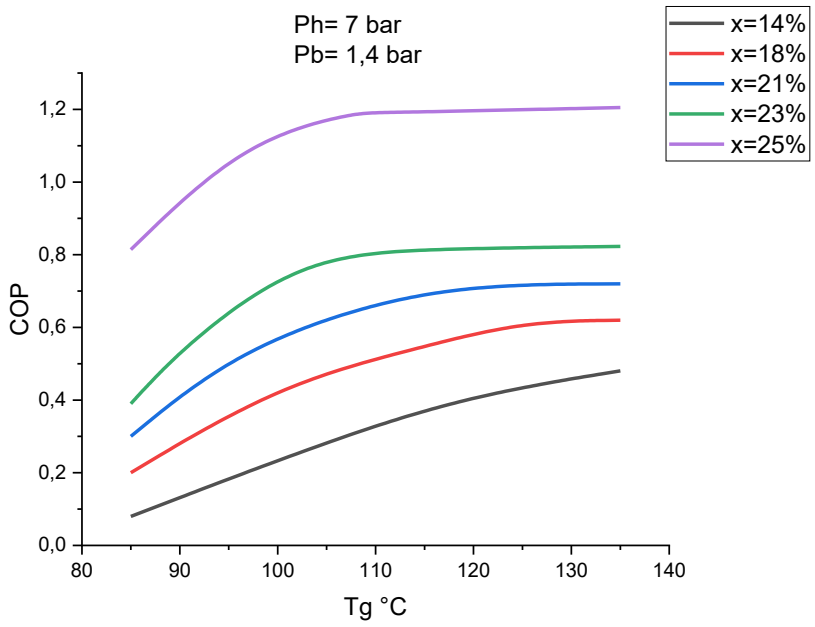


Figure IV. 5 COP variation with generator temperature for different refrigerant mass concentrations at Pb=1.4 bar, Ph=7bar

At Tg=85°C, the COP start to increases from 0.08, 0.202, 0.305, 0.390 and 0.814 for the all ammonia concentrations (x_{NH_3}= 14%, 18%, 21%, 23%and 25%) respectively.

At low ammonia concentrations (x_{NH_3} = 14%, 18%, and 21%), the COP exhibits a gradual increase with the generator temperature. This behavior suggests that the rise in thermal energy

supplied to the generator improves the ammonia desorption process, leading to better cooling performance. When the temperature of generator (Tg) between 120 to 135 °C, the COP values are 0.480, 0.620, and 0.720 for ammonia concentrations of 14%, 18%, and 21%, respectively.

For higher ammonia concentrations (x_{NH_3}= 23% and 25%), the system response can be divided into two operating zones. In the first zone, an increase in generator temperature leads to a noticeable enhancement in COP, indicating improved separation between ammonia and water. In the second zone, after a critical generator temperature is reached, the COP tends to level off and shows only minor variation with further temperature increase. This stabilization occurs around Tg ≈ 117 °C, where the COP reaches 0.817 for x_{NH_3} = 23%. For x_{NH_3} = 25%, a maximum COP of about 1.192 is obtained at Tg = 108 °C.

Beyond these temperatures, further heating of the generator does not significantly improve the system performance, suggesting that the absorption cycle operates near its optimal thermodynamic conditions and additional heat input leads to diminishing efficiency gains.

Figure IV.6 presents the variation of the coefficient of performance (COP) as a function of the evaporator temperature for different ammonia mass fractions at a low pressure of Pb = 1.4 bar and a high pressure of Ph = 7 bar.

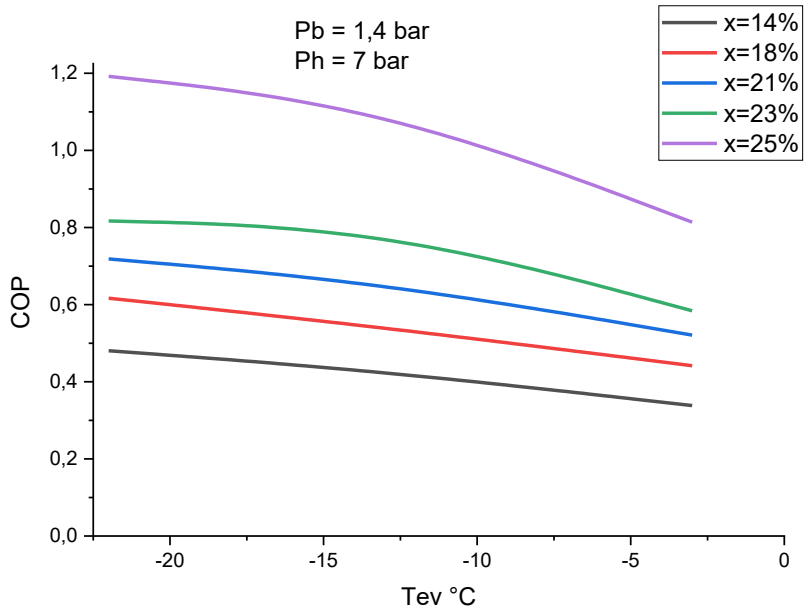


Figure IV. 6 COP variation with evaporator temperature for different refrigerant mass concentrations at Pb=1.4 bar, Ph=7 bar.

For all-ammonia concentrations, the COP decreases when the evaporator temperature increases. At x_{NH_3} = 14%, the COP decreases from 0.480 at Tev = −22 °C to 0.338 at Tev = −3 °C. A similar decreasing trend is observed for x_{NH_3}= 18%, where the COP decreases from 0.620 to 0.4415, and for x_{NH_3} = 21%, where it drops from 0.7185 to 0.521. This behavior is attributed to the reduction in the refrigeration effect and the increase in irreversibilities as the evaporator temperature rises.

For higher ammonia concentrations, the COP values remain significantly higher. At x_{NH_3} = 23%, the COP decreases from 0.817 at Tev = −22 °C to 0.584 at Tev = −3 °C. The maximum COP is obtained for x_{NH_3} = 25%, with values of 1.192 at Tev = −22 °C and 0.814 at Tev = −3 °C. These results indicate that increasing the ammonia concentration improves the thermodynamic performance of the system due to the higher refrigerant mass fraction and reduced solution circulation ratio.

IV.4.1.3. For Pb = 1.7 bar

The **Figure IV.7** presents the evolution of the coefficient of performance (COP) as a function of the generator temperature (Tg) for Pb = 1.7 bar.

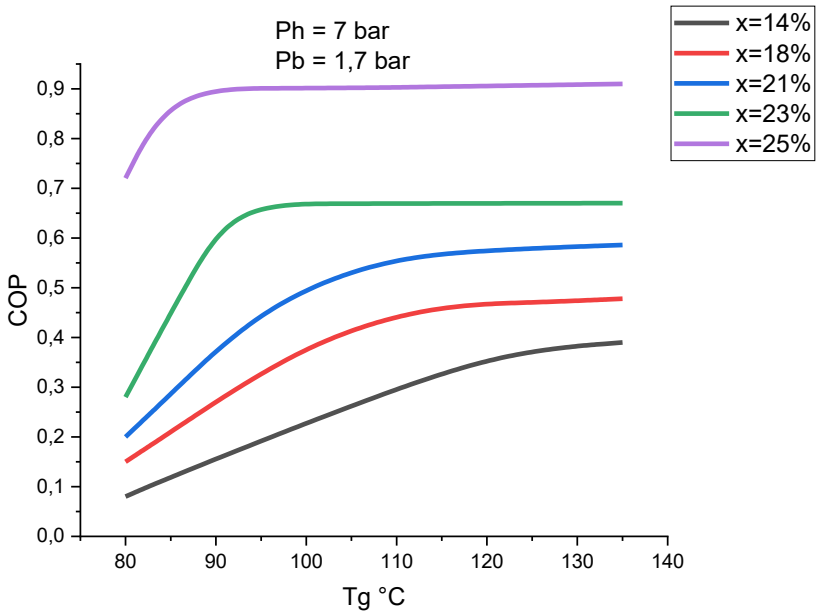


Figure IV. 7 COP variation with generator temperature for different refrigerant mass concentrations at Pb=1.7 bar, Ph=7bar

When Tg=80 °C, the COP start to increases from 0,081, 0,153, 0,206, 0,284 and 0,720 for the all-ammonia concentrations (x_{NH_3}= 14%, 18%, 21%, 23%and 25%) respectively.

For low ammonia concentrations (x_{NH_3} = 14%, 18%, and 21%), the COP increases progressively with the generator temperature, indicating an almost proportional relationship. For a Tg = 135, 130 and 135 °C, the COP reaches values of 0.39, 0.478, and 0.586 for ammonia concentrations of 14%, 18%, and 21%, respectively. This behaviour can be attributed to the enhancement of the desorption process in the generator, where higher thermal input increases the separation of ammonia from the solution, leading to a higher refrigerant mass flow rate and improved cooling capacity.

When the ammonia concentration is increased (x_{NH_3}= 23% and 25%), two distinct operating regimes are observed. In the first regime, the COP continues to rise with the generator temperature for all concentrations, confirming that the absorption refrigeration cycle benefits from increased thermal energy supplied to the generator. This phase corresponds to a region where the strong solution is effectively regenerated and the concentration difference between the strong and weak solutions increases.

In the second regime, beyond a critical generator temperature, the COP tends to stabilize and becomes nearly constant. This stabilization begins at approximately Tg = 95 °C for x_{NH_3} = 23%, where the COP reaches about 0.668, and at Tg = 87 °C for x_{NH_3} = 25%, where the COP attains a value of 0.9002. This behaviour indicates that the system approaches thermodynamic equilibrium, and further increases in generator temperature no longer improve ammonia–water separation. Additional heat mainly increases irreversibility without enhancing the refrigeration effect.

Figure IV.8 shows the influence of the evaporator temperature on the COP for various ammonia mass fractions at a boiler pressure of Pb = 1.7 bar.

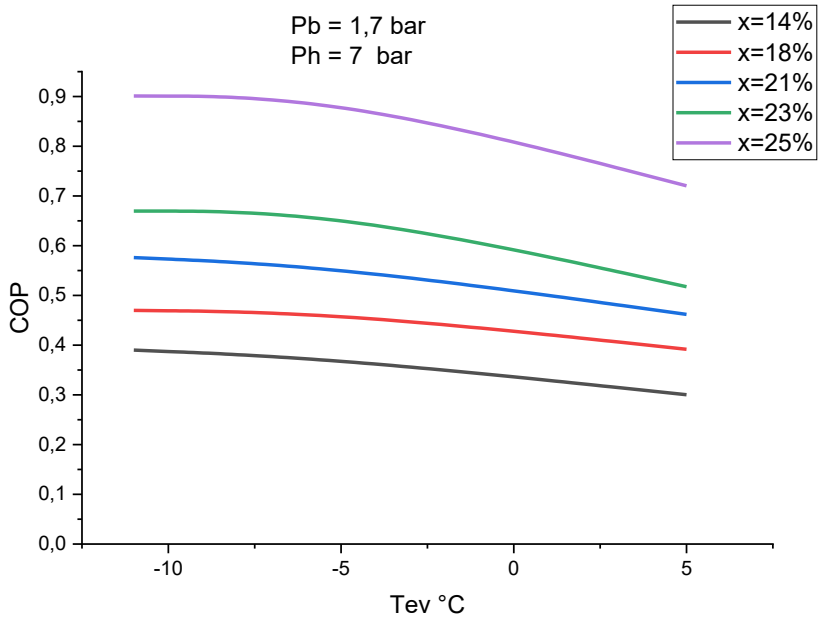


Figure IV. 8 COP variation with evaporator temperature for different refrigerant mass concentrations at Pb=1.7 bar, Ph=7 bar.

The COP decreases with increasing evaporator temperature for all ammonia concentrations. For x_{NH_3}= 14%, the COP decreases from 0.39 at Tev = −11 °C to 0.3002 at Tev = 5 °C. Similarly, for x_{NH_3}= 18%, the COP decreases from 0.47 to 0.3917, and for x_{NH_3}= 21%, it decreases from 0.5762 to 0.4619. This reduction in COP is related to the decrease in the cooling capacity and the increase in thermal irreversibilities at higher evaporator temperatures.

For higher ammonia concentrations, the COP values remain relatively high. At x_{NH_3} = 23%, the COP slightly decreases from 0.6697 at Tev = −11 °C to 0.6684 at Tev = 5 °C, while for x_{NH_3} = 25%, the COP changes marginally from 0.9025 to 0.7204 over the same temperature range. This weak dependence indicates that at high ammonia concentrations, the system operates close to optimal conditions and becomes less sensitive to evaporator temperature variations.

The following **Table IV.1** illustrates the suitable thermodynamic parameters for efficient generator operation for Ph = 7bar, emphasizing its importance in the absorption installation.

Table IV. 1 Best COP values for different pressures and concentrations for Ph=7 bar

Ph (bar)	7					
Pb (bar)	**1**		**1.4**		**1.7**	
x (%)	**COP**	**Tg** (°C)	**COP**	**Tg** (°C)	**COP**	**Tg** (°C)
14	0.505	135	0.480	135	0.390	135
18	0.652	125	0.620	130	0.4778	130
21	0.7565	120	0.720	120	0.586	125
23	0.8984	117	0.817	117	0.668	95
25	1.285	114	1.192	108	0.9002	87

IV.4.2. Second study (Ph=8bar)

In the second study, a parametric study was conducted by varying the low-pressure level (Pb = 1, 1.4, and 1.7 bar), whereas the high-pressure level was maintained constant at Ph = 8 bar.

IV.4.2.1. For Pb = 1bar

The **Figure IV.9** illustrates the variation of the COP as a function of the generator temperature (Tg) for Ph = 8 bar and different ammonia mass fractions in the NH_3/H_2O working solution.

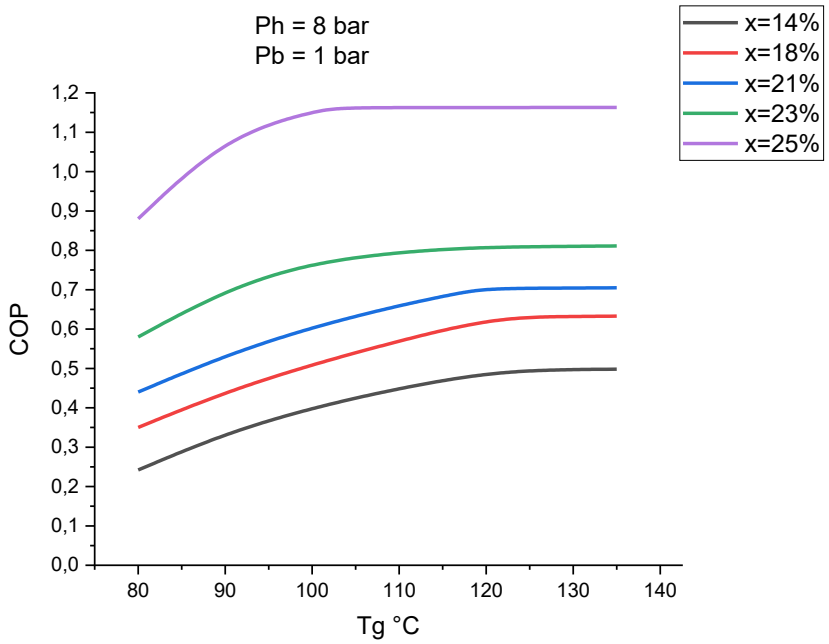


Figure IV. 9 COP variation with generator temperature for different refrigerant mass concentrations at Pb=1 bar, Ph=8bar

The COP start to increases from 0,242, 0,350, 0,441, 0,580 and 0,881 for the all ammonia concentrations (x_{NH_3}= 14%, 18%, 21%, 23%and 25%) respectively.

For low ammonia concentrations (x_{NH_3}= 14%, 18%, and 21%), the COP increases almost linearly with the generator temperature, indicating a proportional relationship between Tg and system performance. At a generator temperature (Tg) are 135, 130 and 120 °C, the COP values are 0.497, 0.632, and 0.703 for ammonia concentrations of 14%, 18%, and 21%, respectively. This trend

can be explained by the enhancement of the desorption process in the generator, where increasing thermal energy promotes the separation of ammonia from the aqueous solution, resulting in a higher refrigerant mass flow rate and improved cooling capacity.

As the ammonia concentration increases (x_{NH_3}= 23% and 25%), the system exhibits two distinct operating regimes. In the first regime, an increase in generator temperature leads to a corresponding increase in COP for all ammonia concentrations, confirming that the absorption cycle benefits from higher thermal input.

In the second regime, beyond a critical generator temperature, the COP tends to stabilize and becomes nearly constant. This behaviour is attributed to the saturation of the absorption cycle, where additional heat supplied to the generator does not significantly increase the ammonia desorption rate. The stabilization occurs beyond Tg ≈ 111.5 °C, where the COP reaches 0.799 for an ammonia concentration of 23%. For x_{NH_3} = 25%, the COP attains a value of 1.162 at Tg = 103 °C, indicating that the system reaches its optimal operating condition at lower generator temperatures for higher ammonia concentrations.

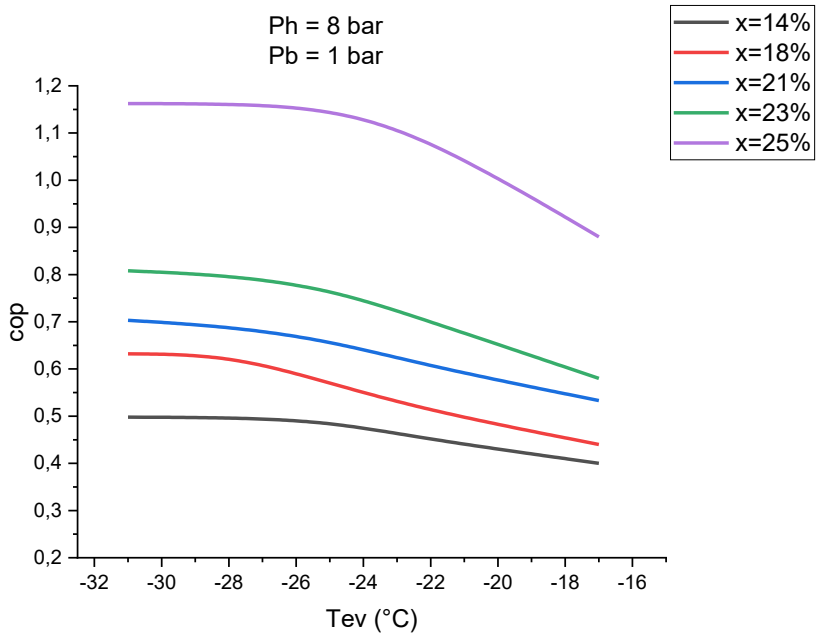


Figure IV. 10 COP variation with evaporator temperature for different refrigerant mass concentrations at Pb=1 bar, Ph=8 bar.

The **Figure IV.10** shows the evolution of the coefficient of performance (COP) as a function of the evaporator temperature (Tev) for different ammonia concentrations at an operating pressure of Ph = 8 bar.

The COP decreases progressively as the evaporator temperature (Tev) increases, indicating a decrease in the efficiency of the refrigeration system at higher evaporator temperatures.

This trend is expected, as an increase in Tev reduces the thermal differential required for the absorption cycle to operate correctly, thus impacting on system efficiency.

A higher ammonia concentration (x_{NH_3} = 23% and 25%) results in a higher COP for all Tev values, demonstrating better system performance with a more concentrated ammonia solution.

At x_{NH_3}=25%, the COP reaches a maximum value greater than 1.163 for the lowest evaporation temperatures (Tev = -31°C), confirming the improved performance with a higher concentration.

Conversely, at x_{NH_3}=14%, COP remains relatively low, not exceeding 0.5, indicating less efficient operation with low ammonia concentration. And about the other concentration 18%, 21% and 23%, the value of COP are 0.632, 0.7032 conversely and 0.799 at Tev=-31C°.

IV.4.2.2. For Pb = 1.4bar

Figure IV.11 illustrates the evolution of the COP as a function of the generator temperature (Tg) for different ammonia mass fractions (x_{NH_3} = 14%, 18%, 21%, 23%, and 25%) at Pb = 1.4 bar and Ph = 8 bar.

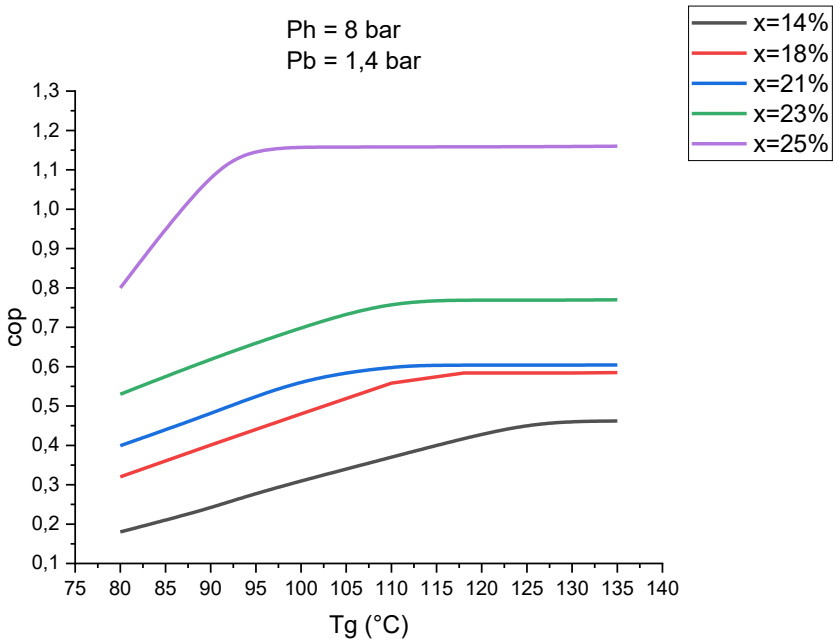


Figure IV. 11 COP variation with generator temperature for different refrigerant mass concentrations at Pb=1.4 bar, Ph=8bar

As the generator temperature increases, the COP increases for all concentrations.
At Tg = 80 °C, the COP values increase significantly with ammonia concentration. For example, for x = 14%, the COP rises from 0.18 to 0.4604 at Tg = 127 °C. Similarly, for x_{NH_3} = 18%, 21%, and 23%, the COP increases from 0.321, 0.399, and 0.532 to 0.5838, 0.6035, and 0.7681 at generator temperatures of 118, 114, and 110 °C, respectively. This behaviour is attributed to the enhancement of the desorption process in the generator, where higher thermal energy promotes ammonia separation from the aqueous solution, leading to an increased refrigerant flow rate and improved cooling capacity.
For the highest ammonia concentration (x_{NH_3}= 25%), the COP reaches a maximum value of 1.157 at Tg = 95 °C, which is significantly higher than the values obtained for lower concentrations and stabilization occurs beyond
Moreover, for high ammonia concentrations, the COP tends to stabilize at elevated generator temperatures, indicating that the system approaches a saturation regime. In this regime, additional heat supplied to the generator does not significantly increase ammonia desorption, and consequently, the COP improvement becomes marginal.

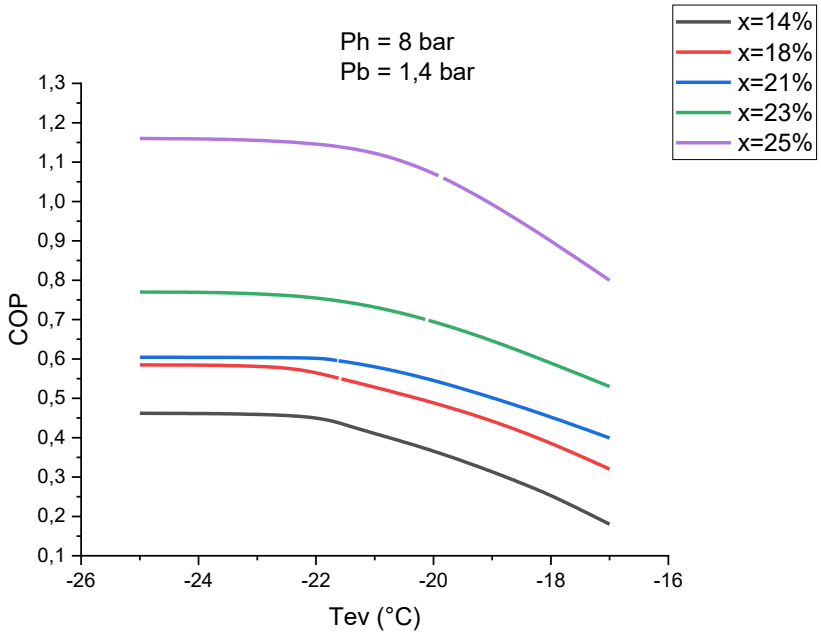


Figure IV. 12 COP variation with evaporator temperature for different refrigerant mass concentrations at Pb=1.4 bar, Ph=8 bar.

Figure IV.12 shows the variation of the COP as a function of the evaporator temperature (Tev) for different ammonia mass fractions (x_{NH_3} = 14%, 18%, 21%, 23%, and 25%) at Pb = 1.4 bar and Ph = 8 bar.

For all ammonia concentrations, the COP are relatively stable from Tev=-25 °C to -22°C, and after decreases when the evaporator temperature to −17 °C.

For instance, for x = 14%, the COP decreases from 0.4604 to 0.180. Similarly, for x_{NH_3} = 18%, 21% and 23% the COP decreases from 0.5839, 0.6035, 0.7681and 1.157 to 0.321, 0.399 and 0.532.

The highest performance is observed for x_{NH_3} = 25%, where the COP decreases from 1.157 at −25 °C to 0.842 at −17 °C.

Furthermore, for a given evaporator temperature, the COP increases significantly with ammonia concentration. Higher ammonia mass fractions reduce the solution circulation ratio and increase the refrigerant mass flow rate, leading to better thermodynamic efficiency of the absorption cycle.

IV.4.2.3. For Pb = 1.7bar

Figure IV.13 illustrates the variation of the coefficient of performance (COP) as a function of the generator temperature (Tg) for different ammonia mass fractions (x_{NH_3}= 14%, 18%, 21%, 23%, and 25%) at a high pressure of 8 bar and a low pressure of 1.7 bar.

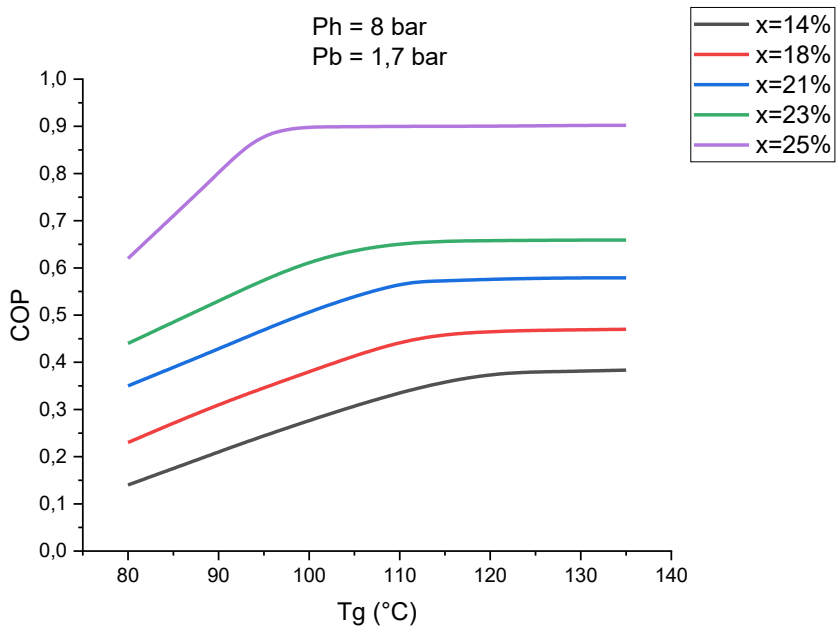


Figure IV. 13 COP variation with generator temperature for different refrigerant mass concentrations at Pb=1.7 bar, Ph=8bar

At a generator temperature of 80 °C, the COP values increase with ammonia concentration (x_{NH_3} = 14%, 18%, 21%, 23%, and 25%), where the values of COP are (0.14, 0.23, 0.35, 0.44 and 0,62) respectively.

Then the coefficient of performance (COP) begins to increases until it stabilizes relatively after the Tg=128°C, 118°C, 114°C and 110 °C for x_{NH_3} = 14%, 18%, 21% and 23% respectively.

For higher ammonia concentrations (x_{NH_3}=25%), two operating regions can be observed. In the first region, the COP increases rapidly to 0.898 at Tg = 95°C. In the second region, the COP tends to stabilize at higher generator temperatures, suggesting that the system approaches a saturation condition where additional heat input does not significantly increase the refrigerant mass flow rate.

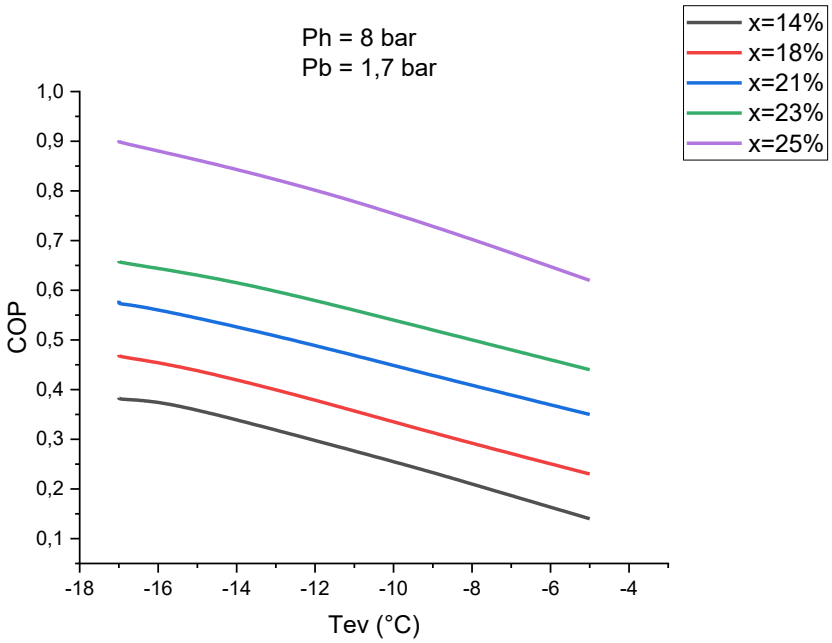


Figure IV. 14 COP variation with evaporator temperature for different refrigerant mass concentrations at Pb=1.7 bar, Ph=8 bar.

Figure IV.14 illustrates the influence of the evaporator temperature (Tev) on the coefficient of performance (COP) for various ammonia mass fractions (x_{NH_3} = 14%, 18%, 21%, 23%, and 25%) at Pb = 1.7 bar and Ph = 8 bar.

A general decline in COP is observed as Tev increases from −17 °C to −5 °C for all ammonia concentrations.

At Tev = −17 °C, the COP reaches 0.380, 0.466, 0.572, 0.656, and 0.898 for ammonia concentrations of 14%, 18%, 21% and 23%, respectively, while it decreases to 0.14, 0.233, 0.350 and 0.441, at Tev = −5 °C.

The highest COP values correspond to x_{NH_3} = 25%, with a decrease from 0.898 to 0.620 over the same temperature range.

These results show that lower evaporator temperatures improve system performance.

The COP is strongly influenced by both Tev and ammonia concentration, and the best performance is achieved with concentrated ammonia solutions operating at lower evaporator temperatures for Pb = 1.7 bar.

The **Table IV.2** shows the appropriate thermodynamic parameters for generator operation, including concentration, temperature, and pressure, which are critical for improving the overall system performance when Ph= 8 bar.

Table IV. 2 Best COP values for different pressures and concentrations for Ph=8 bar

Ph (bar)	8					
Pb (bar)	1		1.4		1.7	
X (%)	COP	Tg (°C)	COP	Tg (°C)	COP	Tg (°C)
14	0.497	135	0.4604	127	0.380	127
18	0.632	130	0.5838	118	0.466	118
21	0.7032	120	0.6035	114	0.572	114
23	0.799	111.5	0.7681	110	0.656	110
25	1.162	103	1.157	95	0.898	95

IV.4.1. Third study (Ph=10bar)

In the third study, a parametric analysis was performed by varying the low pressure (Pb = 1, 1.4, and 1.7 bar), while keeping the high-pressure constant at Ph = 10 bar.

IV.4.3.1. For Pb = 1bar

The **Figure IV.15** illustrates the evolution of the coefficient of performance (COP) as a function of the generator temperature (Tg) for a high pressure (Ph=10bar) and a low pressure (Pb=1bar), considering different ammonia concentrations (x_{NH_3}).

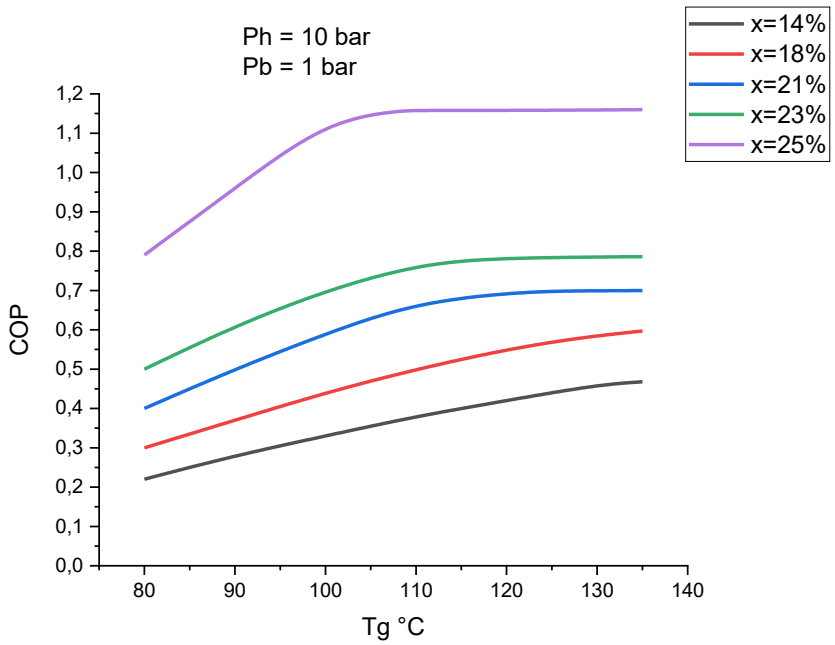


Figure IV. 15 COP variation with generator temperature for different refrigerant mass concentrations at Pb=1 bar, Ph=10 bar

For a generator temperature of 80 °C, an increase in the ammonia concentration in the working solution leads to a significant enhancement in system performance. The COP rises from 0.22 at (x_{NH_3}=14%) to 0.794 at (x_{NH_3}=25%), with intermediate values of 0.30, 0.401, and 0.52 for ammonia concentrations of 18 %, 21 %, and 23 %, respectively.

It can be observed that at lower concentrations, the COP increases progressively with the generator temperature. However, at higher temperatures, this increase slows down due to the thermodynamic limitations of the cycle. For instance, at x_{NH_3} = 21%, the COP reaches 0.698 at Tg = 122°C, while for x_{NH_3}= 18%, it is 0.597 at Tg = 130°C. Similarly, for x_{NH_3} = 14%, the COP decreases to 0.468 at Tg = 135°C.

At higher ammonia concentrations, the COP attains greater values. For x_{NH_3} = 23%, the COP reaches 0.782 at Tg = 118.2°C, while for x_{NH_3} = 25%, it peaks at 1.157 at Tg = 108°C. Initially, an increase in generator temperature (Tg) leads to a continuous improvement in COP. However, beyond these temperatures, the COP stabilizes, indicating a saturation effect where additional thermal energy no longer significantly enhances system efficiency.

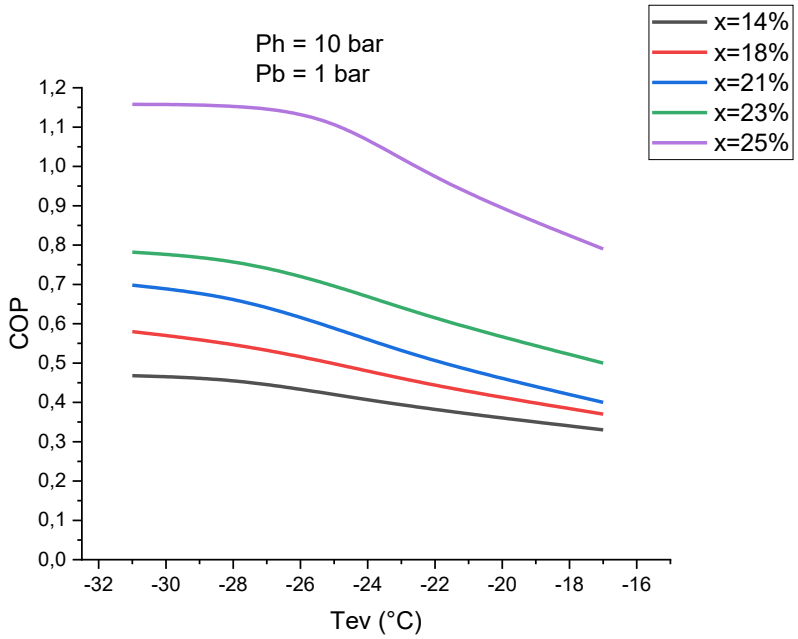


Figure IV. 16 COP variation with evaporator temperature for different refrigerant mass concentrations at Pb=1 bar, Ph=10 bar.

The **Figure IV.16** illustrates the variation of the coefficient of performance (COP) as a function of the evaporator temperature (Tev) for different ammonia concentrations at an operating pressure of Ph = 10 bar and Pb=1bar

The COP decreases as (Tev) increases, indicating a reduction in the efficiency of the refrigeration system at higher evaporator temperatures. This trend is expected, as an increase in Tev reduces the temperature difference between the evaporator and the generator, thereby enhancing heat transfer and cycle efficiency.

For the same evaporator temperature, a higher ammonia concentration (x_{NH_3} = 23% and 25%) results in a higher COP, indicating improved system performance.

At x_{NH_3} = 25%, the COP reaches a maximum value of 1.157 at Tev = -31°C, demonstrating increased efficiency compared to lower concentrations.

Conversely, at x_{NH_3} = 14%, the COP is significantly lower (0.468 at Tev = -31°C), reflecting reduced efficiency for lower ammonia concentrations.

And when the COP decrease where Tev = -17 °C, the valour are (0.33, 0.37, 0.40, 0.51 and 0.79) for the ammonia concentration (14%, 18%, 21%, 23% and 25%)
The decrease in COP with increasing Tev is explained by the decrease in the thermodynamic efficiency of the system.

IV.4.3.2. For Pb = 1.4 bar

Figure IV.17 shows the evolution of the coefficient of performance (COP) as a function of the generator temperature (Tg) for different ammonia mass fractions (x_{NH_3}= 14%, 18%, 21%, 23%, and 25%) at a high pressure of 10 bar and a low pressure of 1.4 bar.

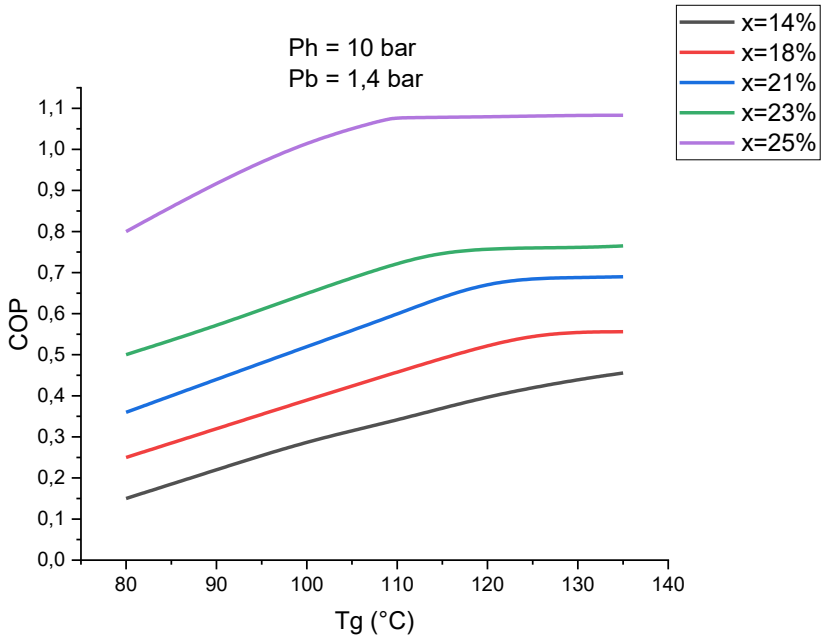


Figure IV. 17 COP variation with generator temperature for different refrigerant mass concentrations at Pb=1.4 bar, Ph=10 bar

At Tg = 80 °C, the COP increases with ammonia concentration, ranging from 0.15 for x_{NH_3} = 14% to 0.807 for x_{NH_3} = 25%, highlighting the positive effect of concentrated ammonia solutions on system efficiency. As the generator temperature rises, the COP improves for all concentrations. For x = 14%, the COP increases from 0.15 at Tg = 80 °C to 0.455 at Tg = 135 °C. Similarly, for x_{NH_3} = 18%, 21%, and 23%, the COP rises from 0.250, 0.360, and 0.501 at 80 °C to 0.555, 0.684, and 0.759 at generator temperatures of 127, 120, and 117 °C, respectively. The maximum COP is obtained for x_{NH_3} = 25%, reaching 1.075 at Tg = 109 °C and are tends to stabilize, which indicates that higher ammonia concentrations allow the system to achieve optimal performance at lower generator temperatures. Then are tends to stabilize, suggesting that the system approaches a saturation state where additional thermal input does not significantly increase the refrigerant mass flow rate.

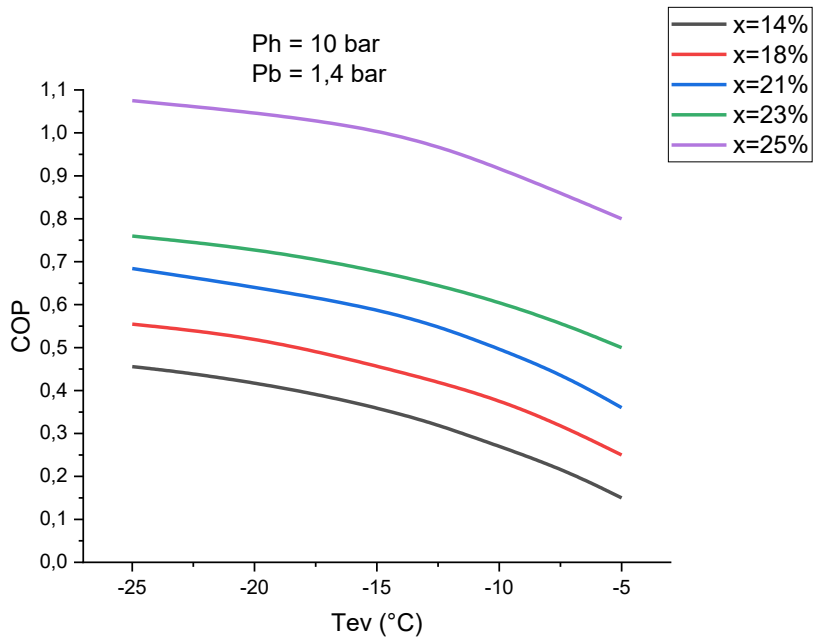


Figure IV. 18 COP variation with evaporator temperature for different refrigerant mass concentrations at Pb=1.4 bar, Ph=10 bar.

Figure IV.18 illustrates the variation of the coefficient of performance (COP) with the evaporator temperature (Tev) for different ammonia mass fractions (x_{NH_3} = 14%, 18%, 21%, 23%, and 25%) at a high pressure of 10 bar and a low pressure of 1.4 bar.

For all ammonia concentrations, the COP decreases as the evaporator temperature increases from −25 °C to −5 °C. When x_{NH_3} = 14%, the COP decreasing from 0.455 at Tev = −25 °C to 0.151 at Tev = −5 °C. A similar trend is observed for x = 18%, where the COP decreases from 0.455 to 0.254 over the same temperature range. For x_{NH_3} = 21% and x_{NH_3} = 23%, the COP decreases from 0.684 and 0.759 at −25 °C to 0.362 and 0.508 at −5 °C, respectively.

The highest performance is obtained for x_{NH_3} = 25%, with the COP decreasing from 1.057 at −25 °C to 0.802 at −5 °C.

This behaviour indicates that lower evaporator temperatures enhance the refrigeration effect and improve the driving force for mass and heat transfer in the evaporator and absorber.

IV.4.3.3. For Pb = 1.4 bar

The **Figure IV.19** illustrates the evolution of the coefficient of performance (COP) as a function of the generator temperature (Tg) for a high pressure (Ph=10bar) and an low pressure (Pb=1.7bar), considering different ammonia concentrations (x_{NH_3})

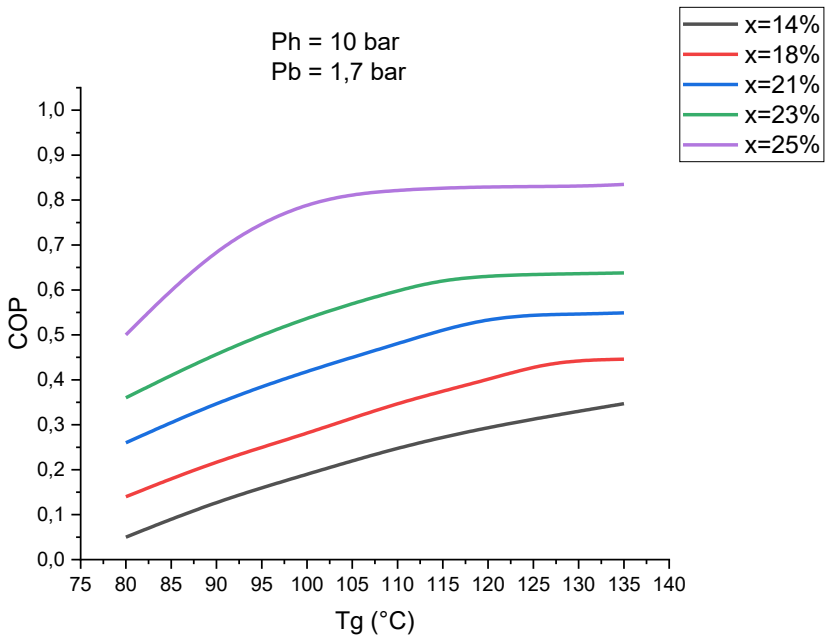


Figure IV. 19 COP variation with generator temperature for different refrigerant mass concentrations at Pb=1.7 bar, Ph=10 bar

For a generator temperature of 80 °C, an increase in the ammonia concentration in the working solution leads to a significant enhancement in system performance. The COP rises from 0.05 at (x_{NH_3}=14%) to 0.501 at (x_{NH_3}=25%), with intermediate values of 0.14, 0.26, and 0.36 for ammonia concentrations of 18 %, 21 %, and 23 %, respectively.

It can be observed that at lower concentrations, the COP increases progressively with the generator temperature.

For instance, at x= 11%, the COP reaches 0.374 at Tg = 135°C, while for x_{NH_3}= 18%, it is 0.442 at Tg = 127°C.

Also for x_{NH_3}=21% and 23% the COP increases but then this increase slows down due to the thermodynamic limitations of the cycle, at Tg= 120°C, 117°C when the valour of COP are 0.543 and 0.632, respectively.

And at higher ammonia concentrations (x_{NH_3}=25%), the COP stabilizes early when the valour are 0.823 at lower temperature of generator Tg = 109 °C for other concentrations, indicating a saturation effect where additional thermal energy no longer significantly enhances system efficiency.

Although increasing the ammonia concentration enhances the COP, the improvement becomes marginal at high generator temperatures. This behaviour reveals the existence of an optimal generator temperature for achieving maximum system performance.

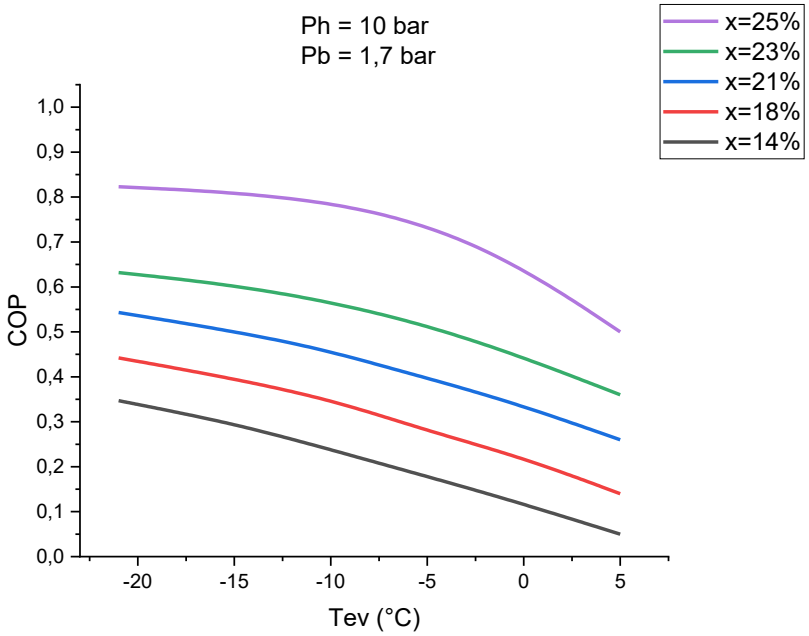


Figure IV. 20 COP variation with evaporator temperature for different refrigerant mass concentrations at Pb=1.7 bar, Ph=10 bar.

Figure IV.20 illustrates the variation of the coefficient of performance (COP) with the evaporator temperature (Tev) for different ammonia concentrations x_{NH_3}= 14%, 18%, 21%, 23%, and 25%) at a high pressure of 10 bar and a low pressure of 1.7 bar.

For all ammonia concentrations, the COP decreases as the evaporator temperature increases from −21 °C to 5 °C. When x_{NH_3} = 14%, the COP decreasing from 0.374 at Tev = −21 °C to Lowest value 0.05 at Tev = −5 °C compared to all concentrations.

A similar trend is observed for x_{NH_3} = 18%, 21% and 23% where the COP decreases from 0.442, 0.543 and 0.632 to 0.14, 0.26 and 0.36, respectively, from Tev = -21°C to 5°C.

At the highest value of the coefficient of performance (COP) at x_{NH_3} = 25%, the COP decreases slowly from 0.823 at Tev=-21°C, then after -5°C it accelerates its decline until it reaches 0.501 at Tev=5°C.

The **Table IV.3** summarizes the optimal thermodynamic operating parameters at the generator level when Ph= 10bar (ammonia concentration, temperature, and pressure), which play a crucial role in ensuring efficient operation of the absorption refrigeration system.

Table IV. 3 Best COP values for different pressures and concentrations for Ph=10 bar

Ph (bar)	**10**					
Pb (bar)	**1**		**1.4**		**1.7**	
X (%)	**COP**	**Tg (°C)**	**COP**	**Tg (°C)**	**COP**	**Tg (°C)**
14	0.468	135	0.4556	135	0.374	135
18	0.597	130	0.5547	127	0.442	127
21	0.698	122	0.6841	120	0.543	120
23	0.782	118.2	0.7598	117	0.632	117
25	1.157	108	1.075	109	0.823	109

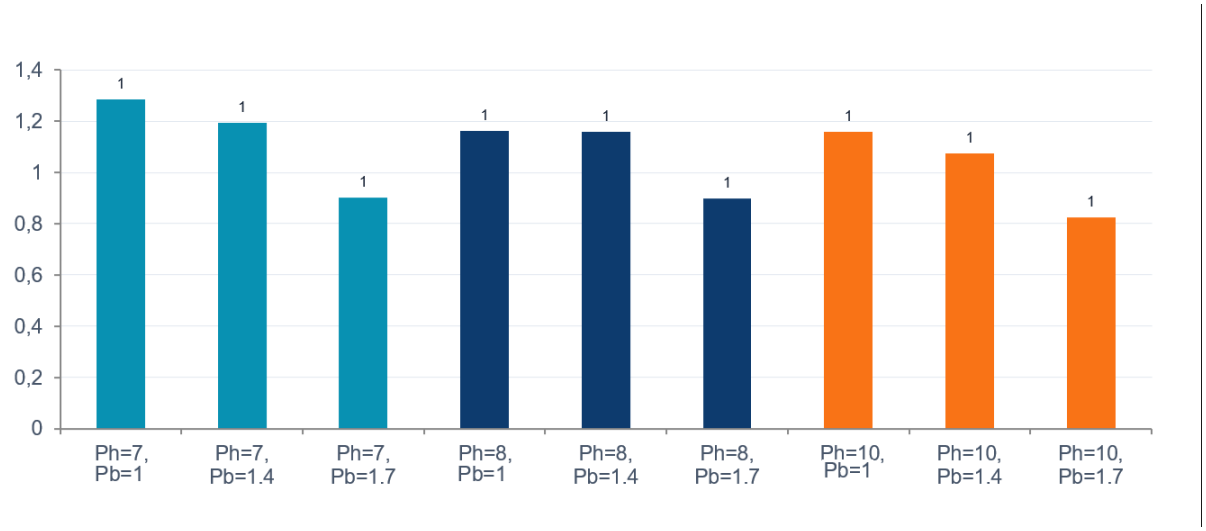


Figure IV. 21 Effect of High Pressure (Ph) on Maximum COP — x = 25%

The **Figure IV.21** illustrates the effect of high pressure on maximum COP for x = 25%, where at a fixed ammonia mass concentration of x=25%, the high pressure (Ph) has a clear negative effect on the maximum COP: Ph=7 bar yields the highest COP of 1.285 (at Pb=1 bar), making it the best overall configuration, while increasing Ph to 8 bar lowers the COP to 1.162 (at Pb=1 bar), a drop of about 9.6% compared to Ph=7 bar, and Ph=10 bar gives a very similar COP of 1.157 (at Pb=1 bar), showing that the COP plateaus and becomes largely insensitive to further increases in Ph beyond 8 bar. The chart also shows that, for every Ph level, the COP consistently decreases as the low pressure (Pb) increases from 1 to 1.4 to 1.7 bar, confirming that operating at the lowest available Pb is preferable for maximizing performance regardless of the chosen Ph.

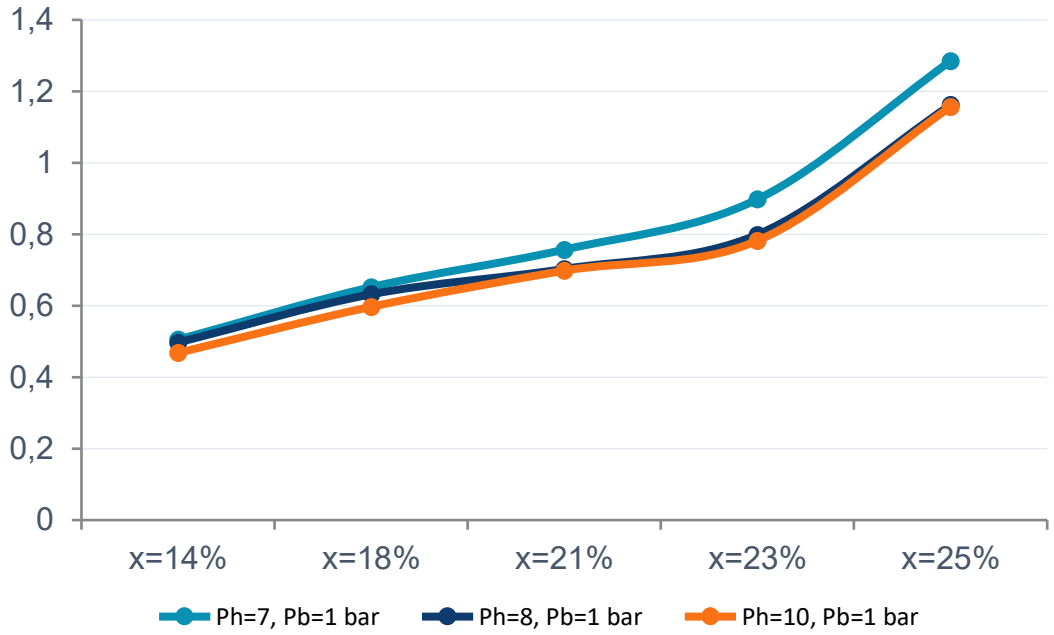


Figure IV. 22 Effect of Ammonia Mass Concentration on COP

As shown in the **Figure IV.22**, the COP increases steadily with the ammonia mass concentration (x) across all three pressure levels (Ph=7, 8, and 10 bar, with Pb=1 bar fixed), rising from around 0.47–0.50 at x=14% to between 1.17 and 1.29 at x=25%, with the most significant jump

occurring between x=23% and x=25%. This improvement is largely explained by the fact that a higher x reduces the solution circulation ratio (the mass of solution required per kg of refrigerant), which improves thermodynamic efficiency. Based on these results, x=25% is identified as the optimal concentration in this study, since further increases could raise pressure constraints and associated safety issues. Notably, the positive effect of concentration on COP is consistent across all pressure levels, with the lowest pressure (Ph=7 bar) consistently yielding the highest COP and the curves converging closely between x=18% and x=23% before diverging again at x=25%.

IV.5. Model validation

To assess the accuracy and reliability of our developed models, the obtained results were compared with coefficient of performance (COP) values reported in prior research.

Wei Wu et al. [133] carried out an experimental study on a compression-assisted absorption heat pump employing the ammonia–water working pair. The findings revealed a significant coefficient of performance (COP) of 1.271 under conditions where the generator temperature was maintained at 115 °C and the evaporator temperature at -10 °C.

In another study, Al-Rbaihat et al. [134] reported a maximum COP of 0.8483 under optimized operating conditions. The study considered a generator pressure of Ph = 14.5 bar, an evaporator pressure of Pb = 2.8 bar, a generator temperature (Tg) of 135 °C, and an evaporator temperature (Tev) of -6 °C. These results highlight the importance of precise control of temperatures and pressures in improving the overall efficiency of the system.

And also, Khan et al. [135] reported a COP of 0.8 based on the first law of thermodynamics. Their system operated optimally at a generator temperature of 120 °C and an evaporator temperature of -2.2 °C.

Predicted COP values align closely with literature. Deviation < 3% in all cases, validating the reliability and accuracy of the developed thermodynamic model.

These comparative studies highlight the influence of thermal conditions and system parameters on the thermodynamic performance of refrigeration systems, providing a meaningful reference framework for evaluating the results derived from our model.

IV.6 Conclusion

The thermodynamic study of the single-effect NH_3/H_2O solar absorption refrigeration system reveals that system performance is strongly influenced by key operating parameters, including ammonia concentration, generator temperature, evaporator temperature, and the high- and low-pressure levels.

These results demonstrate that increasing the ammonia concentration generally improves the coefficient of performance (COP), with the highest values achieved for $x_(NH_3)$ = 25%. However, this improvement exhibits diminishing returns beyond a critical generator temperature, indicating the existence of an optimal operating range for maximum efficiency.

The COP increases with generator temperature for all pressure levels, particularly at moderate ammonia concentrations, due to enhanced desorption and higher refrigerant mass flow rates. Conversely, at higher concentrations, the COP tends to stabilize after a threshold temperature, reflecting a thermodynamic saturation of the absorption cycle. Evaporator temperature shows an inverse relationship with COP: lower Tev values enhance cooling performance by increasing the temperature differential and driving mass transfer, whereas higher Tev reduces the cycle efficiency.

Comparative analysis with literature confirms the validity of the developed model, with predicted COP values aligning closely with experimental and theoretical studies. Parametric analysis across different high-pressure levels (Ph = 7, 8, 10 bar) and low-pressure levels (Pb = 1, 1.4, 1.7 bar) identifies optimal operating conditions that balance thermal input, solution concentration, and pressure constraints to maximize performance.

In summary, the study provides a comprehensive understanding of the operational behaviour of NH_3/H_2O solar absorption systems single effect, highlighting that careful selection of ammonia concentration, generator and evaporator temperatures, and operating pressures is essential to achieve high thermodynamic efficiency and reliable system performance under varying solar conditions.

General conclusion

General conclusion

This thesis presents a comprehensive thermodynamic investigation aimed at improving the performance and energy efficiency of solar-driven absorption refrigeration systems using the ammonia–water (NH_3–H_2O) working pair. The research focused on the development of a detailed mathematical model, implemented under Engineering Equation Solver (EES), to analyze the behavior of a single-effect absorption refrigeration cycle under various operating conditions. Particular attention was given to the influence of generator temperature, evaporator temperature, absorber and condenser pressures, and ammonia mass concentration on system performance.
Through systematic parametric analysis and thermodynamic interpretation, this work identifies optimal operating regions that enhance system stability and maximize the coefficient of performance (COP). The combination of theoretical modeling and comparison with literature data has provided reliable insights for the practical design and optimization of solar absorption refrigeration systems suitable for medium-temperature solar applications, particularly in high solar potential regions.
The main key outcomes and findings derived from the present research work can be summarized as follows:

Solar resource and system suitability
- High solar irradiation levels make solar-driven absorption refrigeration technically feasible and energetically attractive.
- Single-effect absorption systems are well adapted to medium-temperature solar collectors due to their moderate generator temperature requirements (90–120°C).
- Solar absorption refrigeration represents an environmentally sustainable alternative to conventional vapor compression systems by reducing electrical demand and greenhouse gas emissions.

Thermodynamic modeling and validation
- A steady-state thermodynamic model of a single-effect NH_3–H_2O absorption refrigeration system was successfully developed and solved using EES.
- The model allowed accurate calculation of thermodynamic states, mass flow rates, energy balances, and performance indicators.
- The predicted COP values ranged approximately between 0.8 and 1.285, which are consistent with literature data, confirming the validity and reliability of the developed model.

Effect of generator temperature
- The COP increases with generator temperature up to an optimal value, beyond which it stabilizes.
- At elevated generator temperatures, additional heat input mainly increases thermodynamic irreversibility rather than significantly improving refrigeration capacity.
The optimal generator temperature decreases as ammonia mass concentration increases, indicating improved desorption efficiency at higher refrigerant fractions.

Effect of ammonia mass concentration

- Ammonia mass concentration strongly influences system performance and internal circulation ratio.
- Increasing ammonia concentration within the studied range improves COP by reducing the required generator heat per unit of refrigerant produced.
- However, excessive ammonia concentration may increase system pressure levels and operational constraints; therefore, reducing the ammonia mass concentration to an optimal range ensures balanced performance, system stability, and safe operation.
- An optimal concentration region around 25% was identified under the investigated operating conditions.

Effect of evaporator temperature and pressure levels

- Increasing evaporator temperature was observed to decrease the COP under the investigated operating conditions.
- This behavior is attributed to the modification of the low-pressure level and the ammonia–water equilibrium state, which reduces the concentration difference between the strong and weak solutions and increases the circulation ratio.
- As a result, the required generator heat input increases relative to the refrigeration effect, leading to a reduction in overall system performance.
- Higher absorber (low-side) pressure slightly reduces the maximum achievable COP.
- The best performance region was obtained at:

High pressure ≈ 7 bar
Low pressure ≈ 1 bar
Ammonia concentration ≈ 25%
Generator temperature ≈ 110–115°C
Under these conditions, the maximum COP reached approximately 1.285.

Overall Contribution

- The study demonstrates the existence of optimal thermodynamic operating regions for solar-driven NH_3–H_2O absorption systems.
- The results highlight that performance improvement does not depend solely on increasing ammonia concentration, but rather on carefully adjusting and, when necessary, reducing the ammonia mass concentration to achieve thermodynamic balance and operational reliability.
- The presented parametric analysis provides practical guidelines for the design and optimization of solar absorption refrigeration systems in regions with high solar potential.

Perspectives and Future Work

Although the present study provides a detailed thermodynamic analysis of a single-effect NH_3/H_2O solar absorption refrigeration system, several research directions may further enhance system performance and practical implementation:

- Dynamic modeling

The current work is based on steady-state analysis. Future research may focus on dynamic modeling to evaluate transient behavior under variable solar irradiation and ambient conditions, especially for real climatic conditions in Algeria.

- Experimental validation

The development of a pilot-scale experimental setup would allow validation of the numerical results and provide deeper insight into real system losses, heat transfer limitations, and operational constraints.

- Exergy analysis

A detailed exergy study could identify the main sources of irreversibility within system components (generator, absorber, condenser and evaporator) and support further thermodynamic optimization.

- Economic optimization

A techno-economic analysis considering investment cost, payback period, and life-cycle assessment would strengthen the feasibility study for industrial and commercial applications.

- Advanced control strategies

Future work may investigate intelligent control systems to regulate generator temperature, pressure levels, and ammonia mass concentration in order to maintain optimal performance under fluctuating solar conditions.

- Integration with advanced solar collectors

Coupling the absorption system with high-efficiency evacuated tube or concentrating solar collectors may improve thermal supply stability and extend operating range.

- Reduction and optimization of ammonia mass concentration

Further investigation into adjusting and optimizing ammonia mass concentration could improve system safety, reduce pressure constraints, and enhance long-term operational stability without significantly compromising performance.

Final Closing Sentence

In conclusion, this research establishes a solid thermodynamic foundation for the optimization of solar-driven NH_3–H_2O absorption refrigeration systems and opens the way for further developments toward efficient, sustainable, and economically viable solar cooling technologies.

References

1. Laine, H.S., Salpakari, J., Looney, E.E., Savin, H., Peters, I.M., Buonassisi, T.: Meeting Global Cooling Demand with Photovoltaics during the 21st Century. Energy Environ. Sci. 12, 2706–2716 (2019). https://doi.org/10.1039/C9EE00002J
2. Net Zero by 2050 – Analysis, https://www.iea.org/reports/net-zero-by-2050
3. The Future of Cooling – Analysis, https://www.iea.org/reports/the-future-of-cooling
4. Laboratory (CSL), N.C.S.: Scientific Assessment of Ozone Depletion 2018: Executive Summary, https://csl.noaa.gov/assessments/ozone/2018/executivesummary/#section-4
5. Akbari, H., Pomerantz, M., Taha, H.: Cool surfaces and shade trees to reduce energy use and improve air quality in urban areas. Sol. Energy. 70, 295–310 (2001). https://doi.org/10.1016/S0038-092X(00)00089-X
6. Siddiqui, M.U., Said, S.A.M.: A review of solar powered absorption systems. Renew. Sustain. Energy Rev. 42, 93–115 (2015). https://doi.org/10.1016/j.rser.2014.10.014
7. Aliane, A., Abboudi, S., Seladji, C., Guendouz, B.: An illustrated review on solar absorption cooling experimental studies. Renew. Sustain. Energy Rev. 65, 443–458 (2016). https://doi.org/10.1016/j.rser.2016.07.012
8. Derghout, Z., Ziani, L., Gherfi, A., Rouag, D.: Performance and energy saving evaluation of solar absorption refrigeration systems in northeastern algeria. Int. J. Innov. Technol. Soc. Sci. (2024). https://doi.org/10.31435/ijitss.4(44).2024.2987
9. Said, S.A.M., Spindler, K., El-Shaarawi, M.A., Siddiqui, M.U., Schmid, F., Bierling, B., Khan, M.M.A.: Design, construction and operation of a solar powered ammonia–water absorption refrigeration system in Saudi Arabia. Int. J. Refrig. 62, 222–231 (2016). https://doi.org/10.1016/j.ijrefrig.2015.10.026
10. SIERES, J. et FERNÁNDEZ-SEARA, J. Evaluation of the column components size on the vapour enrichment and system performance in small power NH_3–H_2O absorption refrigeration machines. *International Journal of Refrigeration*, 2006, vol. 29, n° 4, p. 579–588.
11. Chikh, M.E.A., Benramdane, M., Aliane, A., Abdesselam, B.: Impact of ammonia-water concentrations on solar absorption refrigeration performance. Renew. Energy Sustain. Dev. 11, 72–84 (2025). https://doi.org/10.21622/resd.2025.11.1.1223
12. Goswami, D.Y., Kreith, F., Kreider, J.F.: Principles of Solar Engineering, Second Edition. CRC Press, Philadelphia, PA (2000)
13. Solar Radiation Resource: Measurement, Modeling, and Methods. 176–212 (2022). https://doi.org/10.1016/B978-0-12-819727-1.00101-1
14. Golubets, D., Voropay, N., Dyukarev, E., Aslamov, I.: Evaluation of Cloud Fraction Data for Modelling Daily Surface Solar Radiation: Application to the Lake Baikal Region. Atmosphere. 16, (2025). https://doi.org/10.3390/atmos16121405
15. Chekirou, W.: Etude Et Analyse D'une Machine Frigorifique Solaire À Adsorption, Doctorat these, (2008)
16. Duffie, J.A., Beckman, W.A.: Solar Engineering of Thermal Processes. Wiley (1991)
17. Kalogirou, S.A.: Solar Energy Engineering: Processes and Systems. ScienceDirect (2014)

18. Iqbal, M.: An Introduction to Solar Radiation. , University of British Columbia, Canada (1983)
19. Mamajek, E.E., Prsa, A., Torres, G., Harmanec, P., Asplund, M., Bennett, P.D., Capitaine, N., Christensen-Dalsgaard, J., Depagne, E., Folkner, W.M., Haberreiter, M., Hekker, S., Hilton, J.L., Kostov, V., Kurtz, D.W., Laskar, J., Mason, B.D., Milone, E.F., Montgomery, M.M., Richards, M.T., Schou, J., Stewart, S.G.: IAU 2015 Resolution B3 on Recommended Nominal Conversion Constants for Selected Solar and Planetary Properties, http://arxiv.org/abs/1510.07674, (2015)
20. Przystupa, K.: Selected aspects of electricity generation in a private photovoltaic installation. MATEC Web Conf. 252, 01004 (2019). https://doi.org/10.1051/matecconf/201925201004
21. Wald, L.: Solar Radiation Energy (Fundamentals).
22. NA: Chapter 3: Fundamentals of Solar Energy and Solar Radiation. (2000)
23. Reda, I., Andreas, A.: Solar Position Algorithm for Solar Radiation Applications (Revised). (2008)
24. Holbrow, C.H.: Build your own analemma, http://arxiv.org/abs/1302.0765, (2013)
25. An Introduction to Solar Geometry for Solar Cell Optimization - Technical Articles, https://eepower.com/technical-articles/an-introduction-to-solar-geometry-for-solar-cell-optimization/
26. Vician, P., Palacka, M., Ďurčanský, P., Jandačka, J.: Determination of Optimal Position of Solar Trough Collector. Procedia Eng. 192, 941–946 (2017). https://doi.org/10.1016/j.proeng.2017.06.162
27. Thorstensen, J.: Coordinates, time, and the sky.
28. Fraknoi, A., Morrison, D., Wolff, C.: Astronomy 2e. (2016)
29. Brownson, F.: Solar Resource Assessment and Economics, https://courses.ems.psu.edu/eme810/node/484
30. Rueda, J.A., Ramírez, S., Sánchez, M.A., Guerrero, J. de D., Rueda, J.A., Ramírez, S., Sánchez, M.A., Guerrero, J. de D.: Sun Declination and Distribution of Natural Beam Irradiance on Earth. Atmosphere. 15, (2024). https://doi.org/10.3390/atmos15081003
31. Szokolay, S.V.: Solar geometry. PLEA, Department of Architecture, The University of Queensland Brisbane 4072 (1996)
32. Zidani, C.: Conception et modélisation des systèmes photothermiques. Applications aux systèmes photothermiques alimentés par fibres optiques, https://dspace.univ-tlemcen.dz/handle/112/2300, (2012)
33. Bernard, R., MENGUY, G., Schwartz, M.: Le rayonnement solaire, Conversion thermique et applications, https://scholar.google.com/scholar?hl=en&as_sdt=0%2C5&q=%5B27%5D%09R.Bernard%2C+G.+Menguy+et+M.+Schwartz%2C+%E2%80%98Le+rayonnement+solaire%2C+Conversion+thermique+et+applications%27&btnG=
34. Angle horaire | Association Méridienne, http://www.meridienne.org/atelier/glossaire/angle-horaire/
35. Jean, M.: Conversion thermique du rayonnement solaire. AFME (Agence française pour la maîtrise de l'énergie), France (1975)

36. Ghrici, A.: Contribution à l'optimisation de l'efficacité énergétique des systèmes frigorifiques à Adsorption solaires, Doctorate thesis, http://dspace1.univ-tlemcen.dz//handle/112/20176, (2023)
37. Bekkouche, S.M.E.A.: Modelisation du comportement thermique de quelques dispositifs solaires., https://dspace.univ-tlemcen.dz/handle/112/4381, (2014)
38. Daguenet, M.: Les Séchoirs solaires: théorie et pratique. UNESCO (1985)
39. Vasar, C., Prostean, O., Prostean, G.: Evaluating solar radiation on a tilted surfaces - a study case in Timis (Romania). IOP Conf. Ser. Mater. Sci. Eng. 106, 012026 (2016). https://doi.org/10.1088/1757-899X/106/1/012026
40. Yettou, F.: Conception et réalisation d'un système de cuisson solaire destiné au site saharien (Ghardaïa, Algérie), Doctorate thesis, https://fr.scribd.com/document /825238241/Elec-Yettou-Fatiha-2-1, (2015)
41. de Simón-Martín, M., Alonso-Tristán, C., González-Peña, D., Díez-Mediavilla, M.: New device for the simultaneous measurement of diffuse solar irradiance on several azimuth and tilting angles. Sol. Energy. 119, 370–382 (2015). https://doi.org/10.1016/j.solener.2015.06.001
42. Hadj Ammar, A.M.: Étude et dimensionnement d'un réfrigérateur solaire à adsorption dans la région saharienne d'Algérie, http://dspace.univ-ouargla.dz/jspui/handle/123456789/23480, (2020)
43. Lenzen, M.: Current State of Development of Electricity-Generating Technologies: A Literature Review. Energies. 3, 462–591 (2010). https://doi.org/10.3390/en3030462
44. Bouraiou, A., Necaibia, A., Boutasseta, N., Mekhilef, S., Dabou, R., Ziane, A., Sahouane, N., Attoui, I., Mostefaoui, M., Touaba, O.: Status of renewable energy potential and utilization in Algeria. J. Clean. Prod. 246, 119011 (2020). https://doi.org/10.1016/j.jclepro.2019.119011
45. Riva Nanda I., Agung Pambudi N., Aziz M.,: Review on the Progress of Solar Water Heaters and Their Future Perspectives - 2023 - Energy Technology - Wiley Online Library, https://onlinelibrary.wiley.com/doi/10.1002/ente.202300191?utm_medium=article&utm_source=researchgate.net
46. Ab Kadir, M.Z.A., Rafeeu, Y., Adam, N.M.: Prospective scenarios for the full solar energy development in Malaysia. Renew. Sustain. Energy Rev. 14, 3023–3031 (2010). https://doi.org/10.1016/j.rser.2010.07.062
47. Infante Ferreira, C., Kim, D.-S.: Techno-economic review of solar cooling technologies based on location-specific data. Int. J. Refrig. 39, 23–37 (2014). https://doi.org/10.1016/j.ijrefrig.2013.09.033
48. Marzouk, O.A.: Solar Heat for Industrial Processes (SHIP): An Overview of Its Categories and a Review of Its Recent Progress. Solar. 5, (2025). https://doi.org/10.3390/solar5040046
49. Evangelisti, L., De Lieto Vollaro, R., Asdrubali, F.: Latest advances on solar thermal collectors: A comprehensive review. Renew. Sustain. Energy Rev. 114, 109318 (2019). https://doi.org/10.1016/j.rser.2019.109318
50. Almasri, R.A., Abu-Hamdeh, N.H., Esmaeil, K.K., Suyambazhahan, S.: Thermal solar sorption cooling systems - A review of principle, technology, and applications. Alex. Eng. J. 61, 367–402 (2022). https://doi.org/10.1016/j.aej.2021.06.005

51. Sarbu, I., Sebarchievici, C.: Review of solar refrigeration and cooling systems. Energy Build. 67, 297–308 (2013). https://doi.org/10.1016/j.enbuild.2013.08.022
52. Kalkan, N., Young, E.A., Celiktas, A.: Solar thermal air conditioning technology reducing the footprint of solar thermal air conditioning. Renew. Sustain. Energy Rev. 16, 6352–6383 (2012). https://doi.org/10.1016/j.rser.2012.07.014
53. Choudhury, B., Chatterjee, P.K., Sarkar, J.P.: Review paper on solar-powered air-conditioning through adsorption route. Renew. Sustain. Energy Rev. 14, 2189–2195 (2010). https://doi.org/10.1016/j.rser.2010.03.025
54. Aliane, A.-E.: Utilisation de l'énergie solaire thermique pour la production du froid, Dotorate thesis, http://dspace1.univ-tlemcen.dz//handle/112/14085, (2019)
55. Al-Yasiri, Q., Szabó, M., Arıcı, M.: A review on solar-powered cooling and air-conditioning systems for building applications. Energy Rep. 8, 2888–2907 (2022). https://doi.org/10.1016/j.egyr.2022.01.172
56. Maheshwar, C.: Cooling India - February 2018. 13, 66–75 (2018)
57. Alazazmeh, A., Mokheimer, E.: Review of Solar Cooling Technologies. J. Appl. Mech. Eng. 04, (2015). https://doi.org/10.4172/2168-9873.1000180
58. Raihan Uddin, M., Mahmud, S., Salehin, S., Abdul Aziz Bhuiyan, M., Riaz, F., Modi, A., Salman, C.A.: Energy analysis of a solar driven vaccine refrigerator using environment-friendly refrigerants for off-grid locations. Energy Convers. Manag. X. 11, 100095 (2021). https://doi.org/10.1016/j.ecmx.2021.100095
59. Otanicar, T., Taylor, R.A., Phelan, P.E.: Prospects for solar cooling – An economic and environmental assessment. Sol. Energy. 86, 1287–1299 (2012). https://doi.org/10.1016/j.solener.2012.01.020
60. Aguilar, F.J., Quiles, P.V., Aledo, S.: Operation and Energy Efficiency of a Hybrid Air Conditioner Simultaneously Connected to the Grid and to Photovoltaic Panels. Energy Procedia. 48, 768–777 (2014). https://doi.org/10.1016/j.egypro.2014.02.089
61. Triki, Z., Selloum, A., Chiba, Y., Tahraoui, H., Mansour, D., Amrane, A., Zamouche, M., Kebir, M., Zhang, J.: Exergy Analysis of a Solar Vapor Compression Refrigeration System Using R1234ze(E) as an Environmentally Friendly Replacement of R134a. Front. Heat Mass Transf. 22, 1107–1128 (2024). https://doi.org/10.32604/fhmt.2024.052223
62. Pal A., Uddin K., Thu K., Saha B.B.: Environmental Assessment and Characteristics of Next Generation Refrigerants | Collections | Kyushu University Library. Evergreen. 5, (2018). https://doi.org/10.5109/1936218
63. Riffat, S.B., Ma, X.: Thermoelectrics: a review of present and potential applications. Appl. Therm. Eng. 23, 913–935 (2003). https://doi.org/10.1016/S1359-4311(03)00012-7
64. Riffat, S.B., Qiu, G.: Comparative investigation of thermoelectric air-conditioners versus vapour compression and absorption air-conditioners. Appl. Therm. Eng. 24, 1979–1993 (2004). https://doi.org/10.1016/j.applthermaleng.2004.02.010
65. Zeyghami, M., Goswami, D.Y., Stefanakos, E.: A review of solar thermo-mechanical refrigeration and cooling methods. Renew. Sustain. Energy Rev. 51, 1428–1445 (2015). https://doi.org/10.1016/j.rser.2015.07.011
66. Braimakis, K.: Solar ejector cooling systems: A review. Renew. Energy. 164, 566–602 (2021). https://doi.org/10.1016/j.renene.2020.09.079

67. Sankarlal, T., Mani, A.: Experimental investigations on ejector refrigeration system with ammonia. Renew. Energy. 32, 1403–1413 (2007). https://doi.org/10.1016/j.renene.2006.05.008
68. Kim, D.S., Infante Ferreira, C.A.: Solar refrigeration options – a state-of-the-art review. Int. J. Refrig. 31, 3–15 (2008). https://doi.org/10.1016/j.ijrefrig.2007.07.011
69. Abdullah, S., Zubir, M.N.B.M., Muhamad, M.R.B., Newaz, K.M.S., Öztop, H.F., Alam, M.S., Shaikh, K.: Technological development of evaporative cooling systems and its integration with air dehumidification processes: A review. Energy Build. 283, 112805 (2023). https://doi.org/10.1016/j.enbuild.2023.112805
70. Allouhi, A., Kousksou, T., Jamil, A., Bruel, P., Mourad, Y., Zeraouli, Y.: Solar driven cooling systems: An updated review. Renew. Sustain. Energy Rev. 44, 159–181 (2015). https://doi.org/10.1016/j.rser.2014.12.014
71. Abu-Hamdeh, N.H., Alnefaie, K.A., Almitani, K.H.: Design and performance characteristics of solar adsorption refrigeration system using parabolic trough collector: Experimental and statistical optimization technique. Energy Convers. Manag. 74, 162–170 (2013). https://doi.org/10.1016/j.enconman.2013.04.043
72. Mukram T, A., Daniel, J.: Solar Passive Building Cooling: Recent Trends and Novel Approaches. (2019)
73. Hassan, H.Z., Mohamad, A.A.: A review on solar-powered closed physisorption cooling systems. Renew. Sustain. Energy Rev. 16, 2516–2538 (2012). https://doi.org/10.1016/j.rser.2012.02.068
74. Fernandes, M.S., Brites, G.J.V.N., Costa, J.J., Gaspar, A.R., Costa, V.A.F.: Review and future trends of solar adsorption refrigeration systems. Renew. Sustain. Energy Rev. 39, 102–123 (2014). https://doi.org/10.1016/j.rser.2014.07.081
75. Fan, Y., Luo, L., Souyri, B.: Review of solar sorption refrigeration technologies: Development and applications, https://hal.univ-smb.fr/hal-00529546
76. Sapienza, A., Santamaria, S., Frazzica, A., Freni, A.: Influence of the management strategy and operating conditions on the performance of an adsorption chiller. Energy. 36, 5532–5538 (2011). https://doi.org/10.1016/j.energy.2011.07.020
77. Ullah, K.R., Saidur, R., Ping, H.W., Akikur, R.K., Shuvo, N.H.: A review of solar thermal refrigeration and cooling methods. Renew. Sustain. Energy Rev. 24, 499–513 (2013). https://doi.org/10.1016/j.rser.2013.03.024
78. Srikhirin, P., Aphornratana, S., Chungpaibulpatana, S.: A review of absorption refrigeration technologies. Renew. Sustain. Energy Rev. 5, 343–372 (2001). https://doi.org/10.1016/S1364-0321(01)00003-X
79. Sharma, D.K., Sharma, D., Ali, A.H.H.: A state of the art on solar-powered vapor absorption cooling systems integrated with thermal energy storage. Environ. Sci. Pollut. Res. 27, 158–189 (2020). https://doi.org/10.1007/s11356-019-06941-x
80. Guercio, A., Curto, D., Franzitta, V., Frascati, M., Milone, D., Martorana, P., Mantegna, M.: Energy Analyses and Optimization Proposals for Hotels in Sicily: A Case Study. Sustainability. 16, (2023). https://doi.org/10.3390/su16010146
81. Nikbakhti, R., Wang, X., Hussein, A.K., Iranmanesh, A.: Absorption cooling systems – Review of various techniques for energy performance enhancement. Alex. Eng. J. 59, 707–738 (2020). https://doi.org/10.1016/j.aej.2020.01.036

82. de'Rossi, F., Mastrullo, R., Mazzei, P.: Working fluids thermodynamic behavior for vapor compression cycles. Appl. Energy. 38, 163–180 (1991). https://doi.org/10.1016/0306-2619(91)90031-R
83. Sarbu, I., Sebarchievici, C.: General review of solar-powered closed sorption refrigeration systems. Energy Convers. Manag. 105, 403–422 (2015). https://doi.org/10.1016/j.enconman.2015.07.084
84. Triché, D.: Étude numérique et expérimentale des transferts couplés de masse et de chaleur dans l'absorbeur d'une machine à absorption ammoniac-eau., https://theses.hal.science/tel-01696252, (2016)
85. Abdulateef, J., Sopian, K., Alghoul, M.: Optimum design for solar absorption refrigeration systems and comparison of the performances using ammonia-water, ammonia-lithium nitrate and ammonia-sodium thiocyanate solutions. Int. J. Mech. Mater. Eng. 3, 17–24 (2008)
86. Chikh, M.E.-A., Benramdane, M., Aliane, A., Abdesselam, B., Embarek, N.: Contribution to the improvement of sorption installations (single and double effect absorption, using the H2O - LiBR binary couple). Stud. Eng. EXACT Sci. 6, e14788–e14788 (2025). https://doi.org/10.54021/seesv6n1-029
87. Grossman, G.: Solar-powered systems for cooling, dehumidification and air-conditioning. Sol. Energy. 72, 53–62 (2002). https://doi.org/10.1016/S0038-092X(01)00090-1
88. Gomri, R.: Investigation of the potential of application of single effect and multiple effect absorption cooling systems. Energy Convers. Manag. 51, 1629–1636 (2010). https://doi.org/10.1016/j.enconman.2009.12.039
89. Kharal, N.: Selection of Novel Technology For Wastewater Treatment. (2017)
90. Ali, D., Ratismith, W.: A semicircular trough solar collector for air-conditioning system using a single effect NH3–H2O absorption chiller. Energy. 215, 119073 (2021). https://doi.org/10.1016/j.energy.2020.119073
91. López-Pérez, L.A., Torres-Díaz, T., Grajales, S.G.P., Prieto, J.J.F., Romero, D.J., Pérez, J.A.H., Huicochea, A.: Solar Water Heating System with Absorption Heat Transformer for Annual Continuous Water Heating. Processes. 12, (2024). https://doi.org/10.3390/pr12081650
92. Benramdane M., Ghernaout Mea., Abboudi S.,: Contribution to improving the performance coefficient of a solar absorption refrigeration system. Int. J. Res. Rev. Appl. Sci. IJRRAS ISSN 2076-734X EISSN 2076-7366. November 2014, 71–81 (2014)
93. Benramdane M., Abboudi S., Ghernaout Mea.,: Contribution to the Simulation and Parametric Analysis of the Operation of a Solar Concentration Thermal Installation | IIETA, https://www.iieta.org/journals/ijht/paper/10.18280/ijht.370210
94. Jakob, U.: Overview on Small Capacity Systems. (2008)
95. Wang, Y., Li, M., Du, W., Ji, X., Xu, L.: Experimental investigation of a solar-powered adsorption refrigeration system with the enhancing desorption. Energy Convers. Manag. 155, 253–261 (2018). https://doi.org/10.1016/j.enconman.2017.10.065
96. Kumar, B., Selvarasan, I., Annadurai, G., Ramalingam, S.: Thermodynamic analysis of a single effect lithium bromide water absorption system using waste heat in sugar industry. Therm. Sci. 22, 507–517 (2018)

97. Ramesh, R., Murugesan, S.N., Narendran, C., Saravanan, R.: Experimental investigations on shell and helical coil solution heat exchanger in NH3-H2O vapour absorption refrigeration system (VAR). Int. Commun. Heat Mass Transf. 87, 6–13 (2017). https://doi.org/10.1016/j.icheatmasstransfer.2017.06.010
98. Wang, S., Li, S., Xu, M., Jin, Z., Xu, C.: Simulation research on absorption refrigeration system based on NH3-H2O-LiBr vapor-liquid equilibrium calculation model. Therm. Sci. 26, 1825–1840 (2022)
99. Kilic, B., Ipek, O.: Thermodynamic analysis of absorption cooling system with LiBr-Al2O3/water nanofluid using solar energy. Therm. Sci. 26, 135–146 (2022)
100. Papadopoulos, A.I., Gkouletsos, D., Champilomatis, V., Giannakakis, A., Kousidis, V., Hassan, I., Seferlis, P.: Systematic assessment of working fluid mixtures for absorption refrigeration based on techno-economic, environmental, health and safety performance. Energy Convers. Manag. 223, 113262 (2020). https://doi.org/10.1016/j.enconman.2020.113262
101. Táboas, F., Vallès, M., Bourouis, M., Coronas, A.: Flow boiling heat transfer of ammonia/water mixture in a plate heat exchanger. Int. J. Refrig. 33, 695–705 (2010). https://doi.org/10.1016/j.ijrefrig.2009.12.005
102. Kang, Y.T., Akisawa, A., Kashiwagi, T.: Experimental correlation of combined heat and mass transfer for NH3–H2O falling film absorption. Int. J. Refrig. 22, 250–262 (1999). https://doi.org/10.1016/S0140-7007(98)00076-0
103. Jiménez-García, J.C., Rivera, W.: Parametric analysis on the experimental performance of an ammonia/water absorption cooling system built with plate heat exchangers. Appl. Therm. Eng. 148, 87–95 (2019). https://doi.org/10.1016/j.applthermaleng.2018.11.040
104. Emamifar, A.: Thermodynamic analysis of a hybrid absorption two-stage compression refrigeration system employing a flash tank with indirect subcooler. J. Comput. Appl. Res. Mech. Eng. JCARME. 12, 145–159 (2023). https://doi.org/10.22061/jcarme.2022.8591.2154
105. Park, C.W., You, D.Y., Kim, H.J., Im, I.-T.: Performance analysis for the characteristics of double/single effect hybrid type absorption chiller. Int. J. Air-Cond. Refrig. 18, 23–29 (2010). https://doi.org/10.1142/S2010132510000046
106. Pirkandi, J., Amiralaei, A., Omian, M.: Performance analysis of a combined cooling, heating and power system based on micro gas turbine from the point of view of exergy. J. Comput. Appl. Res. Mech. Eng. JCARME. 12, 77–93 (2022). https://doi.org/10.22061/jcarme.2021.7514.1999
107. Enoki, K., Watanabe, F., Akisawa, A., Takei, T.: Experimental Investigation of the Effect of Generator Temperature on the Performance of Solution Transportation Absorption Chiller. Int. J. Air-Cond. Refrig. (2017). https://doi.org/10.1142/S201013251 7500286
108. Yıldırım, E., Yeşilata, B.: Düşük Sıcaklıkta Isı Kaynağı Kullanan Bir Absorbsiyonlu Soğutma Sisteminin Termoekonomik Optimizasyonu. Isı Bilimi Ve Tek. Derg. 33, 111–117 (2013)
109. Kumar, V., Pandya, B., Patel, J., Matawala, V.: Cut-off temperature evaluation and performance comparison from energetic and exergetic perspective for NH3-H2O absorption refrigeration system. Therm. Sci. Eng. Prog. 4, 97–105 (2017). https://doi.org/10.1016/j.tsep.2017.09.007

110. Narváez-Romo, B., Chhay, M., Zavaleta-Aguilar, E., Simões-Moreira, J.R.: A Critical Review of Heat and Mass Transfer Correlations for LiBr-H 2 O and NH 3 -H 2 O Absorption Refrigeration Machines Using Falling Liquid Film Technology. Appl. Therm. Eng. (2017). https://doi.org/10.1016/j.applthermaleng.2017.05.092
111. Waghare, P., Sathyabhama, A.: Performance analysis of ammonia-based vapour absorption refrigeration system. Mater. Today Proc. 51, 1503–1509 (2022). https://doi.org/10.1016/j.matpr.2021.10.279
112. Book: Basic Refrigeration and Air Conditioning by P. N. Ananthanarayanan, Second Edition, Tata Mc-Graw-Hill Publishing Company Limited 2000, https://gnindia.dronacharya.info/ME/6thSem/Downloads/RefrigerationAirConditioning/Books/Refrigeration-Air-Conditioning-text-book-1.pdf
113. Site web: Climatrol, T.: Advances in Condenser and Evaporator Technology - Climatrol Corporation - Manufacturer of Water Cooler & Cold Storage Rooms, https://climatrolcorp.com/advances-in-condenser-and-evaporator-technology/, accessed on: 25/05/2024.
114. Stel, H., Ofuchi, E.M., Sabino, R.H.G., Ancajima, F.C., Bertoldi, D., Marcelino Neto, M.A., Morales, R.E.M.: Investigation of the Motion of Bubbles in a Centrifugal Pump Impeller. J. Fluids Eng. 141, (2018). https://doi.org/10.1115/1.4041230
115. PHE Plate Heat Exchanger for HVAC solutions - Ba-32-40 by Nordic Tec, https://nordictec-store.com/ba-32-serie-0032mplate-1-thread-/77-plate-heat-exchanger-nordic-ba-32-40-1-230kw.html
116. Kumbhar, A., Gulhane, N., Pandure, S.: Theoretical Analysis of Hybrid Chiller. Energy Procedia. 109, 487–496 (2017). https://doi.org/10.1016/j.egypro.2017.03.082
117. Dione, F., Thiam, A., Cisse, E.I., Diouf, D., Maiga, A.S.: Theoretical study of an NH3–H2O absorption chiller powered by a linear Fresnel system modelled by combining ray tracing and CFD. Results Eng. 20, 101410 (2023). https://doi.org/10.1016/j.rineng.2023.101410
118. Ramanathan, A., Gunasekaran, P.: Simulation of absorption refrigeration system for automobile application. Therm. Sci. 12, 5–13 (2008). https://doi.org/10.2298/TSCI0803005R
119. Mohamed, H., Brahim, A.B.: Modeling of the absorption phase of a cycle with solar absorption using the couple NH3–H2O for in-sight energy storage. Int. J. Hydrog. Energy. 42, 8624–8630 (2017). https://doi.org/10.1016/j.ijhydene.2016.06.183
120. Akam, S.A. ; Ouchiha, Z.; Said, N.; Bellal, B.; Expérimentation d'une Boucle à Absorption NH3-H2O'', Rev. Energ. Ren. : Valorisation (1999) 17-22.
121. Kherris, S., Makhlouf, M., Asnoun, A.: SARM: Simulation of Absorption Refrigeration Machine. J. Renew. Energ. 11, 587–594 (2008). https://doi.org/10.54966/jreen.v11i4.108
122. Narváez-Romo, B., Chhay, M., Zavaleta-Aguilar, E.W., Simões-Moreira, J.R.: A critical review of heat and mass transfer correlations for LiBr-H2O and NH3-H2O absorption refrigeration machines using falling liquid film technology. Appl. Therm. Eng. 123, 1079–1095 (2017). https://doi.org/10.1016/j.applthermaleng.2017.05.092
123. Sun, X., Wang, Q., Wu, S., Zhao, X., Wei, L., Li, K., Hao, J., Wei, L., Zhai, S., An, Q.: Metal chlorides-promoted ammonia absorption of deep eutectic solvent. Int. J. Hydrog. Energy. 47, 16121–16131 (2022). https://doi.org/10.1016/j.ijhydene.2022.03.101

124. Altamirano, A., Pierrès, N.L., Stutz, B.: Review of small-capacity single-stage continuous absorption systems operating on binary working fluids for cooling: Theoretical, experimental and commercial cycles. Int. J. Refrig. 106, 350–373 (2019). https://doi.org/10.1016/j.ijrefrig.2019.06.033
125. Wu, W., Wang, B., Shi, W., Li, X.: An overview of ammonia-based absorption chillers and heat pumps. Renew. Sustain. Energy Rev. 31, 681–707 (2014). https://doi.org/10.1016/j.rser.2013.12.021
126. Wang, K., Abdelaziz, O., Kisari, P., Vineyard, E.A.: State-of-the-art review on crystallization control technologies for water/LiBr absorption heat pumps. Int. J. Refrig. 34, 1325–1337 (2011). https://doi.org/10.1016/j.ijrefrig.2011.04.006
127. Hang, Y., Qu, M., Zhao, F.: Economical and environmental assessment of an optimized solar cooling system for a medium-sized benchmark office building in Los Angeles, California. Renew. Energy. 36, 648–658 (2011). https://doi.org/10.1016/j.renene. 2010.08.005
128. LEE, Huei-Huang. Programming with MATLAB 2016. Book, Mission (Kansas): SDC Publications, 2016. ISBN 978-1-63057-013-2.
129. TRANSOL, https://photovoltaic-software.com/solar-thermal-softwares/professional-solar-thermal-softwares/transol
130. Allouhi, A., Kousksou, T., Jamil, A., El Rhafiki, T., Mourad, Y., Zeraouli, Y.: Economic and environmental assessment of solar air-conditioning systems in Morocco. Renew. Sustain. Energy Rev. 50, 770–781 (2015). https://doi.org/10.1016/j.rser.2015.05.044
131. Porumb, R., Porumb, B., Balan, M.: Numerical Investigation on Solar Absorption Chiller with LiBr-H2O Operating Conditions and Performances. Energy Procedia. 112, 108–117 (2017). https://doi.org/10.1016/j.egypro.2017.03.1071
132. EES: Engineering Equation Solver | F-Chart Software : Engineering Software, https://fchartsoftware.com/ees/
133. Wu, W., Shi, W., Wang, J., Wang, B., Li, X.: Experimental investigation on NH3–H2O compression-assisted absorption heat pump (CAHP) for low temperature heating under lower driving sources. Appl. Energy. 176, 258–271 (2016). https://doi.org/10.1016/j.apenergy.2016.04.115
134. Al-Rbaihat, R., Alahmer, H., Alahmer, A., Altork, Y., Al-Manea, A., Awwad, K.Y.E.: Energy and exergy analysis of a subfreezing evaporator environment ammonia-water absorption refrigeration cycle: Machine learning and parametric optimization. Int. J. Refrig. 154, 182–204 (2023). https://doi.org/10.1016/j.ijrefrig.2023.07.010
135. Khan, M.M.A., Ibrahim, N.I., Saidur, R., Mahbubul, I.M., Al-Sulaiman, F.A.: Performance assessment of a solar powered ammonia–water absorption refrigeration system with storage units. Energy Convers. Manag. 126, 316–328 (2016). https://doi.org/10.1016/j.enconman.2016.08.004